The National Academies of SCIENCES ENGINEERING MEDICINE
GULF RESEARCH PROGRAM

Safer Offshore Energy Systems 3 Final Report

Project Title: Advanced cement characterization and modeling to evaluate novel additives to improve wellbore integrity
Award Amount: $670,720
Awardee: Oklahoma State University
Award Start Date: 12/01/17
Award End Date: 11/30/20
NAS Grant ID: 2000008865

Project Director: Geir Hareland
Affiliation: Oklahoma State University

Project Key Personnel:

- Runar Nygaard, Oklahoma State University

I. PROJECT SUMMARY (from proposal)

In designing cements, the drilling industry has concentrated only on compressive strength and time to develop sufficient strength and the use of cement bond logs as the main quality indicator. However, to improve the cement integrity and secondly, to quantify the potential leakage path along a wellbore, a better understanding of cements is required. This project's objective is first to improve characterization and understanding of cement to better predict the frequency of magnitude of leakage through cement sheaths and cement plug. The secondary objective is to use this knowledge to investigate how novel cement additives can reduce the potential of leakage and hence improve wellbore integrity.

To investigate wellbore integrity, finite element model (FEM) study of cement integrity has become an important tool to address this issue. The advantage of building the model in several steps is to observe and record stress and deformation changes after each loading. Furthermore, knowing previous deformation and loading history will help to specify initial stress state before final thermal and mechanical loads are applied to the model. Previous simulation studies have given insight into several important phenomena such that cement properties, such as cement shrinkage, strength, and deformability, have significant effects on the casing-cement-formation integrity. The modeling has also shown that the bonding strength between cement and rock is an important factor in wellbore integrity, but very little data exists to incorporate this in models. Lastly, novel additives such as nanoparticles (NPs) have been included in cements, but their effect on cement's properties has not been extensively studied.

The main outputs of the project are an improved modeling capability of wellbore integrity and the magnitude of leakage from wellbores. The secondary output is how NP additives in cements can improve wellbore integrity.

II. PROJECT SUMMARY (from final report)

The NAS GRP funded research project titled: "Advanced cement characterization and modeling to evaluate novel additives to improve wellbore integrity" (Grant Number: 200008865) was an effort to first improve characterization and understanding of cement to better predict the frequency of magnitude of leakage through cement sheaths and cement plug, and then use this knowledge to investigate how novel cement additives can reduce the potential of leakage, and hence improve wellbore integrity.

The main objective of this project was to design new cement mixtures with NP-sized additives that have superior properties to prevent wellbore leakage. This was broken down to the following two sub-objectives.

The first sub-objective was to verify the "life of well" behavior simulations that are calibrated with our experimental laboratory testing. These simulations investigated wellbore cement integrity using finite element modeling used to observe and record stress and deformation changes after each pressure and temperature change throughout the life of a well. The FEM was to be verified and calibrated for different cement mixtures and individual additives, including NPs. The model could then be applied as a "fit for purpose" simulator with capabilities to optimize the cement design to ensure appropriate cement properties and behavior, and to potentially reduce cementing cost. It also gives the operator or service company a simulator that can be applied proactively in the cement planning. Knowing the cement deformation and loading history helps to specify initial stress state before final thermal and mechanical loads are applied to the model. Several important phenomena of cement properties, such as cement shrinkage, compressive and tensile strength, and deformability, have significant effects on the casing-cement-formation integrity; these important model properties were determined from laboratory experiments.

The second sub-objective was to quantify the benefits of individual nano additives for use in cement to improve the quality of cement to prevent or reduce potential problems such as gas leakage, cement fractures, cement permeability, and weak bonding. Specifically, this project investigated new nano additives and particle sizes, the mechanisms of the cement fluid loss and wellbore strengthening potential, cement body permeability reduction, the bonding between the cement and casing, and the formation and the stress state in the cement during thickening and the final cement stress state. The additives investigated are NPs from bentonite, typical cement weighting additives and classic types of cement used in the oil and gas industry. The laboratory study investigated the cement slurry's properties including dynamic fluid losses and thickening time, as well as advanced characterization of the cement compressive strength and bonding strength to rock and casing, and deformation properties including shrinkage.

III. PROJECT RESULTS

Accomplishments

We reached the objectives; we accomplished these milestones through the completion of 9 tasks.
The 9 tasks are: 1) Cement Life Cycle Strength Modeling, 2) Preparation and Experimental Setups for the Project, 3) Cement Fluid Loss and Rheology Testing, 4) Testing of Cement Thickening Time, 5) Cement

Core Tensile Bond Testing, 6) Cement Core Compressive Strength Testing, 7) Cement Setting Pressure and Strength Testing, 8) Cement Core Permeability Testing, and 9) Model Validity of the Correlation Model. The key results of each of the tasks are described below.

Task 1 - Cement Life Cycle Strength Modeling

A FEM was created to replicate the life of a well from the geologic conditions to the production of the well. The Finite Element Analysis (FEA) model was created and simulated using ANSYS™ 19.1. The model is a 3D poroelastic model that utilizes a 3D mesh composed of 18,384 CPT216 brick elements. The element dimensions are designed such that they are smaller towards the center of the model (center of the wellbore) while increasing in size towards the boundaries. This configuration calculates the stress patterns more accurately in the casing, cement, and near rock formation while saving computational time by having larger elements towards the boundaries.

The 3D model has a length of 1.5 m in the x and y directions and 0.05 m in the z-direction. The model geometry is determined based on the Kirsch analytical solution such that the ratio of the model size and the radius of the wellbore is greater than ten, to represent a good approximation to the infinite case (Fjaer et al. 2008; Jaeger et al. 2007). The model is surrounded by frictionless supports on all six edge faces to represent infinite supports. The dimensions of the borehole, casing thickness, and cement sheath thickness are based on the wells discussed in the case studies.

The mechanical FEM simulates the drilling, completion, and production process including the initial conditions (in-situ stresses), drilling conditions (mud weight applied to the borehole), cement conditions (cement density, thus hydrostatic pressure applied to the borehole), and production conditions (production pressure). The rock formation and hardened cement are modeled using poroelastic properties while the casing is modeled using linear elastic properties.

The staged approach uses the property of superposition to build the model's initial conditions before the next load step is implemented (Weideman and Nygaard 2014). The details of the load steps were as follows:

- **Step 1:** The model is loaded with horizontal (σ_H & σ_h) and vertical (σ_V) in-situ stresses.
- **Step 2:** The borehole is drilled, and a mud weight is applied to the rock formation.
  Step 3: Casing is added to the borehole with the mud weight being applied to the inner and outer surfaces of the casing and the borehole.
- **Step 4:** This step represents the completion of the wellbore and has two parts.
  - Cement slurry is pumped into the well. A hydrostatic pressure caused by the cement slurry is applied to the outer surface of the casing and the wellbore while the inner casing surface has the mud weight pressure.
  - Cement hydrates and hardens. The cement elements are added to the model with a framework stress, pore pressure, and zero shrinkage assuming the cement is fully bonded to the rock formation and outer casing surface. The hardened cement is inserted with zero deformation but with a framework stress in all three principal directions equivalent to the hydrostatic pressure. The mud weight pressure is still applied to the inner surface of the casing.

The input parameters used for the three case studies, including the source of the value, are listed in Table 1. Obvious input parameters will not be explained.

The simulation depth was chosen to be the depth of the deepest casing string before the production zones in the well. The cement sheath can be assumed to be intact and not damaged from perforations at this location. The true vertical depth (TVD) of the well would not be ideal to model cement sheath integrity, since it is below the perforation and production zones and not acting as a barrier.

The in-situ stress gradients for the Eugene Island Official Protraction Diagram (OPD) were based on Finkbeiner et al. (1996).

At the end of hydration (i.e. start of the simulation), the pore pressure (P_P) is assumed to be equal to that of the surrounding rock formation as described by Bosma et al. (1999). The setting stress of the cement (σ_C) is assumed to be equal to the hydrostatic pressure of the cement slurry (Bosma et al. 1999; Gray et al. 2009; Bois et al. 2012).

The parametric analysis of the stress development parameters is such that the values are tested in extreme cases. The extreme cases for all of the parameters, unless otherwise stated in Table 2, are ± 40% of the base case values, to see how extreme changes can alter the stress development in the cement sheath. Some parameters such as the hydration products and the in-situ stresses will not have that extreme of variation due to physical/chemical constraints (hydration parameters) and wellbore constraints (in-situ stresses).

The cement stress boundaries are maximum stress equal to the fracture pressure of the rock formation (P_FRAC) and minimum stress equal to the mud weight (MW). Any stress values above or below those will result in instability of the borehole during well construction. The cement P_P can either have a minimum value of zero or a maximum P_P equal to P_FRAC with the surrounding rock formation P_P being the base case.

The in-situ stresses were changed such that the horizontal stresses vary from a combination of isotropic to anisotropic stresses, and the vertical stress is off by ± 5%.

All of these scenarios are displayed in Table 2 for the high and low envelopes for the parametric analysis. For the first part of the results analysis for potential cement sheath debonding and cement fracturing, three base case wellbores were simulated in the model. The effective stresses (hoop and radial) of the cement sheath are presented for the casing/cement and cement/rock formation interfaces.

The effective stress results for the base case parameters of the three wells are represented in Table 3. The medium depth well results are considered the standard and the shallow and deep depths are normalized to it. The shadowed coloring indicates tensile stresses, while the others are compressive. The base results show that the medium and deep wells are experiencing tensile stresses in the radial directions, which indicate debonding as described by Bois et al. (2011). The medium depth well is debonding at both the casing/cement and cement/rock interfaces, while the deep well is only

debonding at the casing/cement interface. The shallow depth well is not experiencing any tensile stresses, but it should be noted that the effective stresses are close to the tensile range.

Figure 1 depicts the graphical results of the base case cement sheaths for the three wells. The effective radial stresses are depicted on the left, and the effective hoop stresses are shown on the right. The inner radius of the sheath is the casing/cement interface while the outer radius is the cement/rock formation interface.

For the shallow well, the maximum effective stress is 1 maximum principle stress (MPa) and is not experiencing any tensile stresses. The medium well is experiencing tensile radial stress throughout the cement sheath, and the magnitude is higher along the casing/cement interface, implying that the resulting debonding gap would be greater than along the cement/rock interface. The deep well is only experiencing debonding along the casing/cement interface as indicated in Table 3. The effective hoop stresses for the medium and deep wells are not close to the tensile range (therefore not resulting in tensile fracturing), and consequently not of interest to this discussion.

The results of the medium and deep well base case simulations are in agreement with an analysis from the literature. These two wells experienced debonding after the production step when the mud weight pressure inside the casing changed to a production pressure. Previous studies have documented that changes in thermal cycling can cause cement sheath debonding (Lavrov et al. 2015; Zhang et al. 2017) while Nygaard et al. (2014) concluded that debonding at the casing/cement interface occurs as a result of thermal and pressure changes. An interesting note to point out is Zhang et al. (2017) observed debonding as a result of thermal cycling of cooling fluid at the cement/rock interface, whereas the results shown here conclude that debonding is occurring at the casing/cement interface.

The second part of this analysis is the parametric study of the base case wells to rank the stress contributing factors. The results are shown in Figure 2. The maximum and minimum normalized effective stress values from the three wells are shown. The parameters are ranked from largest to smallest percent change with respect to the effective radial stress at the cement/rock formation interface. The solid bars represent a positive percent change while the checkered bars represent a negative percent change.

Figure 2 shows that the ranking of the parameters is not the same for all three wells. All three have cement P_P listed as the most important contributing factor, but the orders after that change. The medium and deep well are the most similar; both have the same order of parameters until the in-situ stresses. For the shallow well, the σ_C of the cement is more critical than the internal casing pressure (ICP), and the mechanical properties of the surrounding rock formation and cement are different from the other two wells. Overall, the general interpretation of Figure 2 is similar for all three wells: the cement hydration parameters and the ICP are the most critical parameters in the stress development of the cement sheath, followed by the mechanical properties of the rock and cement; and lastly, the in-situ stresses have little impact on the stress development in the sheath.

The results of this study are in agreement with Bois et al. (2011), in which the authors state that the two most critical aspects of cement sheath integrity are the cement hydration parameters and changes in

the pressure in the wellbore. The changes in ICP have already been proven in the literature to be a major cause of cement sheath debonding and will not be discussed in more detail here, but the cement hydration parameters have not been studied as intensely. Simulating the σ_C from the maximum possible value (P_FRAC) to the lowest possible scenario (zero effective stress) significantly affects the cement sheath stress by over 100% in both the radial and hoop stresses. The change in effective stresses is significant enough to take the cement sheath from compressive to tensile and vice versa. The cement P_P acts the same way. A maximum P_P (equal to P_FRAC resulting in negative effective stress) and a minimum P_P (zero P_P) affect the cement stress from 100% to greater than 1,000% in some instances. Both of these parameters are critical in the development of the hydration of cement, but they are not well understood. The upper and lower ranges for both parameters presented in this paper are realistic, but the variation has dramatic results. Therefore, cement hydration should be investigated further to develop a better understanding of how the cement σ_C and P_P develop during hydration.

When designing a cementation plan for completing a well, many factors are taken into account. The cement density is arguably the most critical, but the structural properties of hardened cement are also considered. The only changeable parameters for the cement job are the cement composition, which directly affects the mechanical properties (elastic modulus [E] & Poisson's ratio [v]). From the results of this study, the mechanical parameters have little effect on cement sheath integrity. The effective radial and hoop stresses were less sensitive to changes in the mechanical properties of cement. The maximum change in one of these parameters is not larger than 100%, which will not change any of the baseline effective stress results in Table 3 from being in compression to tension or vice versa. Therefore, changing cement compositions to develop enhanced structural properties is not a dominant factor in cement sheath integrity in terms of tensile fracturing or tensile debonding. This result is not in agreement with Fleckenstein et al. (2001) in which they concluded that ductile cement (high v & low E) would “significantly” reduce tangential (hoop) tensile stresses, but the authors did not take into account the pore pressure of the cement. The results of this paper do agree with Nygaard et al. (2014) in which the mechanical properties of the cement do not affect the radial stresses dramatically.

Another trend seen in Figure 2 for all three wells is that changing the in-situ stresses has less than a 1% effect on the stress development in the cement sheath. This indicates that the geologic location of the well has little impact regarding the potential failure of the cement sheath from normal faulting stress regimes, although the changes of in-situ stresses due to compaction and subsidence, which was not addressed in this study, have been shown to play a factor in casing shear as described by Dusseault et al. (2001).

A final result, that is not as obvious and not explicitly shown from the parametric study, is how the depth of the well affects cement sheath stress. The shallow well is not experiencing debonding at either interface, but both the medium and deep wells are experiencing at least one interface debonding. The medium well is experiencing debonding at both interfaces, while the deep well is only debonding at one interface, implying that there is a depth in which the cement sheath will be at a higher risk to develop gaps. This depth versus the risk of debonding curve may look similar to a bell curve as seen with the three wells presented in this paper. There may be an “optimum” depth that puts wells at a higher risk for debonding, but above and below that depth have less prime conditions. This reasoning would explain why the medium depth well is debonding at both interfaces, but the deep well is only debonding

at one interface. This phenomenon was described by Gray et al. (2009) in which the authors concluded that debonding does not always occur at the deepest locations within a wellbore.

A staged 3D FEM based on actual wellbore dimensions for three wells in the Eugene Island OPD was developed, and a parametric study was performed to rank contributing factors of stress development that lead to potential cement sheath debonding.

The main conclusions of this task are as follows:

- The base case parameters for the medium and deep TVD wells experience debonding on at least one interface between the casing and cement and/or the cement and rock formation, leading to concerns that established wells in the Gulf of Mexico (GoM) are experiencing leakage. However, debonding gaps were not determined in this study, and future simulations are required to determine potential leakage rates.

- Tensile debonding is the most probable form of cement sheath failure for vertical wells in the Eugene Island OPD.

- The cement mechanical properties, E, and v, have little effect on cement sheath stress development, and the variations are not large enough to sway the cement stress into or out of failure.

  The cement hydration properties (σ_C and P_P) and the ICP have the most significant effect on the stress development in the cement sheath. The literature shows that the ICP is critical in cement sheath debonding, but the cement hydration parameters have not been well documented. These two parameters have major assumptions associated with them and need to be studied further to know definitively how they affect cement sheath stress.

- The geographic location of the well has little effect on the potential for cement sheath debonding for vertical wells.

- The depth of the well appears to play a factor in causing cement sheath debonding. The results of this study show that specific depths are more prone to cause debonding than others.

Task 2 - Preparation and Experimental Setups for the Project

During the second and third years of the project, the cement designs were completed for both heavy and light cases as well as for their NP variants. This included the determination of water requirements for the added NPs. A testing matrix was established to describe the required tests for each property being measured. Several iterations of designs for apparatuses used to test the shear and tensile bond strengths between cement and a steel substrate have been evaluated. Final designs for both types of bond testing have been identified and fabricated. Testing procedures have also been established for both. Slurry property evaluation procedures have also been established to include fluid loss testing, rheology testing, and thickening time.

Test matrices of different cement slurries were designed to investigate the effect of the addition of different NPs on the heavy cement (Portland class H) and light cement (Portland class A). Barite NPs, magnetite NPs, and Portland class H NPs were used in the heavy cement slurry; while bentonite NPs, silica NPs and Portland class A NPs were used in the light cement slurry. Three different concentrations (1%, 3%, and 5% by weight of cement [BWOC]) of each NP type were used to provide a better understanding of the effect of NPs concentration on various cement properties. Testings for the different cement properties were conducted by using different experimental test apparatuses detailed in Tasks 3 through 8. Operating procedures were established for the individual tests and respective user manuals provided step-by-step instructions.

Testing Matrices

A base case cement designed to resemble one that would be seen in the field and altered using weight replacements of NPs were designed as described in Tables 4-9.

The testing matrices for the desired properties were designed such that several data points for each property could be acquired in order to ensure reliability in the data. Tables 7, 8, and 9 describe the testing matrices on which the results should be recorded for the heavy and light cement cases.

Slurry Preparation and Core Storage

Each sample was mixed using the formulations described in the respected table and prepared according to API 10A/ISO 10426-1:2000 using an OFI Testing Equipment (OFITE) variable speed blender, as shown in Figure 3, with a handful of notable exceptions.

The first two deviations from the standard regarded the time of mixing and molding procedures. The standard procedure is 15 seconds at 4000 RPM ±200 RPM with the fluid components already in place and the solids added in this time frame; followed by 12,000 RPM ±500 RPM for an additional 35 seconds. The addition of NPs increased the amount of clumping when the solids were added. Because of their tendency to tie up water on their surface, full introduction of the solids became difficult because they would build upon the fluid surface while the liquid underneath simply swirled without much mixing taking place. It was seen that extra time during the low RPM phase was required, along with tapping on the cup and even gentle shaking to bring the liquids and solids into a homogeneous state. This extra time typically ranged from an additional 30-40 seconds and was always followed by the standard high RPM phase for 35 seconds. In an effort to more efficiently disperse the NPs, they were added during the low RPM stage prior to the rest of the solids. Once mixed, the samples were poured into clean molds that were 2 inches in diameter by 4 inches in length and stirred with a thin metal rod while being subjected to external vibration until bubbles stopped forming on the slurry surface, to ensure there was no trapped gas to leave voids within the cement body.

The remaining difference in procedure from the standard applies only to the tests in which cores were made and cured at elevated temperatures. In lieu of a water bath at 170°F, a brine of pH 12 NaOH solution at 194°F was used to mimic the deep well environment that the cement would be exposed to and promote hydration with an elevated pH without the worry of unintentional reaction with the cement. From there, the samples were pulled from the oven and left to cool with the fluid. This procedure deviates from the standard in that a controlled water bath is not used. Instead, it was verified

that the rate of cooling does not exceed that which is specified in API 10A by monitoring the fluid temperature near the cores in a trial that used the same fluid and wrapping procedure. Once cooled, the cores were prepared according to the testing to which they will be subjected.

The samples that were aged at 194°F were allowed to harden for 48 hours before being removed from their molds and placed in the NaOH hydration solution. From there, they were placed in the oven and left to cure for 28 days to add up to a sum of 30 days aging before being prepared for testing.

Cement Design Methodology and Storage

Several rounds of testing were completed to ensure that the designed cement is a viable field cement with which to test against as a base case.

This section describes the process of designing different cement slurries for heavy and light cement, including consideration of higher temperatures for the deeper sub-surface intervals. Portland class H cement was selected for the heavy cement base case. Portland class A cement was selected for light cement base case, due to the lower temperature at shallow intervals. Water requirements for the different cement classes as well as cement additives have been published in API 10A and API RP 10B. However, a hydration/dime test was conducted to measure the exact water requirement for each component of the cement slurries.

Table 4 shows the required amount of seawater measured for each component based on the hydration/dime test. The hydration/dime test was performed at 4000 RPM with seawater and each additive was added gradually (one gram by one gram) until the vortex mouth in the middle of the mixture converges to the size of a dime. The amount of the added component was then recorded and used for the total water requirement calculation of each cement slurry.

Excess seawater that was measured by the dime test and being used in mixing cement containing NPs normally yielded samples with pockets of unreacted water.

Therefore, it was decided to use the same amount of seawater as the base case for all the samples containing different types of NPs, instead of using the dime-test-measured amount of seawater. Figures 4 and 5 show the cross-sections of 5% BWOC NP barite cores with and without the extra water, respectively. It is observed that while both samples still contain large voids, the sample without excess water is missing the numerous small pockets left by the unreacted water. Note that both samples contain 0.15% BWOC of D-air defoamer to reduce bubbles both in number and size. The decision was made to use the same amount of seawater as the base case for all the different NPs recipes as well as to subject the samples to external vibration and stirring to remove any trapped gasses.

The required amount of barite NPs and magnetite NPs at the different concentrations were calculated based on the specified percentage BWOC in the slurry and then substituted for an equal amount of normal barite in the heavy cement slurry. Similarly, the NP bentonite was substituted BWOC for an equal proportion of standard bentonite.

The NP cement additives (class A and H) will be substituted for equal parts of their respective cement.

Tables 5 and 6 show the initial formulas of the heavy and light base cases. The density of heavy cement is 16.7 pounds/gallon (ppg) and the density of light cement is 13.5 ppg. Hydroxyethylcellulose (HEC) is added to the base cases with the recommended amount of 0.5% BWOC. HEC is a typical additive to control fluid loss of cement slurries. Without a fluid loss control additive in cement, it is expected that a cement slurry would not hydrate properly due to the loss of a considerable amount of water during the setting period; which can result in considerable reductions in the mechanical strength of the set cement as well.

Defoamer D-air 5000 from Halliburton was added to the slurries in the recommended amount of 0.15% BWOC to reduce the bubbles in the cement slurries.

If the bubbles are not eliminated, the cured cement samples would have higher porosity which reduces the mechanical strength of the set cement and creates an ineffective seal in the annulus.

Cement Design Results

The main purpose of using a Consistometer is to find the cement thickening time for heavy and light cement slurries measured in Bearden of consistency (Bc). This testing was conducted using the Chandler Model 7322 high pressure high temperature (HPHT) Consistometer. Initially, two consistency tests were conducted to evaluate the setting time of the initial heavy cement slurry. The tests were conducted at 3000 psi and 160°F to simulate a typical downhole condition in the GoM.

The apparatus and sample cup were mounted together as shown in the manual and prepared for the cement slurry. Then the automated test procedure was set up with the desired temperature, pressure, and motor schedule. The samples were poured into the cup and the cup was sealed and lowered into the test cell. The potentiometer mechanism was then mounted. The test cell plug was set in place and the thermocouple was slid into the paddle shaft. The pressure valve was closed and oil was filled into the test cell by turning the cylinder switch to fill until escaping from the thermocouple, which then was sealed with a wrench after the cylinder switch was turned off.

The pump switch was turned to auto, the heater turned on, and the alarm and timer turned to “on” and the motor started. Then the test was initiated, running until the consistency reaches 80 Bc then stopped automatically. The test report was saved and prepared in Excel and all of the instrument parts were cleaned. The consistometer apparatus is shown in Figure 6.

The consistency results, as shown in Figures 7 and 8, indicate that the setting time for this slurry is about 62 to 67 minutes to reach 80 Bc; that is typically an inadequate cement setting time, especially for the deeper well intervals.

For further evaluation of the initial heavy case, the setting time with different concentrations (1%, 3%, 5% BWOC) of barite NPs was tested using the HPHT consistometer at 3000 psi and 160°F. Figure 9 illustrates the cement consistency results for various concentrations of barite NPs, indicating that the setting time (to reach 80 Bc) slightly increases by increasing barite NPs concentration. However, the results do not imply a significant effect of barite NPs concentration on the slurry setting time. The

measured setting time for all the tests is typically inadequate for well cementing, especially for the deeper well intervals.

Three consistency tests were conducted to evaluate the setting time of the initial light cement slurry. The first test was conducted at 3000 psi and 72°F. The consistency results, as shown in Figure 10, indicate that the setting time for this slurry is about 244 minutes to reach 80 Bc. As expected, the setting time is longer for this test due to the lower temperature (72°F) compared to the previous test's temperature of 160°F.

The second two tests were conducted at 3000 psi and 160°F to simulate a typical downhole condition. The consistency results indicate that the setting times for these slurries are from 62 to 66 minutes to reach 80 Bc, as shown in Figure 11.

These tests indicate that a retarder is necessary, and boric acid (H_3BO_3) was considered a good additive. Testing was done in the consistometer to find the appropriate concentration to get from 180 to 240 minutes of thickening time, which is considered adequate to achieve enough setting time for heavy and light cement.

Initial heavy cement base case was tested with (0.3%, 0.4%, and 0.5% BWOC) boric acid. The tests were done with 3000 psi and 160 °F, and the setting times were, respectively, 129, 202, and 274 minutes, as shown in Figures 12 and 13.

Initial light cement base case was tested with (0.5%, 0.6%, 0.6%, 0.7% BWOC) boric acid. The tests were done with 3000 psi and 160°F, and the setting times were, respectively, 141, 227, 262, and 342 minutes, as shown in Figures 14 and 15.

Based on the tests, the final base case heavy with barite NPs and magnetite NPs will have 0.4% BWOC boric acid, and the final base case light with the bentonite NPs will have 0.6% BWOC boric acid, as shown in Tables 7, 8, and 9.

Nanoparticle Generation

Early attempts at generating reliably sized NPs in-house with a high energy ball grinder as shown in Figure 16 were plagued with issues that ranged from highly inconsistent data to equipment failure. Furthermore, it was seen that in order to reliably generate a consistently small particle size, a large amount of time was required that ultimately yielded very small amounts of product. For these reasons, it was decided to purchase the NPs from a supplier.

Magnetite (Fe_3O_4) NPs with the particle sizes ranging from 50 to 100 nanometers (nm) were purchased from Alfa Aesar. Barite ($BaSO_4$) NPs with a particle size of less than 400 nm were purchased from American Elements Company. Bentonite ($Al_2H_2Na_2O_{13}Si_4$) NPs with a particle size of less than 80 nm were purchased from READ Advanced Materials Company. Silica (SiO_2) fumed NPs with the particle sizes ranging from 200 to 300 nm were purchased from Sigma-Aldrich Company. Portland Cement NP production will be attempted using the EMAX high Energy ball grinder. The apparatus is shown in

Figure 16.

Unconfined Compressive Strength (UCS)
Work done in finalizing the UCS testing procedure was determining a rate of displacement that would load the sample according to ASTM C39. Ideally, the samples would all load at a stressing rate of 35 psi/s; however, a ±7psi/s variance is acceptable. To test this, several cores were prepared and tested at various displacement rates on a percent of the sample length per-second basis. Compressive stress and time were then plotted and the slope of the plastic deformation section was calculated, which determined that a displacement rate of 0.5%/s would be used for this study. Please see Figure 34 for details.

Tensile Strength
Testing procedures regarding the tensile strength of the cement body have been established. The Brazilian tensile test for brittle materials has been adopted over conventional tensile testing for its simplicity in sample making. Initially, the displacement rate was set at 0.0236 inch/min as seen in a similar study; however, upon further review, this rate loaded the sample far too quickly.

The final displacement rate for testing was determined to be such that the sample failure occurred within 2-3 minutes. Preliminary displacement testing (shown in Figure 35) revealed a constant displacement rate of 0.005 in/min to be required.

Additionally, a new set of curved load platens was designed and fabricated according to proven optimum dimensions (Garcia, et al., 2017) for our sample size. Please see Figure 36 for details.

Tensile Bond Strength Experimental Apparatus and Procedure
The experimental apparatus and procedure for the tensile bond strength portion have been fabricated to mount directly to the Mark-10 tabletop load frame. Sample preparation procedures, as well as testing procedures, have also been established.

In order to evaluate the tensile bond strength of the interacting plane between set cement and steel, a testing apparatus was designed and fabricated that mounts securely to the Mark-10 load frame. The setup itself consists of three distinct components; the upper grip; the steel substrate; and the sample holder. Additionally, two separate anchoring methods have been designed and will be discussed later in this section.

The upper grip was made up of a connection similar to a clevis bracket that mounted to the upper connection of the load frame. A heavy-duty eyebolt provided an adjustable anchor point, while a quick connect link allowed the upper grip to connect to the anchor in the sample. Figure 17 visually details this component.

The steel substrate provided the bonding plane of interest and was designed such that the interacting plane matched the geometry of that used for the steel coins in the shear bond testing so that the molds would seal properly. In order to connect it to the sample holder, the round bonding portion was based on a 3”x 3” square. This allowed the sample to be securely seated in the sample holder when a load was

applied. See Figures 18 and 19 for details. In between each test, the surface was also sandblasted in accordance with ASTM C882 to ensure each round of tests had surfaced with similar roughness. Unfortunately, after a few early rounds of testing, pitting was observed, so the decision was made to re-surface the steel in between each testing set by removing 0.005”- 0.01”, depending on the extent of the damage; sandblasting would then follow.

The sample holder was designed and fabricated out of plain carbon steel and mounted securely to the Mark-10 load frame. To accommodate the sample base, a squared slot was cut into the steel roughly 0.05” larger than the steel substrate base. This allowed for a snug fit to minimize the potential for movement during testing. Figure 20 shows how the sample and sample holder go together.

In order to connect the cement half of the sample to the load frame, a secure point was established. Initially, it was thought that the tensile strength of the cement body, low as it is, would overcome the bonding strength by a significant amount. This early assumption produced the first of two anchoring methods that used a series of nuts and washers on a 3/8” eyebolt (see Figure 21) that was placed into the cement slurry immediately following mixing. Once hardened, the anchor was to mechanically distribute the load to the cement body and ultimately to the interaction plane causing failure at that point. Unfortunately, this proved ineffective because the bond strength was close to that of the tensile strength. Furthermore, it is likely that the loading was not distributed uniformly as originally thought and created a high-stress point at the very bottom point of the anchor. This point failed early which then transferred the load to the area around the edges of the washers. Because of the reduced cross-sectional area, the stress built rapidly as the load increased which, when combined with the already failed point at the bottom of the anchor; provided the perfect path for failure across the cement body to occur.

As a new approach, threaded connections were put together and attached to the cement core using a high strength, two-part epoxy. After the cores were allowed to harden for 48 hours, they were removed from the molds and the tops were planed using a tile saw. The excess cuttings were rinsed away using deionized (DI) water followed by an acetone flush to remove residual water from the pores. Once the epoxy was applied according to the instructions, the samples were left half-submerged in DI water for an additional 24 hours. While this approach did not present the entire solution, there was no tensile failure seen within the cement samples. Instead, the majority of failures occurred at the cement-epoxy contact; two samples partially failed at the cement-steel interface. This confirmed the concept, and the testing itself was further modified to reduce the stress accumulation at the epoxy interface.

In an effort to reduce the likelihood of failure away from the bonded surface, the cross-sectional area of the cement-steel interface was reduced by adding a 2” outer diameter (OD) rubber washer between them. This allowed only the cement in the 1” inner diameter (ID) eye of the washer to interact with the steel substrate, therefore reducing the load required to cause bond failure at this point. Additionally, the difference between the bonded area and the cross-sectional area of the cement core would cause the stress at the interacting plane to increase four times faster than the rest of the sample, if uniform loading is assumed. An annotated sketch of this set up is provided in Figure 22.

Once the samples were prepared and ready for testing, they were gently dried and secured to the upper grip by threading an eye bolt into place. The upper grip was then adjusted by adjusting the backing of the top eye bolt until the data recorder consistently read 1 pound-force (lbf). This ensured that the sample was properly aligned.

The upper grip was then backed off until no load was recorded on the data recorder to provide a common 0 lbf starting point for all samples. A constant displacement of 0.05 mm/s was then applied until failure occurred, at which point the resulting load data was saved and the bonded interface was examined for signs of failure other than debonding, as shown in Figure 23.

In order to calculate the bond strength at the interface, first, the diameter of the bonded section was taken at three points roughly 120° from each other (seen in Figure 24) and averaged. The calculated average diameter was then used with the respective load at failure for each sample to find the tensile bond strength using Equation 1.

Shear Bond Strength Experimental Apparatus and Procedure

To date, several iterations of designs have been evaluated for testing the shear bond strength, and a final design has been selected and fabricated. The procedures for this design have also been established and refined.

Evaluating the shear bond strength went through several phases of the experimental set up before settling on the current apparatus. Initially, three steel bases were fabricated to resemble ASTM C882/882M. Each steel base matched the 2" diameter of a cement core with failure angles cut at 45°, 60°, or 75° (see Figure 25). They were then secured inside of a rolled piece of thin sheet metal to form a mold that was filled with cement and left to sit for 24 hours. This design ultimately failed because the makeshift mold did not create uniform cores, and the cement/steel bond typically failed when being removed from the mold.

The third design iteration did away with the core mold design outlined in ASTM C882/C882M in favor of a cheaper alternative that would allow for quicker sample turnover and therefore more data. Drawing from the setup used in Zhang's 2016 study, the shear bond strength between cement and steel was evaluated using a testing apparatus that resembles the split core test. Two halves of an aluminum alloy-6061 cylinder make up the main body of the sample holder that is able to freely slide past each other along the induced failure plane they create. One side contains a centrally placed, 2-inch diameter hole that houses the cement side of the sample puck and therefore applies the shearing load to the sample. The other side has a matching hole; whose depth matches the thickness of the steel coin substrates used for testing to the nearest 5/1000th of an inch. This side acts as the support for samples during load testing and as a means of aligning the cement/steel transition zone of the sample to the failure plane of the sample holder. In order to confidently test at the desired angle across multiple samples, flat edges were milled along the length of the complete cylinder tangent to the arc from which they were cut. Parallel faces were milled diametrically opposite of the first and together correspond to form loading angles that are 15°, 30°, and 45° away from the induced failure plane. This means that the setup is able to reliably test the shear bond strength at angles of 45°, 60°, and 75° from the horizontal. Please see Figures 26, 27, and 28 for detailed sketches of the setup.

In order to verify that the aluminum selected to fabricate the sample holder halves was safe to use, load simulations were ran using the design program Solidworks. These models used the properties of 6061 alloy aluminum to match the aluminum used to fabricate the sample holders, as well as a 2-inch cylinder in place of the cement/steel puck that would be there in testing. This 2-inch cylinder was modeled to have the properties of plain carbon steel so that it would act as a hard inclusion for simulation purposes. The model was bound such that the steel cylinder was in full contact with the sample holder halves; the interacting plane between the sample holder halves was fixed as a roller so that only lateral movement parallel to the planes was allowed and assumed frictionless; the loaded platen had an external load applied, and the platen opposite of the loaded side was fully fixed to act as a base. This is further illustrated in Figure 29.

Results from the simulation showed that when subjected to 1100 lbf, (which is the maximum compressive strength of the Mark-10 load frame), a local stress concentration appears where the steel cylinders top edge makes contact with the inner wall of the top half, see Figure 30. The von Mises value given to this area is around 1005 psi, which is significantly lower than the yield strength value given for 6061 aluminum of 7998 psi (according to the software material description). In fact, the stress concentration at that point does not approach the yield strength until 8750 lbf is applied to the system, see Figure 31.

It was concluded from these simulations that the testing apparatus is fully capable of handling the full load range of the Mark-10 load frame, and if it is necessary, loads of up to 8750 lbf can be applied without plastic deformation of the aluminum occurring. It should also be reiterated here that the limits stated were derived using an inclusion significantly harder than the cement. In other words, the formation of the stress concentrations seen in this model is unlikely because the cement would yield and distribute the load. Furthermore, the limit of 8750 lbf is set to protect the sample holders in the event that the sample was incorrectly placed and the steel coin was preventing displacement.

Sample Preparation and Testing Procedure

Before applying the slurry, each steel substrate was prepared according to ASTM C882 and placed into the flat end of a disposable cylinder mold. Once poured, a layer of DI water was placed on top of the cement to avoid shrinking and the samples were left to harden for 72 hours in order to match the age of the tensile bond strength samples. After being removed from the mold, the samples resembled those in Figure 32.

The samples were then placed into the testing apparatus at the desired testing angle and aligned on the Mark-10 tabletop load frame (Figure 33). A constant displacement rate was then applied until failure occurred.

Because of the expected low values of the bond strength, and the geometry of the setup is similar to a split-core test, it was initially decided to stray from the loading procedure recommended in ASTM C882/882M and use the constant displacement rate of 0.2 in/min recommended for Brazilian testing (García et al., 2017). It was seen, however, that this displacement rate was too high and caused rapid loading of the sample, which is both dangerous and likely to produce unreliable results due to the rapid loading. The displacement rate was then reduced to 0.02 in/min, which resulted in gradual loading and

failure within a more favorable time window. It was seen, however, that testing at this loading rate took several minutes to complete, which, in turn led to concerns about fatiguing the bond. Further investigation revealed that in a study evaluating the adhesive strength between concrete and steel reinforcement bars, a displacement rate of 0.05mm/s was used for three separate methods (Jasiczak et al., 2017). Because of its proven applicability and relatively low displacement rate, 0.05mm/s (0.11811 in/min) was selected as the displacement rate for testing in this study.

Once failure occurred, the test was stopped, data recorded in Excel, and the steel substrate was analyzed for failure other than debonding. The shear bond strength was then calculated using Equations 2, 3, and 4. Where μ_s is the static friction coefficient and was assumed to be 0.3 for a lubricated aluminum-aluminum contact; F is the normal load on the interacting plane; A is the bonded area, and θ was measured from the horizontal plane.

Fluid Loss Testing Methodology

An OFITE HPHT fluid loss tester was used with a quantitative filter paper (2-5 microns) to find the cement slurries' fluid loss for both heavy and light cement. The test cup was mounted with a screen mesh (#170-18) and the standard FANN paper filter (2-5 microns) in the bottom of the test cup, then sealed with rubber O-rings on both sides to prevent leaking, and then closed.

The cement sample was made and poured into the test cell up to ¼ inch from the top; the mesh filter was mounted with rubber O-rings on both sides and then closed. A high-pressure nitrogen (N_2) cylinder was connected to the top (upstream) and bottom (downstream) of the test cell. All the valves were closed and the heater turned on. The sample temperature was allowed to raise to 100°F for light cement or 150°F for heavy cement. After that, the upstream pressure was raised and adjusted to 600 psi and the back pressure (downstream) raised and adjusted to 100 psi. The subsequent differential pressure on the slurry is then 500 psi. The test was started and a timer was turned on. Samples of fluid were collected every minute through the test by opening the valve in the bottom of the cell and the accumulated amount of fluid was set for about 10-15 minutes to clear; then it was recorded. The apparatus is shown in Figure 37.

Rheology Testing Methodology

Rheology tests were modeled with Bingham Plastic correlation. A Fann 35A Viscometer was used together with an OFITE heating cup in the procedure. The rotor dimensions are a radius of 1.7245 cm and height of 3.8 cm. The rotational speed can be selected from 3, 6, 100, 200, 300, and 600 RPM. The purpose of this test is to determine the cement slurry rheology properties. The temperature of the slurry was set to 150°F for heavy cement and 100°F for light cement. The apparatus is shown in Figure 38. The Bingham Plastic formulas used are presented as Equations 5, 6, 7, and 8. The cement was mixed according to the recipes and pour into the heating cup. The cup was moved up to the level over the bob and rotor. The temperature was turned on and when the desired temperature was reached, the test was started. The test was running for 1 minute at each speed, then the reading was recorded. The Bingham Plastic model was used to calculate the Shear Stress and recorded for the different Shear rates of 3, 6, 100, 200, 300, 600 RPM. The plastic viscosity and the yield point were calculated and recorded for each sample.

Thickening Time Methodology

The Chandler Model 7322 HPHT consistometer, as shown in Figures 6A and 6B, was used to determine the thickening time. Then, the thickening time was tested with the final base case and the different NPs to determine the final thickening time. The tests were done with a temperature of 160°F and pressure at 3000 psi for both heavy and light cement. The tests were ended when the consistency reached 80 Bc, and the thickening time was recorded.

Task 3 - Cement Fluid Loss and Rheology Testing

The experimental results of the cement fluid loss and rheology along with a brief discussion of the results are presented in this section.

Cement Fluid Loss Testing

The fluid loss results for the control case of light cement and the mean values are shown in Table 12. The tests were conducted using (2-5 micron) filter paper, and all of the tests were terminated after a few minutes because of the total loss of their filtrate.

The fluid loss results for light cement containing bentonite NPs at a concentration of 1% BWOC and the mean values are shown in Table 13. It is noticeable that bentonite NPs slightly reduced the filtration. The fluid loss results for light cement containing bentonite NPs at a concentration of 3% BWOC bentonite NPs and the mean values are shown in Table 14. By increasing the concentration of bentonite NPs in the cement, a reduction of the filtrate was detected. The fluid loss results for heavy cement containing bentonite NPs at a concentration of 5% BWOC bentonite NPs and the mean values are shown in Table 15. The results show that a meaningful reduction of filtrate happened when small concentrations of bentonite NPs were used in the light cement. By increasing the bentonite NPs concentration in the light cement formulation, filtration slightly reduced. The fluid loss results were depicted in Figure 39, showing the trend of fluid loss for light cement containing different concentrations of bentonite NPs.

The fluid loss results for light cement containing ground cement class A at a concentration of 1% BWOC and the mean values are shown in Table 16. The results show that light ground cement class A do not have a significant influence on the filtration. The fluid loss results for light cement containing ground cement class A at a concentration of 3% BWOC and the mean values are shown in Table 17. The fluid loss results for light cement containing ground cement class A at a concentration of 5% BWOC and the mean values are shown in Table 18. An increase in the concentration of ground cement class A did not affect the fluid loss. The fluid loss results were depicted in Figure 40, showing the trend of fluid loss for light cement containing different concentrations of ground cement class A.

The fluid loss results for the control case of heavy cement and the mean values are shown in Table 47. The tests were conducted using (2-5 micron) filter paper. The fluid loss results for heavy cement containing ground cement class H at a concentration of 1% BWOC and the mean values are shown in Table 48. The fluid loss results for heavy cement containing ground cement class H at a concentration of 3% BWOC and the mean values are shown in Table 49. The fluid loss results for heavy cement containing ground cement class H at a concentration of 5% BWOC and the mean values are shown in Table 50. The fluid loss results were depicted in Figure 65, showing the trend of fluid loss for heavy cement containing different concentrations of ground cement class H. The results suggest that increasing the ground

cement class H concentration in the heavy cement formulation slightly increased the fluid loss compared to the base case.

The fluid loss results for heavy cement containing magnetite NPs at a concentration of 1% BWOC and the mean values are shown in Table 70. It is noticeable that Magnetite NPs generally did not reduce the filtration. The reason might be the fact that pore throat size of the filter paper is much larger than the magnetite NPs size. The fluid loss results for heavy cement containing magnetite NPs at a concentration of 3% BWOC and the mean values are shown in Table 71. By increasing the concentration of magnetite NPs in the cement, a reduction of filtrate was detected. The fluid loss results for heavy cement containing magnetite NPs at a concentration of 5% BWOC and the mean values are shown in Table 72. This test showed that a meaningful reduction of filtrate can happen at the higher concentrations of magnetite NPs in the heavy cement. Figure 84 shows the fluid loss results for heavy cement with magnetite NPs. Adding 3% and 5% BWOC magnetite NPs in the cement sample reduces the fluid loss compared to the base case, except for the 1% BWOC magnetite NPs which had a higher fluid loss. The reason behind the discrepancy between the filtration results for 1% and 3% or 5% needs more tests to be conducted to have conclusive results. There could be a threshold NPs concentration in combination with the other solid materials in cement slurry to be able to reduce filtration.

The fluid loss results for heavy cement containing 1% BWOC barite NPs and the mean are shown in Table 73. It shows that barite NPs at low concentration can slightly reduce the filtration. The fluid loss results for heavy cement containing 3% BWOC barite NPs and the mean are shown in Table 74. The fluid loss results for heavy cement containing 5% BWOC barite NPs and the mean are shown in Table 75. By increasing the concentration of barite NPs, filtration reduces for this heavy cement slurry. Figure 85 shows the fluid loss results for the heavy cement base case and barite NPs. The 1% and 3% BWOC barite NPs had nearly the same fluid loss as the base case, while 5% BWOC barite NPs had a lower fluid loss. These results are in accordance with the previous findings in other research related to the application of barite NPs in cement.

Cement Rheology Testing

Cement rheology for all of the heavy cement cases as well as the light cement base case have been evaluated. The rheology tests were performed with the temperature of 150°F for heavy cement and 100°F for light cement. All tests were started when the temperatures in the slurry reached 150°F for heavy cement and 100°F for light cement. The readings were recorded after running for 1 minute at each speed, 600, 300, 200, 100, 6, and 3 RPM, respectively. The Bingham plastic and the Power-law models were used to approximate the pseudo-plastic behavior of the cement.

Table 20 presents the rheology results for the light cement base case. Table 21 shows the average measurements for light cement base case and the calculated plastic viscosity (PV) and yield point (YP) values based on the Bingham plastic model are 41.8 cp and 62 lbf /$(100\ ft)^2$, respectively. Table 22 presents the rheological measurements for light cement containing 1% BWOC bentonite NPs. Table 23 shows the average measurements for light cement containing 1% BWOC bentonite NPs and the calculated PV and YP values based on the Bingham plastic model are 41 centipoise (cp) and 60.2 lbf/$(100\ ft)^2$, respectively. Table 24 presents the rheological measurements for light cement containing 3% BWOC bentonite NPs. Table 25 shows the average measurements for light cement containing 3%

BWOC magnetite NPs and the calculated PV and YP values based on the Bingham plastic model are 40.8 cp and 66.5 lbf/(100 ft)^2, respectively. Table 26 presents the rheological measurements for light cement containing 5% BWOC bentonite NPs. Table 27 shows the average measurements for light cement containing 5% BWOC bentonite NPs and the calculated PV and YP values based on the Bingham plastic model are 37.3 cp and 68.2 lbf/(100 ft)^2, respectively. The summary of all the rheology results for light cement with bentonite NPs is shown in Figure 42. The shear stress doesn't seem to be affected by the addition of bentonite NPs. Little to no deviation at all from the base case can be depicted in Figure 42.

Table 28 presents the rheological measurements for light cement containing 1% BWOC ground cement class A. Table 29 shows the average measurements for light cement containing 1% BWOC ground cement class A and the calculated PV and YP values based on the Bingham plastic model are 32 cp and 84 lbf/(100 ft)^2, respectively. Table 30 presents the rheological measurements for light cement containing 3% BWOC ground cement class A. Table 31 shows the average measurements for light cement containing 3% BWOC ground cement class A and the calculated PV and YP values based on the Bingham plastic model are 36 cp and 79 lbf/(100 ft)^2, respectively. Table 32 presents the rheological measurements for light cement containing 5% BWOC ground cement class A. Table 33 shows the average measurements for light cement containing 5% BWOC ground cement class A and the calculated PV and YP values based on the Bingham plastic model are 38 cp and 80 lbf/(100ft)^2, respectively. The summary of all the rheology results for light cement with ground cement class A is shown in Figure 43. All the samples containing ground cement class A have slightly higher shear stress than the base case. The higher PV is probably related to the higher specific surface area of the NPs in the ground cement class A compared to the normal cement class A.

Table 34 presents the rheology results for the heavy cement base case. Table 35 shows the average measurements for heavy cement base case and the calculated PV and YP values based on the Bingham plastic model are 76 cp and 135 lbf/(100 ft)^2, respectively. Table 51 presents the rheology results for the heavy cement containing 1% BWOC ground cement class H. Table 52 shows the average measurements for heavy cement containing 1% BWOC ground cement class H and the calculated PV and YP values based on the Bingham plastic model are 39 cp and 223 lbf/(100 ft)^2, respectively. Table 53 presents the rheology results for the heavy cement containing 3% BWOC ground cement class H. Table 54 shows the average measurements for heavy cement containing 3% BWOC ground cement class H and the calculated PV and YP values based on the Bingham plastic model are 20 cp and 260 lbf/(100 ft)^2, respectively. Table 55 presents the rheology results for the heavy cement containing 5% BWOC ground cement class H. Table 56 shows the average measurements for heavy cement containing 5% BWOC ground cement class H and the calculated PV and YP values based on the Bingham plastic model are 25 cp and 251 lbf/(100 ft)^2, respectively. The summary of all the rheology results for heavy cement containing ground cement class H is shown in Figure 66. All the samples containing ground cement class H have higher shear stress than the base case.

Table 76 presents the rheology results for the heavy cement base case. Table 77 shows the average measurements for heavy cement base case and the calculated PV and YP values based on Bingham plastic model are 161 cp and 50 lbf/(100 ft)^2, respectively. Table 78 presents the rheological measurements for heavy cement containing 1% BWOC magnetite NPs. Table 79 shows the average measurements for heavy cement containing 1% BWOC magnetite NPs and the calculated PV and YP

values based on Bingham plastic model are 193 cp and 47 lbf/(100 ft)^2, respectively. Table 80 presents the rheological measurements for heavy cement containing 3% BWOC magnetite NPs. Table 81 shows the average measurements for heavy cement containing 3% BWOC magnetite NPs and the calculated PV and YP values based on the Bingham plastic model are 191 cp and 54 lbf/(100 ft)^2, respectively. Table 82 presents the rheological measurements for heavy cement containing 5% BWOC magnetite NPs. Table 83 shows the average measurements for heavy cement containing 5% BWOC magnetite NPs and the calculated PV and YP values based on the Bingham plastic model are 219 cp and 66 lbf/(100ft)^2, respectively. The summary of all the rheology results for heavy cement with magnetite NPs is shown in Figure 86. All the magnetite NPs have higher shear stress than the base case. That is probably related to the fact that NPs have a higher specific surface area compared to the normal barite and they are responsible for the possible higher plastic viscosity and yield point.

Table 84 presents the rheological measurements for heavy cement containing 1% BWOC barite NPs. Table 85 shows the average measurements for heavy cement containing 1% BWOC barite NPs and the calculated PV and YP values based on the Bingham plastic model are 212 cp and 53 lbf/(100 ft)^2, respectively. Table 86 presents the rheological measurements for heavy cement containing 3% BWOC barite NPs. Table 87 shows the average measurements for heavy cement containing 3% BWOC barite NPs and the calculated PV and YP values based on the Bingham plastic model are 204 cp and 46 lbf/(100 ft)^2, respectively. Table 88 presents the rheological measurements for heavy cement containing 5% BWOC barite NPs. Table 89 shows the average measurements for heavy cement containing 5% BWOC barite NPs and the calculated PV and YP values based on the Bingham plastic model are 168 cp and 66 lbf/(100 ft)^2, respectively. The summary of all the rheology results for heavy cement with barite NPs is shown in Figures 87. All the barite NPs have higher shear stress than the base case. Same as the discussion for the magnetite NPs, the higher PV probably is related to the higher specific surface area of the NPs compared to the normal barite.

Task 4 - Testing of Cement Thickening Time

The first phase of testing on the light cement was performed to determine the right concentration of the retarder additive at 160°F. It was decided not to use any retarder for tests being done on light cement at 100°F. The consistency tests on the light cement slurries were done at 3000 psi and the temperature 100°F and 160°F for the light cement. The thickening time tests for all of the heavy cement formulations were evaluated at 3000 psi and the temperature 160°F. Thickening time was determined when cement consistency reached 80 Bc.

Two sets of experiments were performed using bentonite NPs, the third set with ground cement class A and the fourth set with ground cement class H. The first set of tests was performed with the light cement control case and Bentonite NPs, temperature 100°F, and 3000 psi, as shown in the summarized results in Table 62 and Figures 45 and 46. The thickening time was slightly higher than the control case for 1% and 5% BWOC Bentonite NPs, while 3% BWOC Bentonite NPs had a slightly lower thickening time than the control case.

Another round of tests was performed using bentonite NPs and the results can be seen in Figures 77 and 78. The thickening time was lower than the control case for all the Bentonite NPs; it was 5.29% lower for

1% and 1.39% lower for 3% and 5% BWOC Bentonite NPs. The summary of results from Round 2 is outlined in Table 63.

The results from Round 1 and 2 were combined as shown in Table 64 and Figure 79. The thickening time was almost the same for all the tests. The percent change from the control case for all the Bentonite NPs was 1.11% lower for 1%, 1.39% lower for 3% BWOC Bentonite NPs, and 3.06% higher for 5% BWOC Bentonite NPs, as shown in Figure 80.

Figures 47 and 48 show the light base case with (1%, 3%, and 5% BWOC) light cement NPs. The thickening time was lower than the base case for all the light cement NPs. The results were almost the same for all the light cement NP concentrations: a little higher for the 5% BWOC light cement NP than the 1% and 5% BWOC light cement NPs.

Figures 49 and 50 show the tests with heavy base cases with (1%, 3%, and 5% BWOC) heavy cement NPs. The thickening time was much lower than the base case for all the heavy cement NPs.

Figures 88 and 89 show the first tests; these were done with a higher amount of seawater in the NPs than in the base case, Test 1. The thickening time was higher than the base case for all the barite NPs. The highest result was for the 1% BWOC barite NP and almost the same thickening time resulted for 3% and 5% BWOC barite NPs. Figures 90 and 91 show the repeated heavy base case containing 1%, 3%, and 5% BWOC barite NPs, but now with same amount of seawater in the NPs as in the final base case recipe, Test 2. The thickening time was higher than the base case for all the barite NPs. The results were almost the same for all the barite NP concentration: a little higher for 1% and 3% BWOC barite NP than 5% BWOC barite NP. Figures 92 and 93 show the tests with heavy base cases with (1%, 3% and 5% BWOC) magnetite NPs. The thickening time was higher than the base case for heavy cases containing 1%, 3% and 5% BWOC; magnetite NPs had lower thickening time than the base case.

Task 5 - Cement Core Tensile Bond Testing

Task 5 evaluates the tensile strength of the cement samples, as well as the bond strength between cement and a steel substrate. Tests were carried out according to the testing matrix established in Task 2. The following subsections outline the observations and results.

Tensile Strength

An initial sample set was generated for and tested after 30 days of curing, using the original set of curved plates. A core of each recipe was cut to create 3 Brazilian samples and ground to size using a rotary grinding table.

The samples underwent the same issues as outlined in the UCS section, and as such, the NP barite samples showed a negative correlation between tensile strength and NP barite concentration (see Figure 94). As seen in similar studies, there is an inversion to the improvement provided by the NP magnetite somewhere between 3-5% BWOC as shown in Figure 94. This translates to almost a 35% increase in tensile strength at 3% BWOC. The results are detailed in Table 36. The second round of Brazilian samples yielded results with similar coefficients of variation as the first. The tensile strengths, however, saw an overall increase across all of the samples, which was to be expected when the

procedural corrections were made. Their results are detailed in Table 37. In an effort to verify the data (specifically the trend seen in the NP magnetite samples), small batches of the 1% and 3% NP magnetite samples were created and cured using the same procedure as in the second round samples. The results of these tests showed a 23.9% and 27.5% increase in average tensile strength for the 1% and 3% concentrations, respectively. As of yet, it is unclear what caused this increase, however, the need to make another round of samples was clear. The results and comparison to the second round results are shown in Table 38.

The dramatic increase in strength observed with the spot check samples not only continued but also was seen to dramatically widen the gap between the new and old samples, and the increasing trend of strength with increasing concentrations was lost entirely. Increases in average tensile strength as high as 78.6% were seen compared to the results of the Round 2 samples as detailed in Table 39. The only change discovered between the two samples was the implementation of the new Brazilian apparatus; however, it only changed the arc length of the loaded area marginally, and thus is unlikely to be responsible for this change in results.

Initially, it was thought possible that the aluminum foil used to cover the samples may have leached into and contaminated the samples. This could have caused the formation of extra Ettringite, which, in the less dense base case would have filled in the spaces where the NPs would otherwise be; thus increasing the strength. A combination of scanning electron microscopy (SEM) and quick EDS (energy-dispersive X-ray spectroscopy) was used to test this theory against a base case core that had not been cured in the same manner. The results of this evaluation saw no change in the presence of aluminum in any of the samples and ruled out this possibility. There were, however, large pockets of barite found in the 1% and 3% NP magnetite samples, which indicates uneven mixing. These results are shown in Figures 55 and 56 as well as Tables 40 and 41. This could describe the trend seen for the NP magnetite samples, but the overall increase in strength is as of yet unclear.

Figure 53 shows that the tensile strength of the samples containing bentonite NPs was slightly higher compared to the control samples. The detailed results are presented in Table 90. Tensile strength was measured for the samples containing ground cement class A at different concentrations of 1%, 3%, and 5% BWOC. The results are depicted in Figure 54 and tabulated in Table 91. Similar to the UCS testing, evaluation of the tensile strength by way of the Brazilian testing method has undergone several iterations of testing. The samples for each round of testing were created using the cores made for the UCS testing. The results suggest that increasing the concentration of Bentonite NPs slightly improves the tensile strength while using ground cement class A does not have a significant effect on the cement tensile strength.

Tensile Bond Strength

A trial run of samples was created and tested using the heavy base case cement recipe and failed at the interface, just as predicted. Unfortunately, no solution was added to the top of the slurry after poring and it is likely that cement shrinkage caused the failure.

Another round of samples using the same recipe was created with the addition of NaOH hydration solution added on top of the slurry. These samples failed within the cement body just below the lowest

point of the anchor. It was theorized that the anchor set in the sample was not effectively distributing the load throughout the core and, therefore, a point of high loading was created. Several more sample sets were created with changes in the number and geometry of the washers; all resulted in the same failure. As a new approach, threaded connections were put together and attached to the cement core using a high strength, two-part epoxy. After the cores were allowed to harden for 48 hours, they were removed from the molds and the tops were planed using a tile saw. The excess cuttings were rinsed away using DI water followed by an acetone flush to remove residual water from the pores. Once the epoxy was applied according to the instructions, the samples were left half-submerged in DI water for an additional 24 hours. While this approach did not present the entire solution, there was no tensile failure seen within the cement body. Instead, the majority saw the failure of the epoxy, and two even partially failed at the cement-steel interface. This confirmed the concept, and the testing itself was further modified to reduce the stress accumulation at the epoxy interface.

By reducing the bonded area at the cement-steel interface as discussed in the previous subsection, the samples are more likely to fail at the desired plane as opposed to anywhere else. Once the procedure was established, a sample of each recipe was produced. Despite gentle handling, several of the samples failed at the bond when being removed from the molds for prep. To this end, two batches were created to get a data point for each recipe. Their results are shown in Table 42. Results suggest that as concentration increases, the tensile bond strength increases until it overcomes the tensile strength of the cement body. This type of failure is shown in Figure 57 and implies that when NPs are added, the bonding interface is no longer the point of concern when exposed to tensile loading at concentrations of 5% BWOC.

Shear Bond Strength

Though the shear bond strength results have seen a notable decrease in consistency compared to other tests, they have seen significantly more improvement when evaluating the base case samples and samples with NPs in them. In the base case, NP bentonite and NP cement class A & G were tested; an increase in the shear bond strength was only observed for NP bentonite and NP class G cement. Once fabricated, the apparatus was first tested to establish a procedure and explore the strength values we could expect to see. The samples were made using class A base case cement bonded to steel coins that had been washed with dish soap to remove any residual cuttings or machining oil. After a hydration period of roughly 48 hours, and with an added layer of the hydration solution NaOH, the samples were tested on 8/9/20. This resulted in two main observations. The first observation was that the cement did bond well with the steel substrate. While seemingly obvious, this justified the testing and allowed for a deeper dive into the mechanical response of the bond, which gave rise to the next observation. It was established that the strength of that bond was heavily dependent on the surface condition of the steel and cement itself. This was manifested as a hard division between completely bonded and partially bonded samples and could be easily recognized by analyzing the loading plots. Figure 59 shows the plot of a completely bonded sample, which is characterized by smooth continuous loading followed by rapid unloading. Figure 60 shows the same plot for a partially bonded sample. The partially bonded samples failed significantly earlier and under less load (~78-95% lower failure load). It was seen in the samples that were completely bonded to the steel that the physical surface condition plays a large part in determining the bond strength between steel and cement. Several iterative rounds of testing were completed to verify the repeatability of the testing. It was seen that because the bonding strength is so

contingent on the surface condition of the metal, any variance in preparation would greatly distort the results.

Three full batches of sample sets were prepared and tested using everything learned in the previous experiments from Years One and Two. New steel substrates were fabricated for the purpose to ensure each one had as close to the same surface to bond to as possible; as seen in Figures 62 and 64, a clear increase in shear bond strength is observed as the NP concentrations increase. For NP class A cement, at concentrations of 5% BWOC, a decrease in bond strength is observed. This is detailed in Table 46 and implies a broader range of bonding strength as the NPs concentrations increase. This is likely due to variations in the microstructure of the cement at the interacting plane, in that some samples see higher concentrations of NPs in the bonding zone than others. The variations in composition along this plane come as a result of NPs' tendency to clump during mixing, leaving a non-uniform slurry to be placed on the steel substrate. In practical applications, the use of a dispersant should correct these clumping issues and yield a more uniform bond with a steel substrate.

Task 6 – Cement Core Compressive Strength Testing

Task 6 evaluates the UCS as well as the shear bond strength between set cement and a steel substrate used to represent casing. Standard UCS testing according to ASTM C39 was utilized for the former while an apparatus and testing procedure were devised for the latter. The following subsections describe the progress made with each.

As part of Task 6, UCS testing was completed on samples containing 1%, 3%, and 5% bentonite NP, ground light cement, and ground heavy cement. To date, several iterations of the testing have been completed in an effort to improve the sample variation as well as clarify the effects of each NP additive.

All samples were made was to cover 30 days of curing time; while ambitious, the results proved to be less than desirable due to a handful of issues that are discussed in detail later in this section. Fortunately, this provided us with testing grounds for our procedure, while also confirming the idea that the addition of NP additives will increase the compressive strength even if the exact compressive strengths were not observed. As seen in Tables 43, 44, and 45, the presence of NP additives had a significant impact on the UCS values observed, albeit with very large variation between samples as well as a peculiar trend in the light cement NPs' and bentonite NPs' results.

The first round of samples was done using 1%, 3%, and 5% bentonite NPs (BWOC). The second round was done using 1%, 3%, and 5% light cement NPs (BWOC) and the third with 1%, 3%, and 5% heavy cement NPs (BWOC). The addition of NP bentonite caused a significant increase in compressive strength for samples containing 3% and 5% bentonite NPs (BWOC). The details of the first round of results are available in Table 43 and Figure 69. The second round of samples was an unsatisfactory declining trend with the addition of the light cement NPs. The presence of light cement NP additives showed a negative impact on the UCS values observed as observed in Table 44 and Figure 68. The ground cement class H, even at low concentrations of 1%, 3%, and 5% BWOC, caused an increase in compressive strength. This result, however, did not follow trends seen in previous experimental rounds. The details of the third round of results are available in Table 45 and Figure 70.

By utilizing the stress-strain data obtained in the UCS testing, Young's modulus was calculated according to ASTM C469. The stress-strain slope was taken at 35% and 45% of the critical load so that the stiffness was calculated while the sample was still under deformation. Figures 71, 72, and 73 show Young's modulus results for samples containing different concentrations of bentonite NPs, ground cement class A, and ground cement class H, respectively. Detailed results are shown in tables. Again, a similar trend of results can be observed where a decrease in stiffness is seen when a concentration of 5% (BWOC) is used for bentonite NP, light cement NP, and heavy cement NP. It is still unclear why there are such dramatic changes between the UCS, tensile strength, and Young's modulus values across the same recipes of cement. The reasoning for the dramatic decrease in strength is unclear, particularly for the case of all 5% NP samples.

Task 7 - Cement Setting Pressure and Strength Testing

As cement begins to set, a series of contractions and expansions are observed. The final set permeability of the cement is due to two cycles of expansion and contraction of the cement. Cement passes through two cycles of building its structure during the gelation period. The major causes of the early microfractures are the incomplete cement–water reaction, the low compressive strength of the set cement, and the sudden change in the hydrostatic pressure as the cement changes its phase from liquid-state to solid-state. The first cycle of pressure change is due to the cement's thixotropic behavior (shear-thinning over time). In the second cycle, the cement is more prone to microfractures.

Figure 74 shows the change in applied pressure of 250 psi over time for class G cement at three different densities. Temperature is kept constant throughout the experiment. The highest change in applied pressure is observed at approximately 278 psi for a 16.59 ppg class G cement.

In a separate group of experiments, an initial pressure is applied and the change in pressure with time is observed. Table 61 shows the contraction cycles of ten cement slurry samples at a given applied pressure and temperature. As the applied pressure is decreased, the total contraction increases. This data is also plotted in Figure 76 where the final cement volume contraction at an applied pressure of 250 psi is 6.13cc/420cc. It was found that the real cause of the expansion cycles is due to the cement reacting with water before it sets. Inadequate reaction with water will then contribute to the formation of microcracks. A correlation was created from the presented data and Equation 9 was used to calculate the setting pressure for class G cement at any given hydrostatic pressure. Contraction and setting pressure values from 500 psi and below were calculated using Equation 9.

Task 8 - Cement Core Permeability Testing

After a cement slurry sets and becomes solid, its physical properties such as porosity and permeability need to be evaluated. Cement sheaths show none or very small permeability that is crucial for zonal isolation. Depending on the cement composition, their absolute porosity can vary in a wider range. For each case, four samples were prepared and tested. Figure 80 shows the prepared samples for the porosity and permeability tests. Table 65 shows the porosity measurements and results for light cement samples. Table 66 shows the porosity measurements and results for heavy cement samples. Permeability was measured using the PERG-200 gas permeameter, and all the samples show zero permeability. However, PERG-200 can only measure flow rate as low as 0.01 ml that can result in

permeability in order of micro Darcy, so permeability of the samples may fall in the nano-Darcy range. Figure 81 shows the apparatus PERG-200.

Task 9 - Model Validity of the Correlation Model

The mechanical properties of the cement mixtures determined from the lab experiments (setting stress, Young's modulus, tensile strength, UCS, shear, and tensile bonding parameters) are used in the FEA model to predict cement sheath integrity issues.

A case study was performed on a GoM well (API 427094116400). The drilling report and log data for this well were purchased such that the model could replicate the wellbore. The information used from the reports includes the wellbore dimensions, depths of the casing strings, pore pressure gradients, mud weight gradients, formation fracture pressure gradients, BHP gradient, and the cement slurry design.

The FEA model was created and simulated using ANSYS™ 19.1. The model is a static structural 3D poro-elastic model that uses the traction separation law to model the debonding of the casing/cement and cement/rock formation interfaces. The 3D model uses 25,552 CPT216 quadratic brick elements in which the element size in the interface zones is based on the Turon et al. (2006) approach which uses the element length determined by Hillerborg et al. (1976) and further divides the element length by three to ensure the element size is fine enough to capture the delamination in the cohesive zones. Further refinement of the mesh was conducted using a mesh sensitivity analysis. The maximum micro annuli gap width versus mesh density was analyzed to determine the optimal mesh density.

Figure 81 shows a 2D (left) and 3D (right) cutaway of the model showing the three different materials within it (casing, cement, and rock formation). The 3D model dimensions are 1.5 m in the x and y (i.e. horizontal) directions and 0.05 m in the z (i.e. vertical) direction. A model with a vertical thickness of 0.05 m has 140,440 nodes with a computational run time of approximately 10 minutes. Thicker geometries of 0.5 m and 1.0 m would have 1,110,504 and 2,189,216 nodes, respectively, with at least 12-hour run times for a single simulation. The resulting micro annuli is the same magnitude between 0.05 m and thicker models. Therefore, 0.05 m thickness was chosen. 3D geometry is chosen such that plain-strain assumptions do not have to be made for the model.

The model geometry is determined based on the Kirsch analytical solution such that the ratio of the model size and the wellbore diameter is greater than three to represent a good approximation to the infinite case and to prevent unintentional boundary effects from the thermal distribution throughout the model (Jaeger et al. 2007; Fjaer et al. 2008; Li and Nygaard 2017). The model is constrained using frictionless supports on the top, bottom, and four faces to represent infinite supports. The dimensions of the borehole, casing thickness, and cement sheath thickness are based on the case study well and are shown in Table 67.

The FEM replicates the well's lifecycle similar to Gray et al. (2009) and Weideman and Nygaard (2014). The staged approach uses the property of superposition to build the model's initial conditions before the next load step is implemented. The advantage of performing a staged approach is that the stress and deformation changes can be monitored in each load step. The load steps used were modified from Weideman (2014) and Wise et al. (2019).

The load steps are:

- Step 1: The model is loaded with horizontal (σ_H and σ_h) and vertical (σ_v) in-situ stresses.
- Step 2: The borehole is drilled, and a fluid weight (mud weight, MW) is applied to the rock formation.
  Step 3: The casing is added to the borehole with the fluid weight being applied to the inner and outer surfaces of the casing and the borehole.
- Step 4: This step represents the completion of the wellbore and has two parts:
  - The cement slurry is pumped into the well. A hydrostatic pressure caused by the cement slurry is applied to the outer surface of the casing and the borehole while the inner casing surface has the fluid weight pressure.
  - Cement hydrates and hardens. The cement elements are added to the model with framework stress, pore pressure, and zero shrinkage, assuming the cement is fully bonded to the rock formation and outer casing surface. The hardened cement is inserted with zero deformation but with framework stress in all three principal directions equivalent to the hydrostatic pressure. The fluid weight pressure is still applied to the inner surface of the casing.
- Step 5: The wellbore is producing. The fluid weight pressure is removed from the inner surface of the casing and replaced with the production pressure referenced as the ICP.

At the end of the cement hydration, the P_P of the cement is assumed to be equal to the P_P of the surrounding rock formation (Li and Nygaard 2017; Zhang et al. 2017; Gray et al. 2009). The σ_C is determined from the experiments. The mechanical properties of the cement were determined from the experiments in this project.

A parametric analysis of parameters with uncertainties (in-situ stresses, cement mechanical and thermal properties, rock mechanical and thermal properties, and softening traction-separation law properties) as well as parameters that are easily changeable from an engineering perspective (wellbore dimensions) will be been simulated. The upper and lower bounds of the sensitivity analysis are shown in Table 68. The change in ICP (ΔP) has been shown to cause micro annuli gaps, but numerous parameters within a wellbore can affect the magnitude and initiation of such gaps. The parameters listed in Section 2 are tested with different ΔP's to determine which parameters are contributing factors to micro annuli initiation and magnitude. The ΔP is a reduction in pressure of 29%, 44%, 50%, and 67%. For a reduction of 29%, nanometer gaps were created from the base case curves and micron gaps were initiated at a 44% reduction. A reduction of 50% resulted in micro annuli of approximately. A reduction of 67% resulted in micro annuli of approximately 30 µm. The results for all four percentage reductions are shown in Figure 83 for the maximum and minimum micro annuli gap sizes.

For a reduction of 29%, nanometer-sized gaps occur in the base well, but variations of E_cement, setting stress of the cement (σ_cement), Hole Size, and casing thickness (ω_casing) cause micron-sized gaps to occur. The micro annuli range from a size of 0 µm (no gap/nanometer-size gap) to a maximum gap of 7.2 µm, implying that these four parameters can cause the gap initiation to decrease from 43% to 29% (i.e. lower ΔP). An interesting observation is that the change in hole size affects the gaps created by pressure. A larger hole size results in gaps with a 29% ΔP.

The micro annuli gaps for a 44% reduction in ΔP range in size from 0 μm to 51.2 μm. For the base wellbore, ΔP resulted in a gap of 1.25 μm and variations of τ^o, E_rock, E_cement, v_cement, σ_cement, Hole Size, ω_cement, and ω_casing caused changes in the base gap width. One observation with the 44% reduction is that many of the wellbore parameters could be altered such that the base gaps for ΔP (1.25 μm) can be reduced down to no gap (0 μm). Another observation is that the same trend occurs with the 44% reduction as with the 29% reduction. The hole size variations have effects on gap widths. A similar trend occurs for the casing thickness, except that thicker casings have smaller gaps for ΔP.

The micro annuli gaps for a 50% reduction in ΔP range from a size of 0 μm to 72.2 μm. For the base case with a reduction of 50%, ΔP resulted in a gap of 9.79 μm. Every parameter that caused variations in the base gaps with ΔP 44% reduction caused variations in gap widths with 50% reduction. As with the 44% reduction, ω_casing and Hole Size created large variations in the gap widths for ΔP. With a reduction of 50% in ΔP, three of the parameters can be altered such that the base case gap can be reduced down to no gap (0 μm). The parameters that can be altered such that there is not a gap are ω_casing, Hole Size, and E_cement. All three parameters can eliminate the gap for ΔP, but only E_cement significantly reduced the gap for ΔT (0.1μm).

The micro annuli gaps for a 67% reduction in ΔP range in size from 1.3 μm to 125.2 μm. For the base case with a reduction of 67%, ΔP resulted in a gap of 31.13 μm. Similar to the 50% and 44% reduction, ω_casing and Hole Size have the largest variation in gap width for ΔP. Based on the results from the 67% ΔP reduction, changes in pressure with respect to wellbore parameters are critical.

The results of the parametric analysis are sorted based on their percent change of the maximum gap width (%MGW) from the base micro annuli gap in terms of 1st, 2nd, and 3rd Order Parameters as shown in Table 69. 3rd Order Parameters are defined as parameters with their %MGW less than 10%. 3rd Order Parameters have little to no effect on the development of the gap magnitude and therefore are not critical inputs into the well life cycle model. 2nd Order Parameters are defined as parameters with their %MGW larger than 10% but less than 100%. These parameters have some effect on the gap with a magnitude, but are not critical. Finally, 1st Order Parameters are defined as parameters that have their %MGW larger than 100%. These input parameters (Hole Size and ω_casing) have the largest impact on the gap width development. From the results in Table 69, wellbore cement mechanical properties (setting stress, Young's modulus, bonding properties) are not as critical as the wellbore dimensions and casing thickness.

Summary Section

- **Task 1**: A "well life cycle" FEM was developed; it showed that the cement mechanical properties have little effect on cement sheath stress development, whereas the cement hydration properties had the most significant effect.
- **Task 2**: Test matrices, NP generation, test methodologies, and cement slurry mixture were determined.
- **Task 3**: The addition of the NPs increased the fluid loss for light cement while they had little effect on the heavy cement. The addition of the NPs resulted in increased shear stress from the rheology testing.
- **Task 4**: The addition of the NPs shortened the thickening time than the base cement mixture.

- **Task 5**: The shear bonding of the cement to the steel was improved with the addition of the NPs.
- **Task 6**: Compressive and tensile strength of the cement with NPs added had minimal change in values from the base case mixture.
- **Task 7**: A correlation for determining the setting stress given an applied pressure was determined.
- **Task 8**: The permeability of the cement mixtures was unable to be quantified (due to instrument resolution). However, the permeability is less than micro Darcy (instrument limit).
- **Task 9**: Updated cement properties were used in the "well life cycle" FEM that included debonding gaps. The results showed that the wellbore dimensions had the largest effect on gap size, while the cement mechanical properties were not as critical.

Implications

The most remarkable accomplishment of this project is the quantification of the benefit of using nano-sized materials to enhance mechanical properties of wellbore cements.

Education and Training

Number of students, postdoctoral scholars, or educational components involved in the project:

- K-12 students: 0
- Undergraduate students: 0
- Graduate students: 5
- Postdoctoral scholars: 0
- Citizen Scientists: 0
- Other Trainees: 0

IV. DATA AND INFORMATION PRODUCTS

This project produced data and information products of the following types:

- Data

DATA

Data Management Report:

See attached Data Management Report.

Relationships Between Data Sets:

Different datasets were collected for different cement mixtures. Each set of cement mixtures has a control case wherefrom each dataset varies the concentration of NPs in both the light and heavy cement case. Raw data from the finite element life of well models is included.

Additional Documentation Produced to Describe Data:

The data collected is based on the experimental procedures described in the progress reports and the publications from this work.

Other Activities to Make Data Discoverable:
All relevant data has been (or will be) published in technical conference papers.

Sensitive, Confidential, or Proprietary Data:
N/A

INFORMATION PRODUCTS

Information Products Report:
See attached Information Products Report.

Citations for Project Publications, Reports and Monographs, and Workshop and Conference Proceedings:
N/A

Websites and Data Portals:
GRIIDC Data Portal: https://grp.griidc.org/research-group/about/908

Additional Documentation Produced to Describe Information Products:
N/A

Other Activities to Make Information Products Accessible and Discoverable:
N/A

Confidential, Proprietary, Specially Licensed Information Products:
N/A

V. PUBLIC INTEREST AND COMMUNICATIONS

Most Exciting or Surprising Thing Learned During the Project
Cement is an extremely complex material wherein small changes in one additive can give large effects on the behavior of the cement properties. Cement thickening time depends on both chemical reactions and water requirement. To establish the correct setting time for the cement to thicken, multiple hort with different water contents, retarders and or extenders should match with the cement and additives on the filed corresponding pressure and temperature.

Outcomes Achieved During the Project
Short term outcomes include multiple publications, oral presentations, and collaborations with colleagues. From the project itself, cement mechanical properties determined through the lab experiments have been of use in the FEMs.

Communications, Outreach, and Dissemination Activities of Project
Jarrett Wise's undergraduate college wrote an article about his ongoing research in cement sheath integrity that is partially funded by the NAS-GRP grant. (Link: https://www.hastings.edu/success-stories/wise14-studies-potential-leakage-pathways-in-abandoned-oil-wells-in-published-research-article)

Tables

Table 1: Base case parameters for the three wells in the Eugene Island Official Protraction Diagram and the source of their values.

Parameter	Well			
	Shallow	Medium	Deep	
TVD (m)	797	3,014	6,028	1
Simulation Depth (m)	468	2,697	4,317	*
Hole Size (cm)	44.45	25.08	31.12	1
Casing OD (cm)	33.97	17.78	24.45	1
Casing ID (cm)	32.04	15.94	21.99	1
v Steel	0.30	0.30	0.30	2
E Steel (GPa)	200	200	200	3
Mud Weight (g/cc)	1.13	1.41	1.29	1
ICP (MPa)	5.18	25.6	38.23	1
σ_H (MPa)	7.74	49.49	84.89	4
σ_h (MPa)	6.38	40.76	69.91	4
σ_v (MPa)	9.11	58.23	99.88	4
Pp Rock (g/cc)	0.99	1.35	1.18	1
v Rock	0.27	0.27	0.27	3
E Rock (GPa)	25	25	25	2
Pp Cement (g/cc)	0.99	1.35	1.18	*
v Cement	0.25	0.25	0.25	2
E Cement (GPa)	10	10	10	2
Cement Slurry (g/cc)	1.22	1.53	1.55	1
Cement Stress (MPa)	5.62	40.43	65.61	*

[1]Log, [2]Zhang et al. (2016), [3]Weideman (2014), [4]Finkbeiner et al. (1996)

Table 2: High and low values for the parametric study. These values apply for all three well depth parameters.

Parameter	Low	High
Cement Stress (MPa)	MW	P_{Frac}
Pp Cement (g/cc)	0	P_{Frac}
Isotropic Horizontal Stress Variation	$\sigma_v = \sigma_{v,\,base}$ $\sigma_H = 0.7 \times \sigma_{v,\,base}$ $\sigma_h = \sigma_{H,\,base}$	$\sigma_v = \sigma_{v,\,base}$ $\sigma_H = 1 \times \sigma_{v,\,base}$ $\sigma_h = \sigma_{H,\,base}$
Anisotropic Stress Variation	$\sigma_v = \sigma_{v,\,base}$ $\sigma_H = 0.7 \times \sigma_{v,\,base}$ $\sigma_h = 0.7 \times \sigma_{H,\,base}$	$\sigma_v = \sigma_{v,\,base}$ $\sigma_H = 1 \times \sigma_{v,\,base}$ $\sigma_h = 0.7 \times \sigma_{H,\,base}$
Vertical Stress Variation	$\sigma_v = -5\% \times \sigma_{v,\,base}$ $\sigma_H = \sigma_{h,\,base}$ $\sigma_h = 0.7 \times \sigma_{v,\,base}$	$\sigma_v = +5\% \times \sigma_{v,\,base}$ $\sigma_H = \sigma_{h,\,base}$ $\sigma_h = 0.7 \times \sigma_{v,\,base}$

Table 3: Cement sheath effective stress results for the base case parameters for the three case studies. The shallow and deep well are normalized to the medium well.

Effective Interface Stress	Well: Shallow (%)	Well: Medium (MPa)	Well: Deep (%)
Hoop Stress Casing/Cement	-84%	5.70	167%
Hoop Stress Cement/Rock	-78%	3.70	242%
Radial Stress Casing/Cement	-121%	-2.75	-59%
Radial Stress Cement/Rock	-174%	-0.84	-390%

Compressive	Tensile

Table 4: Seawater Requirements for additives after the "Dime tests" for cement mixing.

Component	Recorded Hydration
Seawater requirement table	(g/g)
Portland Cement Class A	0.4082
Portland Cement Class H	0.3960
Barite	0.2604
Bentonite	3.8462
HEC	285.7143
NPs Barite	1.8018
NPs Magnetite	5.4795

Table 5: The initial formulation of the heavy base case of cement.

Comp	Mass in solution (g)
Seawater	362.68
Class H	850.00
Barite	100.00
HEC	4.25
D-air 5000	1.28

Table 6: The initial formulation of the light base case of cement.

Comp	Mass in solution (g)
Seawater	478.34
Class A	550.00
Bentonite	66.00
HEC	2.75
D-air 5000	0.83

Table 7: Heavy base case final recipe with barite nanoparticles.

HEAVY Cement	Base Case	1% Barite NP	3% Barite NP	5% Barite NP
Comp	Mass (g)	Mass (g)	Mass (g)	Mass (g)
Seawater	362.68	362.68	362.68	362.68
Class H	850.00	850.00	850.00	850.00
Barite	100.00	91.50	74.50	57.50
Barite NP	0.00	8.50	25.50	42.50
Magnetite NP	0.00	0.00	0.00	0.00
HEC	4.25	4.25	4.25	4.25
D-air 5000, 0.15%	1.28	1.28	1.28	1.28
Boric Acid, 0.4%	3.40	3.40	3.40	3.40

Table 8: Heavy base case final recipe with magnetite nanoparticles.

HEAVY Cement	Base Case	1% BWOC Magnetite NP	3% BWOC Magnetite NP	5% BWOC Magnetite NP
Comp	Mass (g)	Mass (g)	Mass (g)	Mass (g)
Seawater	362.68	362.68	362.68	362.68
Cement Class H	850.00	850.00	850.00	850.00
Barite	100.00	91.50	74.50	57.50
Barite NP	0.00	0.00	0.00	0.00
Magnetite NP	0.00	8.50	25.50	42.50
HEC	4.25	4.25	4.25	4.25
D-air 5000, 0.15%	1.28	1.28	1.28	1.28
Boric Acid, 0.4%	3.40	3.40	3.40	3.40

Table 9: Light base case final recipe with bentonite nanoparticles.

LIGHT Cement	Base Case	1% Bentonite NP	3% Bentonite NP	5% Bentonite NP
Comp	Mass (g)	Mass (g)	Mass (g)	Mass (g)
Seawater	478.34	478.34	478.34	478.34
Class A	550.00	550.00	550.00	550.00
Bentonite	66.00	60.50	49.50	38.50
Bentonite NP	0.00	5.50	16.50	27.50
HEC	2.75	2.75	2.75	2.75
D-air 5000, 0.15%	0.83	0.83	0.83	0.83
Boric Acid, 0.6%	3.30	3.30	3.30	3.30

Table 10: Testing matrix for the heavy cement cases.

	Base case	Heavy Barite NPs (BWOC)			Magnetite NPs (BWOC)			Cement H NPs (BWOC)		
NPs Concentration	0	1%	3%	5%	1%	3%	5%	1%	3%	5%
# of consistency tests	3	3	3	3	3	3	3	3	3	3
# of filtration tests	3	3	3	3	3	3	3	3	3	3
# of rheology tests	3	3	3	3	3	3	3	3	3	3
# of UCS tests	4	4	4	4	4	4	4	4	4	4
# of Brazilian tests	6	6	6	6	6	6	6	6	6	6
# of Shear Bond tests	8	8	8	8	8	8	8	8	8	8
# of Tensile Bond tests	2	2	2	2	2	2	2	2	2	2

Table 11: Testing matrices for the light cement cases.

Light										
	Base case	Bentonite NPs (BWOC)			Silica NPs (BWOC)			Cement A NPs (BWOC)		
NPs Concentration	0	1%	3%	5%	1%	3%	5%	1%	3%	5%
# of consistency tests	3	3	3	3	3	3	3	3	3	3
# of filtration tests	3	3	3	3	3	3	3	3	3	3
# of rheology tests	3	3	3	3	3	3	3	3	3	3
# of UCS tests	4	4	4	4	4	4	4	4	4	4
# of Brazilian tests	6	6	6	6	6	6	6	6	6	6
# of Shear Bond tests	8	8	8	8	8	8	8	8	8	8
# of Tensile Bond tests	2	2	2	2	2	2	2	2	2	2

Table 12: Fluid loss results for light cement base case.

	Base Case	Base Case	Base Case	Base Case	Base Case	Mean
Date	2/11/2020	2/11/2020	2/12/2020	2/14/2020	2/18/2020	
Temp	Slurrytemp 100F	Slurrytemp 100F	Slurrytemp 100F	Slurrytemp 100F	Slurrytemp 100F	
Min	ml	ml	ml	ml	ml	ml
0	0	0	0	0	0	0.0
1	34	34	31	30	32	32.2
2	45	46	41	45	46	44.6
3	49	55	50	53	56	52.6
4	50	58	53	54	57	54.4
5	52	61	55	56	60	56.8
6	52	61	55	56	60	56.8

Table 13: Fluid loss results for light cement, 1% BWOC Bentonite nanoparticles.

1%BWOCbentNP	1%BWOCbentNP	1%BWOCbentNP	1%BWOCbentNP	Mean
2/10/2020	2/10/2020	2/14/2020	2/18/2020	
Slurrytemp 100F	Slurrytemp 100F	Slurrytemp 100F	Slurrytemp 100F	
ml	ml	ml	ml	ml
0	0	0	0	0.0
32	34	28	26	30.0
46	47	41	39	43.3
52	50	49	47	49.5
54	53	50	48	51.3
54	53	52	51	52.5
54	53	54	51	53.0

Table 14: Fluid loss results for heavy cement, 3% BWOC magnetite nanoparticles.

	3% BWOC bentNP	3% BWOC bentNP	3% BWOC bentNP	3% BWOC bentNP	3% BWOC bentNP	3% BWOC bentNP	Mean
Date	2/12/2020	2/12/2020	1/13/2020	1/14/2020	1/18/2020	6/8/2020	
Temp	Slurrytemp 100F	Slurrytemp 100F	Slurrytemp 100F	Slurrytemp 100F	Slurrytemp 100F	Slurrytemp 100F	
Min	ml	ml	ml	ml	ml		ml
0	0	0	0	0	0	0	0.0
1	34	30	31	28	29	26	29.7
2	46	43	44	40	41	36	41.7
3	51.5	52	51	50	52	44	50.1
4	53	54.5	51	53	60	50	53.6
5	53	54.5	51.5	55.5	63	56	55.6
6	53	54.5	51.5	55.5	63	58.5	56.0
7	53	54.5	51.5	55.5	63	60.5	56.3

Table 15: Fluid loss results for heavy cement, 5% BWOC bentonite nanoparticles.

	5% BWOC bentNP	5% BWOC bentNP	5% BWOC bentNP	5% BWOC bentNP	5% BWOC bentNP	Mean
Date	2/13/2020	2/13/2020	2/14/2020	2/18/2020	2/19/2020	
Temp	Slurrytemp 100F	Slurrytemp 100F	Slurrytemp 100F	Slurrytemp 100F	Slurrytemp 100F	
Min	ml	ml	ml	ml	ml	ml
0	0	0	0	0	0	0.0
1	29	28	31	23	28	27.8
2	42	40	44	31	42	39.8
3	51	50.5	46	45	53	49.1
4	54.5	55.5	48	54	54	53.2
5	54.5	55.5	48	57	56	54.2
6	54.5	55.5	48	57	56	54.2

Table 16: Fluid loss results for light cement, 1% BWOC light cement nanoparticles.

Light	1% BWOC light cement NP	1% BWOC light cement NP	1% BWOC light cement NP	1% BWOC light cement NP	
Date	7/14/2020	7/16/2020	7/25/2020	7/24/20	Mean
Temp	100	100	100	100	
Min	mL	mL	mL	mL	mL
1	31	27	23	23	26.0
2	43	38	32	32	36.3
3	53	46	40	39	44.5
4	54	55	48	46	50.8
5	55	55.5	54	52	54.1
6	55.5	56	55	57	55.9
7	56	57	57	59	57.3

Table 17: Fluid loss results for light cement, 3% BWOC light cement nanoparticles.

Light	3% BWOC light cement NP	3% BWOC light cement NP	3% BWOC light cement NP	3% BWOC light cement NP	
Date	7/15/2020	7/23/2020	7/23/2020	7/24/20	Mean
Temp	100	100	100	100	
Min	mL	mL	mL	mL	mL
1	26	27	23	22	24.5
2	37	36	34	32	34.8
3	45	44	41	40	42.5
4	53	51	48	47	49.8
5	60	58	54	53	56.3
6	61	59	55	56	57.8
7	62	61	56	57	59.0

Table 18: Fluid loss results for light cement, 5% BWOC light cement nanoparticles.

Light	5% BWOC light cement NP	5% BWOC light cement NP	5% BWOC light cement NP	5% BWOC light cement NP	
Date	7/16/2020	7/23/2020	7/23/20	7/24/20	Avg
Temp	100	100	100	100	
Min	mL	mL	mL	mL	mL
1	26	26	24	22	24.5
2	36	34	34	31	33.8
3	43	42	42	38	41.3
4	49	49	50	44	48.0
5	55	55	54	49	53.3
6	56	58	55	54	55.8
7	57	59	56	58	57.5

Table 19: Fluid loss results for light cement base case.

Recipe	Base Case	Base Case	Base Case	Base Case	MEAN
Date	7/15/19	7/28/19	7/29/19	7/31/19	
Temp	100	100	100	100	
Min	ml	ml	ml	ml	ml
0	0	0	0	0	0.00
1	43	32	31.5	30	34.13
2	52	48.5	48.5	47	49.00
3	56	60.5	60	57.5	58.50
4	59	62	63.5	63.5	62.00
5	62	63	64	66.5	63.88

Table 20: Rheology results for light cement base case.

		Sample #		
Base Case	1	2	3	4
Temp ˚F	100	100	100	100
Date	2/11/2020	2/11/2020	2/14/2020	2/18/2020
% BWOC	0	0	0	0
600	145	148	143	146
300	105	105	101	104
200	90	89	85	89
100	70	70	68	73
6	42	41	40	44
3	32	32	30	34
3 (10m)	32	30	32	38

Table 21: Summarized Rheology results for light cement base case.

Reading		Bingham	Newtonian	μp	τy
Mean	Shear stress	Shear rate	Shear rate	Plastic viscosity	Yield point
0	(lbf/100ft^2)	(1/s)	(1/s)	(cp)	(lbf/100ft^2)
146	155	1070	1022	41.8	62.0
104	110	559	511		
88	94	388	341		
70	75	218	170		
42	44	58	10		
32	34	53	5		
33					

Table 22: Rheology results for light cement containing 1% BWOC bentonite nanoparticles.

	Sample #					
1% Bent NP	1	2	3	4	5	6
Temp ˚F	100F sure	100F sure	100F sure	100F sure	100F sure	100F
Date	2/12/2020	2/12/2020	2/14/2020	2/14/2020	2/18/2020	7/17/2020
% BWOC	1	1	1	1	1	1
600	138	140	153	138	139	145
300	98	99	106	98	99	107
200	85	85	91	84	86	93
100	69	69	73	68	71	75
6	45	42	46	42	45	44
3	34	32	37	33	37	31
3 (10m)	34	32	33	32	34	29

Table 23: Summarized Rheology results for light cement base case with 1% BWOC bentonite nanoparticles.

Reading		Bingham	Newtonian	μp	τy
Mean	Shear stress	Shear rate	Shear rate	Plastic viscosity	Yield point
	(lbf/100ft^2)	(1/s)	(1/s)	(cp)	(lbf/100ft^2)
142	151	1069	1022	41.0	60.2
101	108	558	511		
87	93	388	341		
71	75	218	170		
44	47	58	10		
34	36	52	5		
32					

Table 24: Rheology results for light cement base case with 3% BWOC bentonite nanoparticles.

	Sample #					
3% Bent NP	1	2	3	4	5	6
Temp ˚F	100F sure	100F sure	100F sure	100F sure	100F sure	100F
Date	2/12/2020	2/14/2020	2/14/2020	2/18/2020	2/19/2020	7/17/2020
% BWOC	3	3	3	3	3	3
600	149	145	144	143	151	157
300	112	101	101	102	109	119
200	95	85	86	89	94	102
100	77	71	72	74	71	88
6	49	45	46	46	55	55
3	37	31	34	38	40	33
3 (10m)	35	31	35	35	38	29

Table 25: Summarized Rheology results for heavy cement base case with 3% BWOC bentonite nanoparticles.

Reading		Bingham	Newtonian	μp	τy
Mean	Shear stress	Shear rate	Shear rate	Plastic viscosity	Yield point
	(lbf/100ft^2)	(1/s)	(1/s)	(cp)	(lbf/100ft^2)
148	158	1074	1022	40.8	66.5
107	114	563	511		
92	98	393	341		
76	80	223	170		
49	53	63	10		
36	38	58	5		
34					

Table 26: Rheology results for light cement with 5% BWOC bentonite nanoparticles.

	Sample #					
5% Bent NP	1	2	3	4	5	6
Temp ˚F	100F sure	100F sure	100F sure	100F sure	100F sure	100F
Date	2/13/2020	2/13/2020	2/14/2020	2/14/2020	2/18/2020	7/17/2020
% BWOC	5	5	5	5	5	5
600	150	130	151	152	142	132
300	104	96	106	108	105	114
200	88	80	92	93	92	95
100	73	66	76	76	79	79
6	49	45	51	47	57	49
3	42	35	36	35	45	33
3 (10m)	35	35	36	37	38	27

Table 27: Summarized Rheology results for light cement with 5% BWOC bentonite nanoparticles.

Reading		Bingham	Newtonian	μp	τy
Mean	Shear stress	Shear rate	Shear rate	Plastic viscosity	Yield point
	(lbf/100ft^2)	(1/s)	(1/s)	(cp)	(lbf/100ft^2)
143	152	1074	1022	37.3	68.2
106	112	563	511		
90	96	393	341		
75	80	223	170		
50	53	63	10		
38	40	58	5		
35					

Table 28: Rheology results for light cement with 1% BWOC light cement nanoparticles.

	Sample #			
1% NP	1	2	3	4
˚F	100	100	100	100
Date	7/14/2020	7/16/2020	7/23/2020	7/24/2020
% BWOC	1	1	1	1
600	144	138	160	150
300	109	115	118	121
200	97	93	99	97
100	85	75	83	81
6	38	43	47	45
3	23	30	30	28
3 (10m)	17	31	28	23

Table 29: Summarized Rheology results for light cement with 1% BWOC light cement nanoparticles.

	Shear	Bingham	Newtonian	μp	τy
Mean	Stress	Shear rate	Shear rate	Plastic viscosity	Yield point
	(lbf/100ft^2)	(1/s)	(1/s)	(cp)	(lbf/100ft^2)
148	158	1070	1022	32	84
116	123	559	511		
97	103	388	341		
81	86	218	170		
43	46	58	10		
28	30	53	5		
25					

Table 30: Rheology results for light cement with 3% BWOC light cement nanoparticles.

	Sample #			
3% NP	1	2	3	4
˚F	100	100	100	100
Date	7/15/2020	7/23/2020	7/23/2020	7/24/2020
% BWOC	3	3	3	3
600	135	165	144	154
300	108	117	110	121
200	92	99	98	107
100	74	82	83	91
6	45	48	48	54
3	31	32	31	35
3 (10m)	31	30	32	36

Table 31: Summarized Rheology results for light cement with 3% BWOC light cement nanoparticles.

	Shear	Bingham	Newtonian	μp	τy
Mean	Stress	Shear rate	Shear rate	Plastic viscosity	Yield point
	(lbf/100ft^2)	(1/s)	(1/s)	(cp)	(lbf/100ft^2)
150	159	1070	1022	36	79
114	121	559	511		
99	105	388	341		
83	88	218	170		
49	52	58	10		
32	34	53	5		
32					

Table 32: Rheology results for light cement with 5% BWOC light cement nanoparticles.

	Sample #			
5% NP	1	2	3	4
˚F	100	100	100	100
Date	7/16/2020	7/23/2020	7/23/2020	7/24/2020
% BWOC	5	5	5	5
600	165	155	147	155
300	118	121	111	121
200	101	98	101	101
100	85	81	83	84
6	58	49	50	46
3	35	31	31	30
3 (10m)	31	23	32	30

Table 33: Summarized Rheology results for light cement with 5% BWOC light cement nanoparticles.

	Shear	Bingham	Newtonian	μp	τy
Mean	Stress	Shear rate	Shear rate	Plastic viscosity	Yield point
	(lbf/100ft^2)	(1/s)	(1/s)	(cp)	(lbf/100ft^2)
156	166	1070	1022	38	80
118	125	559	511		
100	107	388	341		
83	89	218	170		
51	54	58	10		
32	34	53	5		
29					

Table 34: Rheology results for heavy cement base case.

	Sample #			
Base Case	1	2	3	4
Temp ˚F	150	150	150	150
Date	7/15/2019	7/15/2019	7/17/2019	7/24/2019
% BWOC	0	0	0	0
600	285	287	300+	300+
300	230	177	245	190
200	187	134	198	143
100	124	88	137	92
6	103	35	53	36
3	30	29	38	28
3 (10m)	48	25	45	28

Table 35: Summarized Rheology results for heavy cement base case.

	Shear	Bingham	Newtonian	μp	τy
Mean	Stress	Shear rate	Shear rate	Plastic viscosity	Yield point
	(lbf/100ft^2)	(1/s)	(1/s)	(cp)	(lbf/100ft^2)
286	305	1079	1022	76	135
211	224	569	511		
166	176	398	341		
110	117	228	170		
57	60	68	10		
31	33	63	5		
37					

Table 36: Brazilian testing results from the first round of samples. Each recipe tested three samples.

	Mean Tensile Strength (psi)	CV (%)	Change from Base Case (%)
Base Case	334.1	6.9%	-
1% NP Barite	438.7	9.2%	27.1%
3% NP Barite	360.8	24.3%	7.7%
5% NP Barite	325.1	6.0%	-2.7%
1% NP Magnetite	408.6	1.6%	20.1%
3%NP Magnetite	466.7	8.1%	33.1%
5% NP Magnetite	430.4	15.7%	25.2%

Table 37: Brazilian testing results from the second round of samples. Each recipe tested six samples.

	Mean Tensile Strength (psi)	CV (%)	Change from Base Case (%)
Base Case	449.8	10.9%	-
1% NP Barite	452.8	12.9%	0.7%
3% NP Barite	468.5	9.4%	4.1%
5% NP Barite	518.6	15.8%	14.2%
1% NP Magnetite	523.3	15.5%	15.1%
3%NP Magnetite	482.2	5.7%	6.9%
5% NP Magnetite	522.6	5.2%	15.0%

Table 38: Spot check sample results showing a profound increase when compared to the second round of samples.

	Average Tensile Strength (psi)	CV (%)	Diff. (%)
1% NP Magnetite Round 2	523.3	15.5%	-
1% NP Magnetite Spot Check	665.3	7.9%	23.9%
3% NP Magnetite Round 2	482.2	5.7%	-
3% NP Magnetite Spot Check	636.1	6.0%	27.5%

Table 39: Results from the third round of Brazilian tests compared to the second round of samples.

	Mean Tensile Strength (psi)	CV (%)	Change from Base Case (%)	Change from Round 2 (%)
Base Case	1031.7	19.5%	-	78.6%
1% NP Barite	927.4	19.8%	-10.6%	68.8%
3% NP Barite	774.1	5.0%	-28.5%	49.2%
5% NP Barite	898.8	10.3%	-13.8%	53.7%
1% NP Magnetite	868.3	11.6%	-17.2%	49.6%
3%NP Magnetite	851.5	9.9%	-19.1%	55.4%
5% NP Magnetite	846.7	16.4%	-19.7%	47.3%

Table 40: Quick EDS results for the marked areas shown in Figure 59. Note the absence of excess aluminum at either point.

Normalized mass concentration [%]

Spectrum	Oxygen	Sodium	Aluminium	Silicon	Sulfur	Calcium	Iron	Barium
1% M 3mm Inside 1	36.05	0.15	0.00	8.10	0.09	54.31	1.31	0.00
1% M 3mm Inside 2	25.59	0.12	0.05	0.36	15.46	1.72	0.17	56.52
Mean	**30.82**	**0.13**	**0.02**	**4.23**	**7.78**	**28.01**	**0.74**	**28.26**
Sigma	**7.40**	**0.03**	**0.03**	**5.47**	**10.87**	**37.18**	**0.80**	**39.97**
SigmaMean	**5.23**	**0.02**	**0.02**	**3.87**	**7.69**	**26.29**	**0.57**	**28.26**

Table 41: Quick EDS results for the marked areas shown in Figure 60. Note the absence of excess aluminum at either point.

Normalized mass concentration [%]

Spectrum	Oxygen	Sodium	Aluminium	Silicon	Sulfur	Calcium	Iron	Barium
3% M 3mm Inside 1	30.54	0.29	0.61	3.73	10.06	13.17	1.08	40.52
3% M 3mm Inside 2	43.70	1.30	0.75	8.61	0.55	39.72	4.68	0.68
Mean	**37.12**	**0.80**	**0.68**	**6.17**	**5.31**	**26.45**	**2.88**	**20.60**
Sigma	**9.31**	**0.71**	**0.10**	**3.45**	**6.73**	**18.77**	**2.55**	**28.17**
SigmaMean	**6.58**	**0.50**	**0.07**	**2.44**	**4.76**	**13.27**	**1.80**	**19.92**

Table 42: Tensile bond strength results.

Tensile Bond Strength			
Recipe	Tensile Load (lbf)	Average Tensile Bond Strength (psi)	Change from Base Case (%)
Heavy Base Case	87	114.4	0%
1% NP Barite 1	103	Tensile Failure	-
3% NP Barite 1	126	Tensile Failure	-
3% NP Barite	107.5	141.4	21%
5% NP Barite 1	163.5	Tensile Failure	-
5% NP Barite 2	122.5	Tensile Failure	-
1% NP Magnetite 1	124.5	162.5	35%
1% NP Magnetite 2	100	130.5	13%
3% NP Magnetite	108.5	141.6	21%
5% NP Magnetite 1	101	Tensile Failure	-
5% NP Magnetite 2	195.5	Tensile Failure	-

Table 43: First Round unconfined compressive strength results with nanoparticles Bentonite.

		Average UCS (psi)	CV (%)	Change From Base Case (%)
Round 1	Light cement Base case	860	5.9%	base case
	1% NP Bentonite	705	9.6%	-18.00%
	3% NP Bentonite	1625	22.5%	89.00%
	5% NP Bentonite	1122	6.2%	30.60%

Table 44: Second round unconfined compressive strength results with nanoparticles light cement.

Round 2	Light cement Base Case	888	14.4%	base case
	1% NP Light cement	842	7.9%	-5.20%
	3% NP Light cement	839	22.7%	-5.50%
	5% NP Light cement	687	20.3%	-22.60%

Table 45: Round 3 unconfined compressive strength Results with nanoparticles heavy cement.

Round 3	Heavy cement Base case	1539	26.8%	base case
	1% NP Heavy cement	1874	12.1%	21.70%
	3% NP Heavy cement	1813	26.2%	17.80%
	5% NP Heavy cement	1629	10.7%	5.80%

Table 46: Averaged results from shear bond tests.

		Mean Shear Bond Strength (psi)	CV (%)	Change from Base Case (%)
	Base Case	67.2	0.213	-
	1% NP Bentonite	29.4	0.177	-0.783
	3% NP Bentonite	33.5	0.126	-0.671
Round 1	5% NP Bentonite	60.9	0.120	-0.099
	Base Case	64.4	0.192	-
	1% NP light cement	59.0	0.060	-0.087
	3% NP light cement	76.8	0.121	0.175
Round 2	5% NP light cement	57.5	0.281	-0.114
	Base Case	89.7	0.115	-
	1% NP heavy cement	79.2	0.357	-0.124
	3% NP heavy cement	109.4	0.115	0.198
Round 3	5% NP heavy cement	138.7	0.212	0.430

Table 47: Fluid loss results for heavy cement base case.

Heavy	Base Case	Base Case	Base Case	Base Case	Base Case	Base Case	Base Case
Date	5/13/2019	7/12/2019	7/15/2019	7/15/2019	7/17/2019	7/24/2019	MEAN
Temp	150	150	150	150	150	150	150
Min	ml	ml	ml	ml	ml	ml	ml
0	0	0	0	0	0	0	0.00
1	24	25	27	32	30	24.5	27.08
2	29	27	28.5	32.5	32.5	31	30.08
3	30	28	29	33.5	33	31.5	30.83
4	30.5	30	29.5	34	33.5	32	31.58
5		32	30			32.5	31.50
6							

Table 48: Fluid loss results for light cement, 1% BWOC heavy cement nanoparticles.

Heavy	1% BWOC heavy cement NP	1% BWOC heavy cement NP	1% BWOC heavy cement NP	1% BWOC heavy cement NP	
Date	7/9/2020	7/24/2020	7/27/2020	7/30/2020	Mean
Temp	150	150	150	150	
Min	mL	mL	mL	mL	mL
1	29	17	30	23	24.8
2	35	25	33	29	30.5
3	36	31	34	31	33.0
4	36.5	37	34.5	31.5	34.9
5	37	38	35	33	35.8
6	37.5	39	35.5	34	36.5
7		40	36	34.5	36.8

Table 49: Fluid loss results for light cement, 3% BWOC heavy cement nanoparticles.

Heavy	3% BWOC heavy cement NP	3% BWOC heavy cement NP	3% BWOC heavy cement NP	3% BWOC heavy cement NP	
Date	7/10/2020	7/24/2020	7/27/2020	7/30/2020	Mean
Temp	150	150	150	150	
Min	mL	mL	mL	mL	mL
1	29.5	16	30	31	26.6
2	34	24	38	36.5	33.1
3	35	30	40	38	35.8
4	36	35	40.5	38.5	37.5
5	36.5	38	41	39	38.6
6	37	38.5	41.5	39.5	39.1
7		39	42	40	40.3

Table 50: Fluid loss results for light cement, 5% BWOC heavy cement nanoparticles.

Heavy	5% BWOC heavy cement NP	5% BWOC heavy cement NP	5% BWOC heavy cement NP	5% BWOC heavy cement NP	
Date	7/13/2020	7/24/2020	7/27/2020	7/30/2020	Mean
Temp	150	150	150	150	
Min	mL	mL	mL	mL	mL
1	23	18	31	28	25.0
2	27	21	37	33	29.5
3	29	32	39	34	33.5
4	31	38	41	34.5	36.1
5	32.5	40	41.5	35	37.3
6	34	41	42	35.5	38.1
7		42	43	36	40.3

Table 51: Rheology results for heavy cement with 1% BWOC heavy cement nanoparticles.

	Sample #			
1% Hgrind	1	2	3	4
Temp ˚F	150	150	150	150
Date	7/9/2020	7/24/2020	7/27/2020	7/30/2020
% BWOC	1	1	1	1
600	300+	300+	300+	300+
300	268	273	277	227
200	216	208	220	177
100	157	154	157	124
6	64	87	65	55
3	46	65	49	42
3 (10m)	57	64	51	55

Table 52: Summarized Rheology results for heavy cement with 1% BWOC heavy cement nanoparticles.

	Shear	Bingham	Newtonian	μp	τy
Mean	Stress	Shear rate	Shear rate	Plastic viscosity	Yield point
	(lbf/100ft^2)	(1/s)	(1/s)	(cp)	(lbf/100ft^2)
300	320	1079	1022	39	223
261	278	569	511		
205	219	398	341		
148	158	228	170		
68	72	68	10		
51	54	63	5		
57					

Table 53: Rheology results for heavy cement with 3% BWOC heavy cement nanoparticles.

	Sample #			
3% Hgrind	1	2	3	4
Temp ˚F	150	150	150	150
Date	7/10/2020	7/24/2020	7/27/2020	7/30/2020
% BWOC	3	3	3	3
600	300+	300+	300+	300+
300	299	277	288	256
200	251	202	223	207
100	194	166	161	149
6	80	93	72	65
3	58	73	52	47
3 (10m)	64	74	55	53

Table 54: Summarized Rheology results for heavy cement with 3% BWOC heavy cement nanoparticles.

	Shear	Bingham	Newtonian	μp	τy
Mean	Stress	Shear rate	Shear rate	Plastic viscosity	Yield point
	(lbf/100ft^2)	(1/s)	(1/s)	(cp)	(lbf/100ft^2)
300	320	1079	1022	20	260
280	298	569	511		
221	235	398	341		
168	178	228	170		
78	83	68	10		
58	61	63	5		
62					

Table 55: Rheology results for heavy cement with 5% BWOC heavy cement nanoparticles.

	Sample #			
5% Hgrind	1	2	3	4
˚F	150	150	150	150
Date	7/13/2020	7/24/2020	7/27/2020	7/30/2020
% BWOC	5	5	5	5
600	300+	300+	300+	300+
300	266	300	260	300+
200	221	253	210	266
100	162	179	158	194
6	71	93	72	81
3	52	80	55	58
3 (10m)	64	79	60	58

Table 56: Summarized Rheology results for heavy cement with 5% BWOC heavy cement nanoparticles.

	Shear	Bingham	Newtonian	μp	τy
Mean	Stress	Shear rate	Shear rate	Plastic viscosity	Yield point
	(lbf/100ft^2)	(1/s)	(1/s)	(cp)	(lbf/100ft^2)
300	320	1079	1022	25	251
275	293	569	511		
238	253	398	341		
173	185	228	170		
79	84	68	10		
61	65	63	5		
65					

Table 57: Average Brazilian testing results for heavy cement nanoparticles.

				Change from
	Mean Tensile Strength (psi)	Mean stdev	CV (%)	Base Case (%)
Base Case	713.3	36.2939151	5.1%	-
1% Hgrind	557.3	111.807	20.1%	-24.6%
3% Hgrind	578.4	166.763873	28.8%	-20.9%
5% Hgrind	543.6	136.11638	25.0%	-27.0%

Table 58: Average Young's modulus testing results for bentonite nanoparticles.

	Overall Youngs Modulus Results for Bentonite NPs		
UCS	Youngs Modulus (ksi)	CV (%)	YM Change from Base Case
Base Case	2138	30.2%	Base Case
1% NP Bentonite	2215	11.2%	3.6%
3% NP Bentonite	2489	36.3%	16.4%
5% NP Bentonite	1787	29.3%	-16.4%

Table 59: Average Young's modulus testing results for light cement nanoparticles.

Overall Youngs Modulus Results for Bentonite NPs			
UCS	Mean Youngs Modulus (ksi)	CV (%)	YM Change from Base Case
Base Case	888	14.4%	Base Case
1% NP light cement	842	7.9%	-5.2%
3% NP light cement	839	22.7%	-5.5%
5% NP light cement	687	20.3%	-22.6%

Table 60: Average Young's modulus testing results for heavy cement nanoparticles.

Overall Youngs Modulus Results for heavy cement NPs			
	Mean Youngs Modulus (ksi)	CV (%)	YM Change from Base Case
Base Case	1539	26.8%	Base Case
1% Heavy cement NPs	1874	12.1%	21.7%
3% Heavy cement NPs	1813	26.2%	17.8%
5% Heavy cement NPs	1629	10.7%	5.8%

Table 61: Cement Setting Pressure and % Contraction.

Applied pressure,psi	Total Contraction, cc/420cc sample	% contraction	Psetting, psi
900	3.1	0.738	17.9
800	3.4	0.810	18.0
750	3.59	0.855	18.1
700	4.1	0.976	18.1
670	4.14	0.986	18.2
500	5.64	1.343	18.4
300	9.62	2.291	18.8
250	11.64	2.772	19.0
50	62.59	14.901	20.4
14.7	224.93	53.555	21.6

Table 62: Round 1, Summarized results for light cement with Bentonite nanoparticles at 100°F and 3000 psi.

Round 1			
Light Cement	Thickening time		Change
100˚F, 3000psi	(HH:MM)	Min	from CC
Control case	3:00	180	
1% Bentonite NPs1	3:05	185	3.06%
3% Bentonite NPs1	2:57	177	-1.39%
5% Bentonite NPs1	3:13	193	7.52%

Table 63: Round 2, Summarized results for light cement with Bentonite nanoparticles at 100°F and 3000 psi.

Round 2			
Light Cement	Thickening time		Change
100˚F, 3000psi	(HH:MM)	Min	from C
Control Case	3:00	180	
1% Bentonite NPs 2	2:50	170	-5.29%
3% Bentonite NPs 2	2:55	177	-1.39%
5% Bentonite NPs 2	2:55	177	-1.39%

Table 64: Combined result for Round 1 and Round 2.

	Round 1		**Round 2**		**Average**		
Light Cement	Thickening time		Thickening time		Thickening time		Change
100˚F, 3000psi	(HH:MM)	Min	(HH:MM)	Min	(HH:MM)	Min	from BC
Control Case	3:00	179.5	3:00	180	3:00	180	
1% Bentonite NPs	3:05	185	2:50	170	2:57	178	-1.11%
3% Bentonite NPs	2:57	177	2:55	0:00	2:56	177	-1.39%
5% Bentonite NPs	3:13	193	2:55	0:00	3:04	185	3.06%

Table 65: Porosity measurement and results for light cement.

Sample #	Lengt (in)	Diameter (in)	Wet weight (g)	Dry weight (g)	Volum (in^3)	Volum (cm^3)	Weight water (g)	Volume water (cm^3)	Porosity (%)
1	0.97	0.99	18.90	14.00	0.74	12.20	4.90	4.90	0.40
2	0.97	0.99	18.40	13.80	0.74	12.20	4.60	4.60	0.38
3	0.93	0.99	18.10	13.60	0.71	11.67	4.50	4.50	0.39
4	0.90	1.00	18.30	14.40	0.70	11.52	3.90	3.90	0.34

Table 66: Porosity measurement and results for light cement.

Sample #	Lengt (in)	Diameter (in)	Wet weight (g)	Dry weight (g)	Volum (in^3)	Volum (cm^3)	Weight water (g)	Volume water (cm^3)	Porosity (%)
1	0.97	1.00	24.30	21.20	0.75	12.36	3.10	3.10	0.25
2	0.88	0.99	21.60	18.80	0.68	11.08	2.80	2.80	0.25
3	0.85	0.99	20.60	17.70	0.66	10.77	2.90	2.90	0.27
4	0.91	0.99	22.20	19.20	0.70	11.55	3.00	3.00	0.26

Table 67: Parameters for the case well in the Gulf of Mexico.

	Parameter	Value	
	TVD (m)	2,623	1
	$Simulation\ Depth$ (m)	1,920	
Dimensions	$Hole\ Size$ (cm)	31.12	1
	$Casing\ OD$ (cm)	24.45	1
	$Casing\ ID$ (cm)	21.68	1
In-Situ Stresses	σ_H (MPa)	38.99	
	σ_h (MPa)	36.98	1,2,3
	σ_v (MPa)	41.00	4
Casing	ν	0.30	5
	E (GPa)	200.00	5
	ρ (kg/m^3)	7,938.00	1
	α (K^{-1})	1.14E-05	5
	κ (W/m·K)	43.00	5
	c (J/kg·K)	490.00	5
Cement	Pp (g/cc)	1.56	
	ρ_{slurry} (g/cc)	1.68	1
	ν	0.18	6
	ρ_{dry} (kg/m^3)	1,965.00	1
	α (K^{-1})	8.64E-06	6
	κ (W/m·K)	0.41	6
	c (J/kg·K)	490	6
Rock	Pp (g/cc)	1.56	1
	ν	0.34	7
	E (GPa)	3.9	7
	ρ (kg/m^3)	2,600.00	7
	α (K^{-1})	1.00E-05	5
	κ (W/m·K)	2.40	5
	c (J/kg·K)	900.00	5
Cement/Rock	τ^o (MPa)	0.42	8
	G_C (J/m^2)	100.00	8
Loads	MW (g/cc)	30.49	1

[1]Log, [2]Breckels and van Eekelen (1982), [3]Wojtanowicz et al. (2000), [4]Meng et al. (2018), [5]Weideman (2014), [6]Cement Database, [7]High Island Log Analysis, [8]Wang and Taleghani (2014)

Table 68: High and low values for the parametric study.

Parameter	Low	High
Dimensions	-40%	$+40\%$
Isotropic Horizontal Stress Variation	$\sigma_v = \sigma_{v,base}$ $\sigma_H = \sigma_{h,base}$ $\sigma_h = \sigma_{h,base}$	$\sigma_v = \sigma_{v,base}$ $\sigma_H = \sigma_{v,base}$ $\sigma_h = \sigma_{v,base}$
Anisotropic Stress Variation	$\sigma_v = \sigma_{v,base}$ $\sigma_H = \sigma_{h,base}$ $\sigma_h = \sigma_{h,base}$	$\sigma_v = \sigma_{v,base}$ $\sigma_H = \sigma_{v,base}$ $\sigma_h = \sigma_{h,base}$
Vertical Stress Variation	$\sigma_v = -5\% \cdot \sigma_{v,base}$ $\sigma_H = \frac{\sigma_v + \sigma_h}{2}$ $\sigma_h = \sigma_{h,base}$	$\sigma_v = +5\% \cdot \sigma_{v,base}$ $\sigma_H = \frac{\sigma_v + \sigma_h}{2}$ $\sigma_h = \sigma_{h,base}$
Cement Stress (MPa)	MW	$P_{fracture}$
Cement Mechanical and Thermal Properties	$25\%\ Quartile$	$75\%\ Quartile$
Rock Mechanical Properties	Min from Log Data	Max from Log Data
Rock Thermal Properties	-40%	$+40\%$
Traction Law Properties	-40%	$+40\%$

Table 69: Wellbore parameters sorted based off their percent change of the maximum gap width (%MGW) from the base gap magnitude. 1st Order Parameters are critical in the development of the gap width magnitude at the casing/cement interface. 2nd Order Parameters have minor effect, and 3rd Order Parameters have little to no effect on the development of the gap widths.

	ΔP	%MGW
1st Order Parameters	$Hole\ Size$	302%
	ω_{casing}	208%
2nd Order Parameters	σ_{cement}	42%
	E_{rock}	40%
	ω_{cement}	34%
	E_{cement}	29%
	τ^{o}	20%
3rd Order Parameters	G_C	3%
	v_{rock}	3%
	v_{cement}	2%
	α_{rock}	0%
	$\delta\sigma_V$	0%
	α_{cement}	0%
	κ_{cement}	0%
	c_{cement}	0%
	κ_{rock}	0%
	c_{rock}	0%
	$\frac{\delta\sigma_H}{\delta\sigma_V}$	0%
	$\frac{\delta\sigma_h}{\delta\sigma_H}$	0%

Table 70: Fluid loss results for heavy cement, 1% BWOC magnetite nanoparticles

Heavy	1% BWOC MagnNP	1% BWOC MagnNP	1% BWOC MagnNP	1%
Date	5/7/2019	7/22/2019	8/5/2019	MEAN
Temp	150	150	150	150
Min	Ml	ml	ml	ml
0	0	0	0	0.00
1	19	20	24	21.00
2	30	31	35	32.00
3	35	36	35.5	35.50
4	36	37	36	36.33
5	37	38	36.5	37.17
6	37.5		37.5	37.50

Table 71: Fluid loss results for heavy cement, 3% BWOC magnetite nanoparticles.

Heavy	3% BWOC MagnNP	3% BWOC MagnNP	3% BWOC MagnNP	3%
Date	5/22/2019	7/22/2019	7/23/2019	MEAN
Temp	150	150	150	150
Min	ml	ml	ml	ml
0	0	0	0	0.00
1	19	19	18	18.67
2	22	23	21	22.00
3	24.5	25.5	23.5	24.50
4	26	27	24.5	25.83
5	26.5	28	25.5	26.67
6	27			27.00

Table 72: Fluid loss results for heavy cement, 5% BWOC magnetite nanoparticles.

Heavy	5% BWOC MagnNP	5%
Date	7/24/2019	MEAN
Temp	150	150
Min	ml	ml
0	0	0
1	17	17
2	24	24
3	24.5	24.5
4	25	25

Table 73: Fluid loss results for heavy cement, 1% BWOC barite nanoparticles

Heavy	1% BWOC BariteNP	1% BWOC BariteNP	1% BWOC BariteNP	1%
Date	8/7/2019	7/26/2019	7/29/2019	MEAN
Temp	150	150	150	150
Min	ml	ml	ml	ml
0	0	0	0	0.00
1	20.5	18	21	19.83
2	29	24	30	27.67
3	32	27	30.5	29.83
4	32.5	28.5	31	30.67
5	33		31.5	32.25

Table 74: Fluid loss results for heavy cement, 3% BWOC barite nanoparticles.

Heavy	3% BWOC BariteNP	3% BWOC BariteNP	3% BWOC BariteNP	3% BWOC BariteNP	3%
Date	5/15/2019	7/26/2019	7/29/2019	8/5/2019	MEAN
Temp	150	150	150	150	150
Min	ml	ml	ml	ml	ml
0	0	0	0	0	0.00
1	17	18.5	22	18	18.88
2	23	27	27	29	26.50
3	28	28.5	29.5	30.5	29.13
4	28.5	29	29.5	31	29.50
5	29.5			31.5	30.50
6				32.5	32.50

Table 75: Fluid loss results for heavy cement, 5% BWOC barite nanoparticles

Heavy	5% BWOC BariteNP	5% BWOC BariteNP	5% BWOC BariteNP	5%
Date	7/31/2019	8/1/2019	8/5/2019	MEAN
Temp	150	150	150	150
Min	ml	ml	ml	ml
0	0	0	0	0.00
1	15	15.5	11.5	14.00
2	21.5	20.5	22	21.33
3	27	23.5	25	25.17
4	29	24	25.5	26.17
5	29.5	24.5	26	26.67
6	30.5	26	26	27.50

Table 76: Rheology results for heavy cement base case.

Base Case	Base Case	Base Case	Base Case
07/15/19	07/15/19	07/17/19	07/24/19
150F	150F	150F	150F
285	287	300+	300+
230	177	245	190
187	134	198	143
124	88	137	92
103	35	53	36
30	29	38	28
48	25	45	28

Table 77: Rheology results for heavy cement base case.

Base Case	Reading		Bingham
	Mean	Shear stress	Shear rate
RPM	Fann 35A	(lbf/100ft^2)	(1/s)
600			1040
300	211	224	529
200	166	176	359
100	110	117	188
6	57	60	28
3	31	33	23
3 (10m)	37		

Table 78: Rheology results for heavy cement containing 1% BWOC magnetite nanoparticles.

1% BWOC MagNP	1% BWOC MagNP
07/22/19	08/05/19
150F	150F
267	300+
217	263
103	200
87	133
46	53
36	41
29	43

Table 79: Rheology results for heavy cement base case with 1% BWOC magnetite nanoparticles.

1% BWOC MagNP	Reading		Bingham
	Mean	Shear stress	Shear rate
RPM	Fann 35A	(lbf/100ft^2)	(1/s)
600			1019
300	240	256	508
200	152	161	
100	110	117	167
6	50	53	7
3	39	41	2
3 (10m)	36		

Table 80: Rheology results for heavy cement base case with 3% BWOC magnetite nanoparticles.

3% BWOC MagNP	3% BWOC MagNP	3% BWOC MagNP
05/22/19	07/22/19	07/23/19
150F	150F	150F
257	300+	300+
231	211	292
136	166	241
126	117	186
73	56	96
45	40	72
66	36	66

Table 81: Rheology results for heavy cement base case with 3% BWOC magnetite nanoparticles.

3% BWOC MagNP	Reading		Bingham
	Mean	Shear stress	Shear rate
RPM	Fann 35A	(lbf/100ft^2)	(1/s)
600			1031
300	245	261	520
200	181	193	350
100	143	152	
6	75	80	19
3	52	56	14
3 (10m)	56		

Table 82: Rheology Results for heavy cement base case with 5% BWOC magnetite nanoparticles.

5% BWOC MagNP
07/24/19
150F
300+
285
220
153
80
60
75

Table 83: Rheology results for heavy cement base case with 5% BWOC magnetite nanoparticles.

5% BWOC MagNP	Reading		Bingham
	Mean	Shear stress	Shear rate
RPM	Fann 35A	(lbf/100ft^2)	(1/s)
600			1037
300	285	304	526
200	220	234	355
100	153	163	185
6	80	85	25
3	60	64	20
3 (10m)	75		

Table 84: Rheology results for heavy cement base case with 1% BWOC barite nanoparticles.

1% BWOC BarNP	1% BWOC BarNP	1% BWOC BarNP	1% BWOC BarNP
07/26/19	07/29/19	08/05/19	08/05/19
150	150	150	150
300+	300+	300+	300+
300	250	300	207
257	190	261	162
160	120	197	111
72	55	90	49
57	42	64	38
58	48	66	42

Table 85: Rheology results for heavy cement base case with 1% BWOC barite nanoparticles.

1% BWOC BarNP	Reading		Bingham
	Mean	Shear stress	Shear rate
RPM	Fann 35A	(lbf/100ft^2)	(1/s)
600			1050
300	264	281	539
200	218	232	369
100	147	157	199
6	67	71	39
3	50	54	34
3 (10m)	54		

Table 86: Rheology results for heavy cement base case with 3% BWOC barite nanoparticles.

3% BWOC BarNP	3% BWOC BarNP	3% BWOC BarNP
07/26/19	07/29/19	08/05/19
150	150	150
300+	300+	300+
272	244	235
194	181	172
126	122	117
68	61	60
68	51	54
67	54	58

Table 87: Rheology results for heavy cement base case with 3% BWOC barite nanoparticles.

3% BWOC BarNP	Reading		Bingham
	Mean	Shear stress	Shear rate
RPM	Fann 35A	(lbf/100ft^2)	(1/s)
600			1029
300	250	267	518
200	182	194	348
100	122	130	178
6	63	67	18
3	58	61	12
3 (10m)	60		

Table 88: Rheology results for heavy cement base case with 5% BWOC barite nanoparticles.

5% BWOC BarNP	5% BWOC BarNP	5% BWOC BarNP
07/31/19	08/01/19	08/05/19
150	150	150
300+	300+	300+
249	235	214
192	182	170
149	136	130
88	88	82
69	69	65
78	74	75

Table 89: Rheology results for heavy cement base case with 5% BWOC barite nanoparticles.

5% BWOC BarNP	Reading		Bingham
	Mean	Shear stress	Shear rate
RPM	Fann 35A	(lbf/100ft^2)	(1/s)
600			1038
300	233	248	527
200	181	193	357
100	138	147	187
6	86	92	27
3	68	72	22
3 (10m)	76		

Table 90: Average Brazilian testing results for light Cement with Bentonite nanoparticles.

	Mean Tensile Strength (psi)	Mean stdev	CV (%)	Change from Base Case (%)
Base Case	302.2	34.6504472	11.5%	-
1% BWOC Bentonite NP	272.3	44.8234305	16.5%	-10.4%
3% BWOC Bentonite NP	279.8	43.9976118	15.7%	-7.7%
5% BWOC Bentonite NP	304.8	29.3121482	9.6%	0.9%

Table 91: Average Brazilian testing results for light cement nanoparticles.

				Change from	
	Mean Tensile Strength (psi)	Mean stdev	CV (%)	Base Case (%)	
Base Case	302.2	34.65045	11.5%	-	
1% Ground cement A	282.5	22.82249	8.1%	-6.7%	
3% Ground cement A	206.7	34.4859	16.7%	-37.5%	
5% Ground cement A	279.8	53.19186	19.0%	-7.7%	

Figures

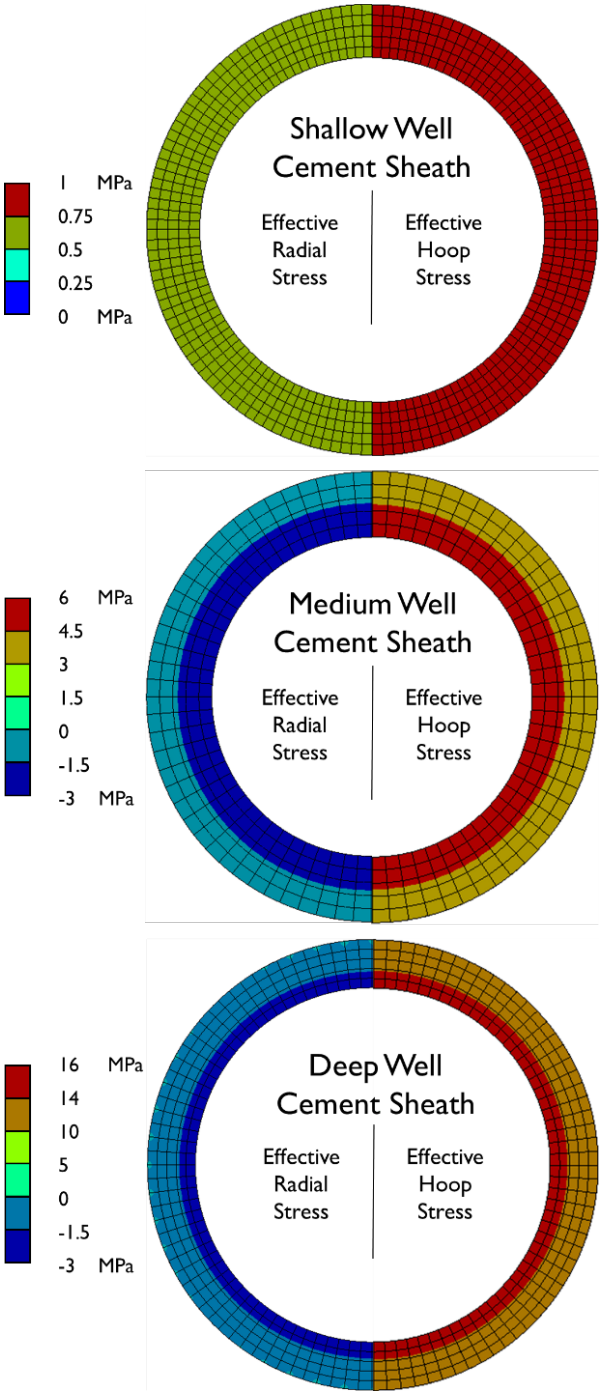

Figure 1: Graphical results of the base case stress values shown in Table 2 for the three case studies: shallow, medium, and deep wells.

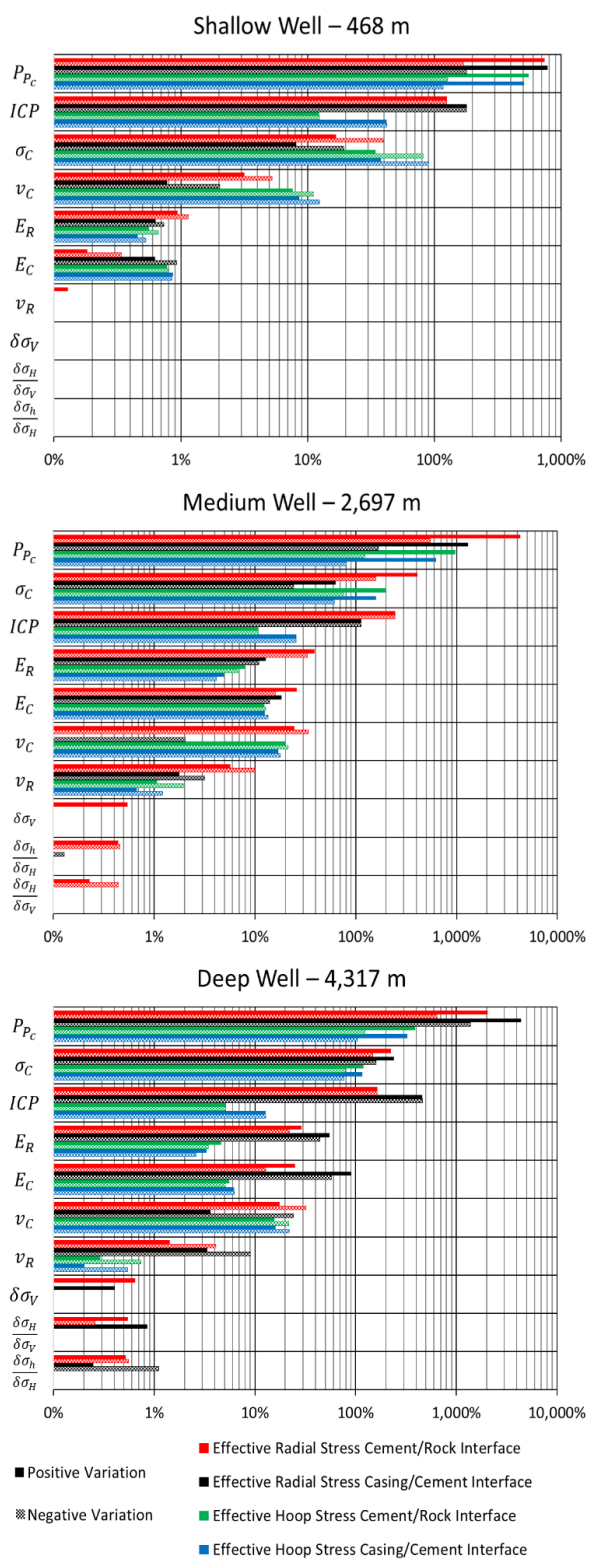

Figure 2: Results of the parametric study ranking the parameters with the largest impact on stress development for the shallow, medium, and deep wells in the Eugene Island Official Protraction Diagram. Note that the y-axis labels are defined in the nomenclature section.

Figure 3: OFI Testing Equipment variable speed mixer.

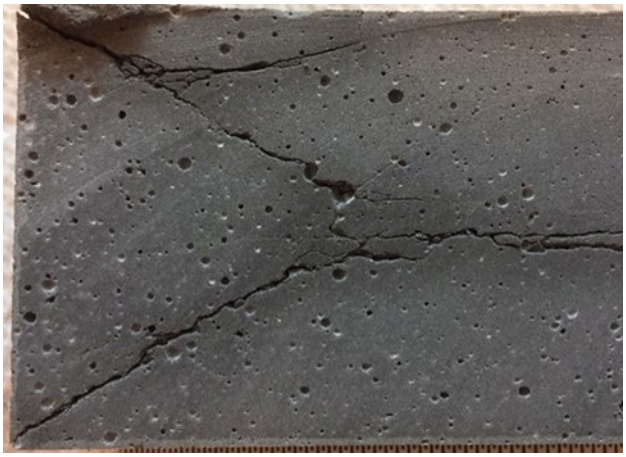

Figure 4: 5% BWOC Barite nanoparticles containing extra water for nanoparticles.

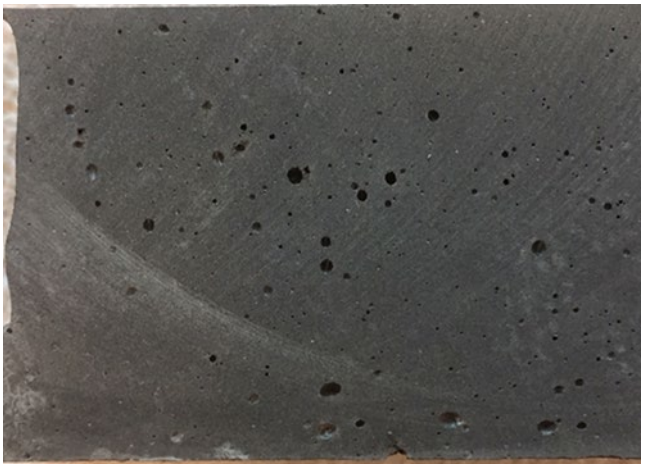

Figure 5: 5% BWOC Barite nanoparticles without extra water for nanoparticles.

Figure 6A (left) and **6B** (right): shows the Chandler Model 7322 HPHT Consistometer.

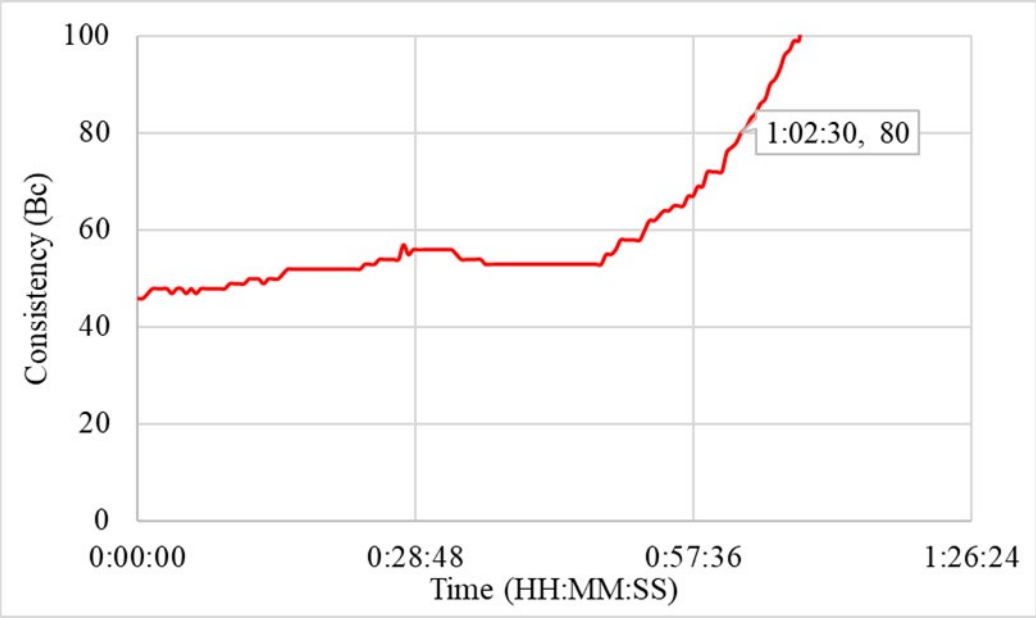

Figure 7: Consistency test of the initial heavy base case.

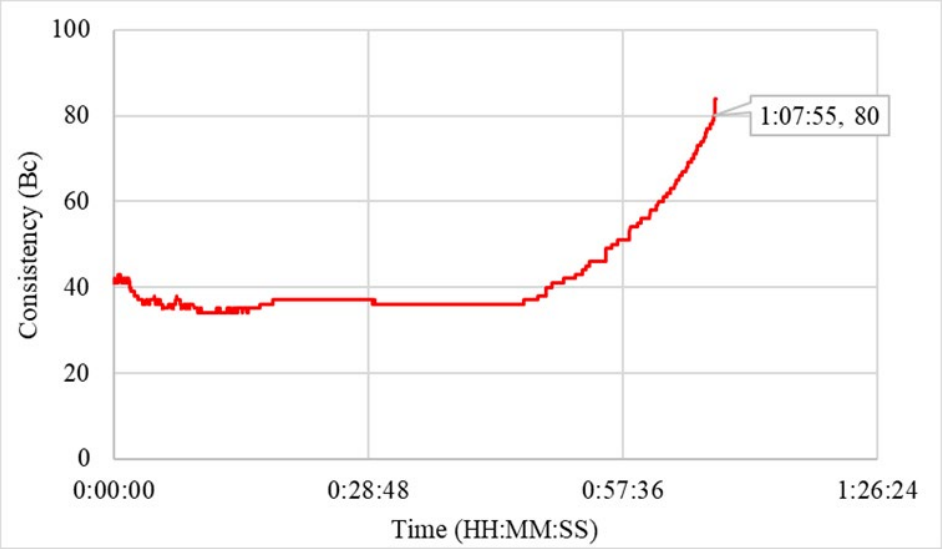

Figure 8: The repeated consistency test of the initial heavy base case.

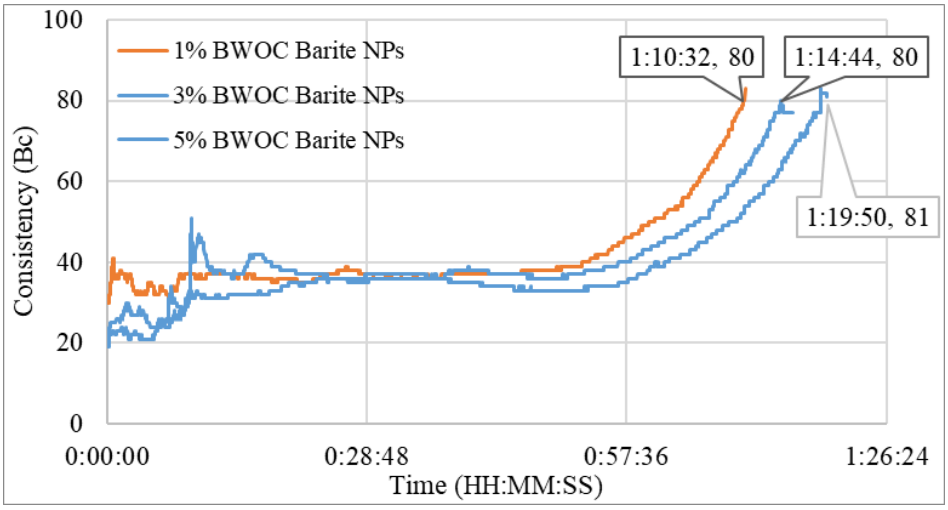

Figure 9: The repeated consistency test of the initial heavy base case with barite nanoparticles.

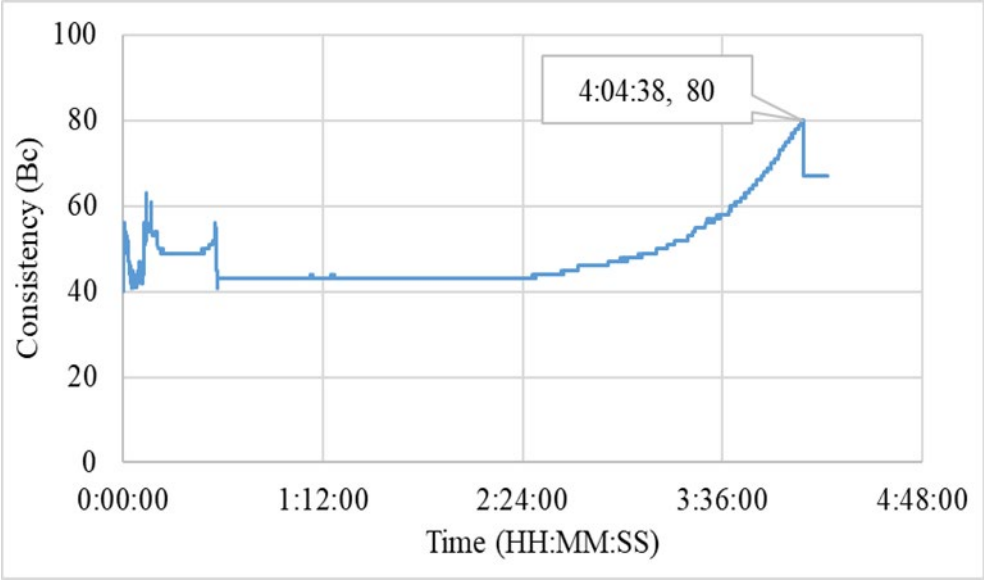

Figure 10: The consistency test of the initial light base case with low temperature.

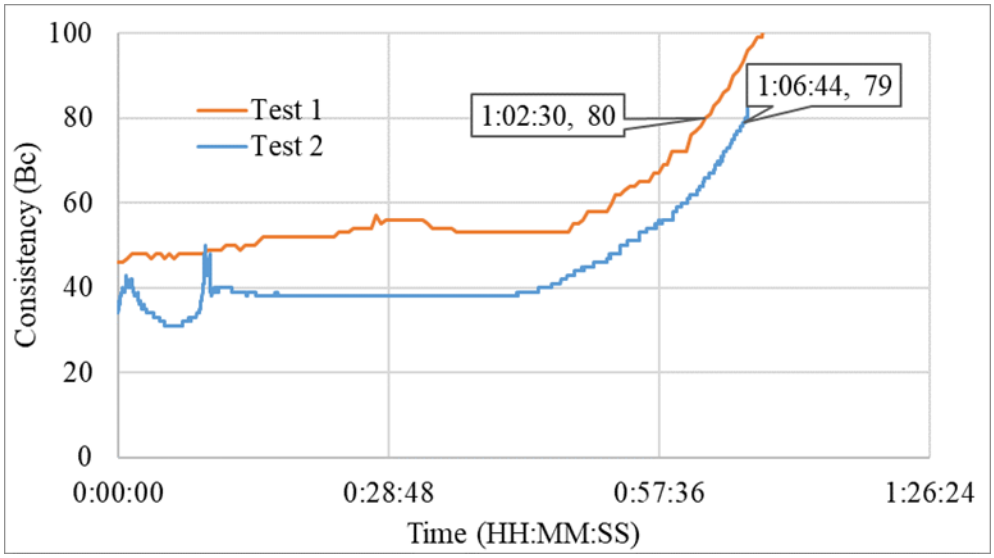

Figure 11: The repeated consistency two tests of the initial light base case.

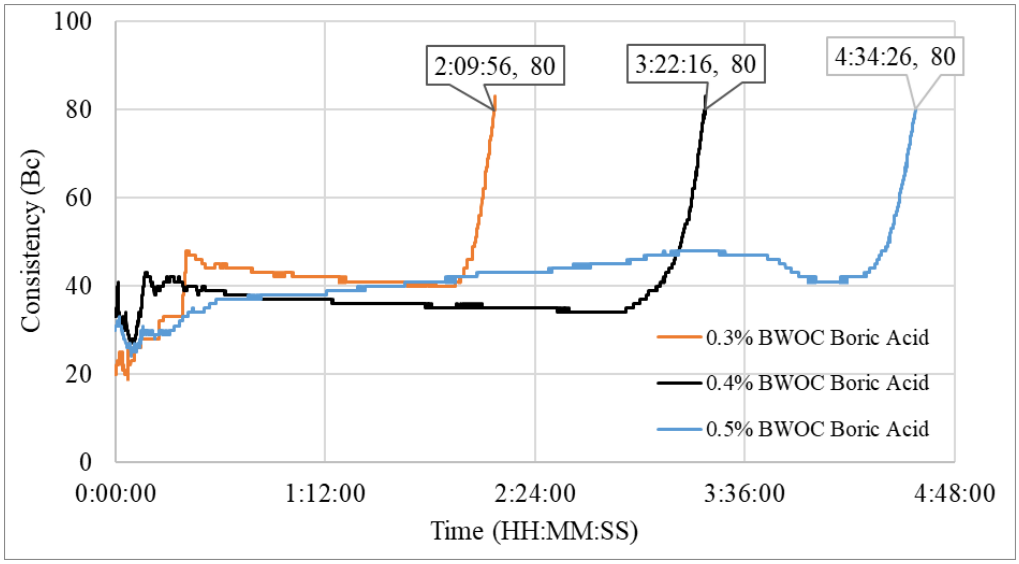

Figure 12: Boric Acid tests with initial heavy base case cement.

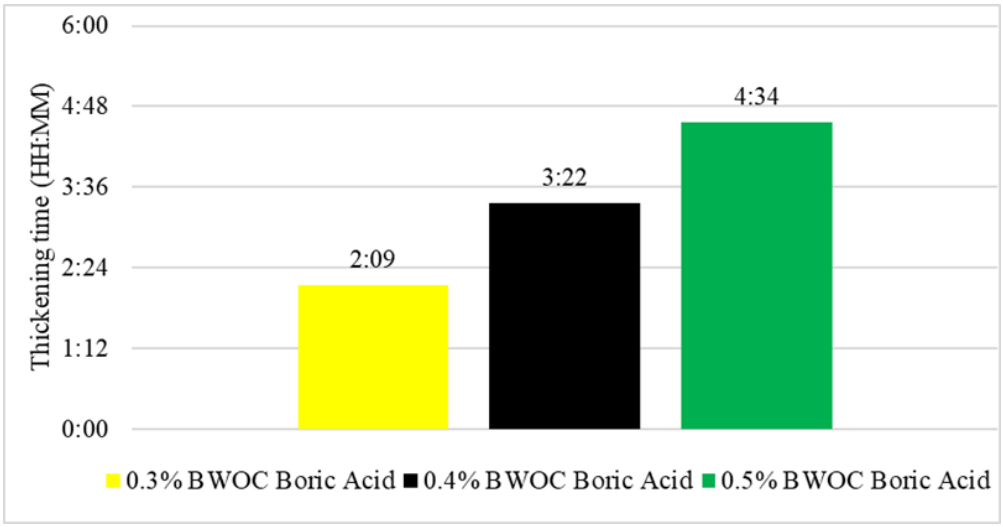

Figure 13: Boric Acid tests with initial heavy base case cement.

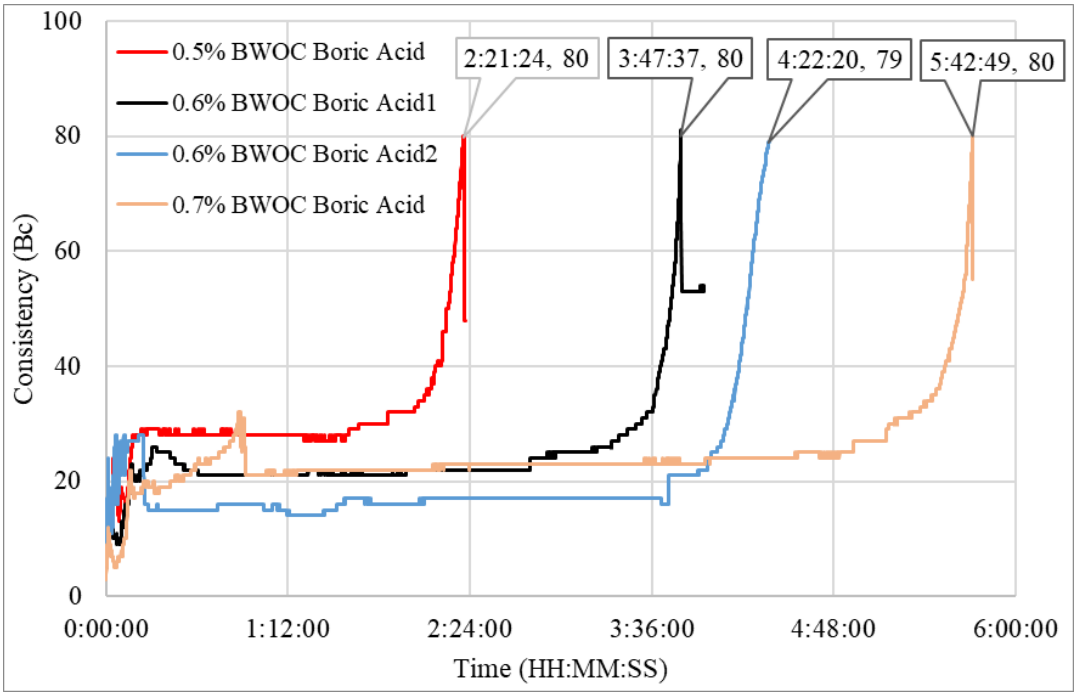

Figure 14: Boric Acid tests with initial light base case cement.

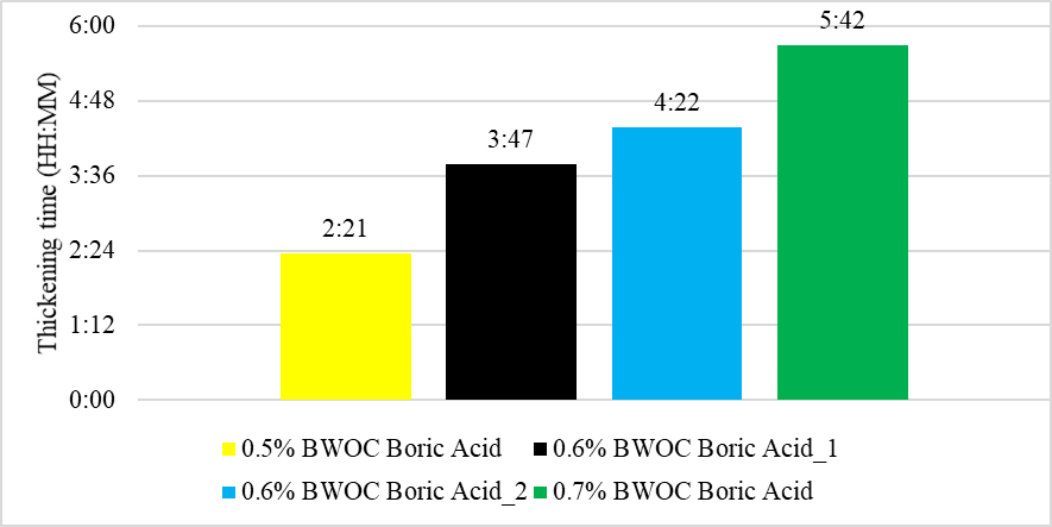

Figure 15: Boric Acid tests with initial light base case cement.

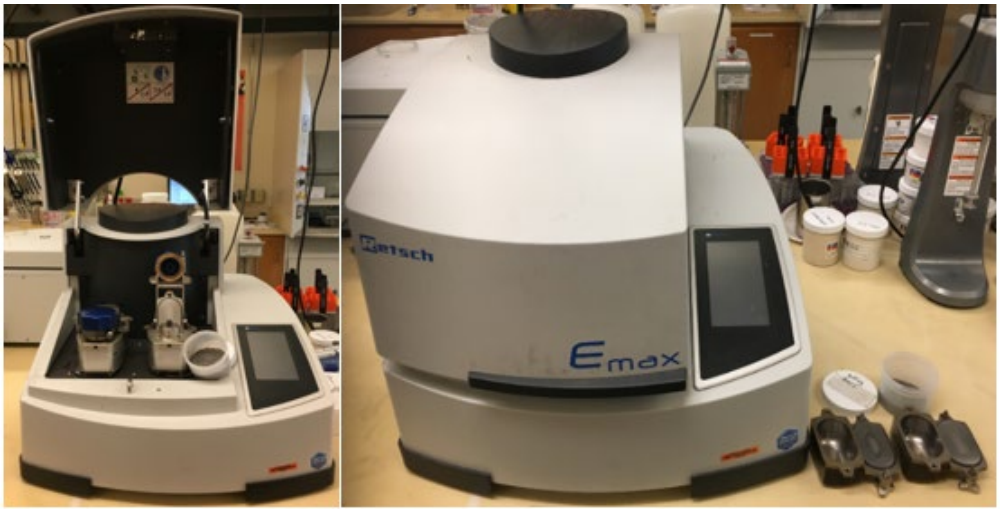

Figure 16: EMAX high energy ball grinder.

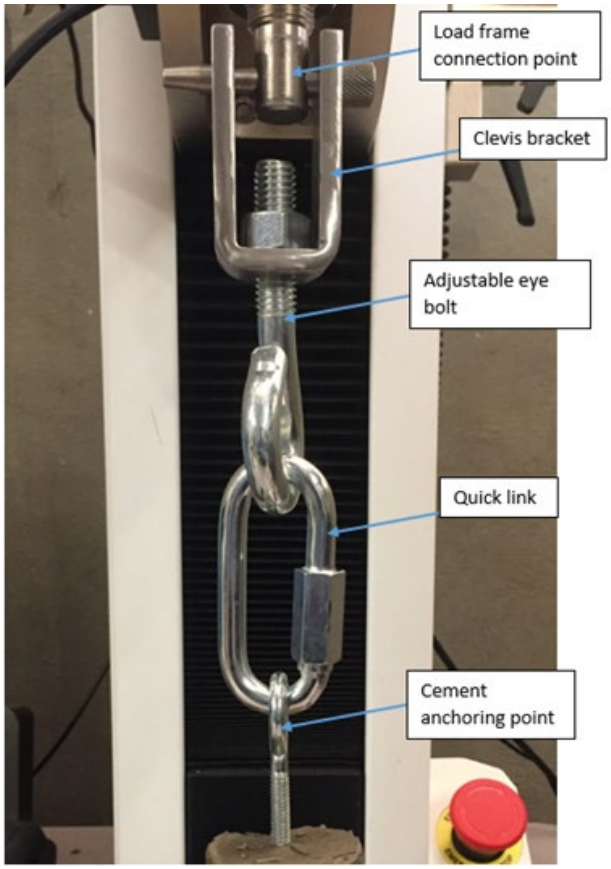

Figure 17: Upper grip of the tensile bond testing apparatus.

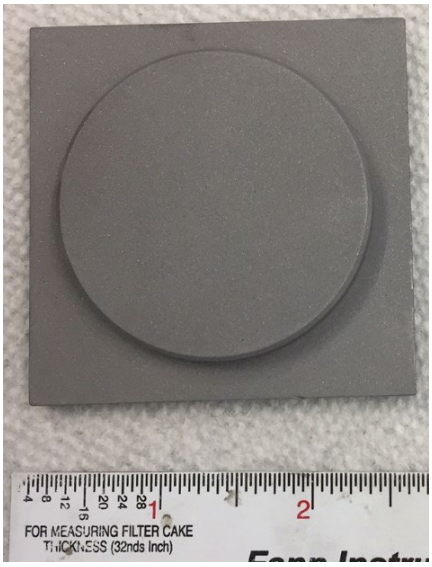

Figure 18: Steel substrate for tensile bond testing.

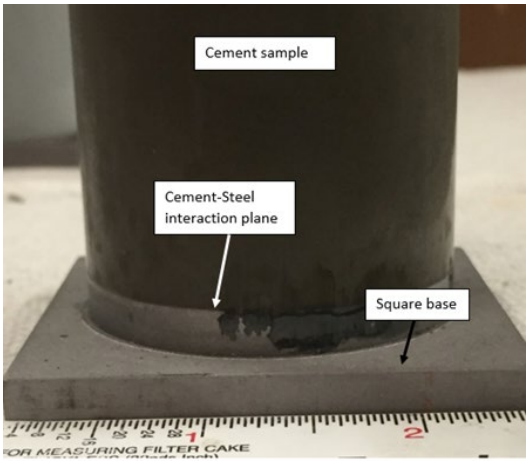

Figure 19: Steel substrate and cement sample.

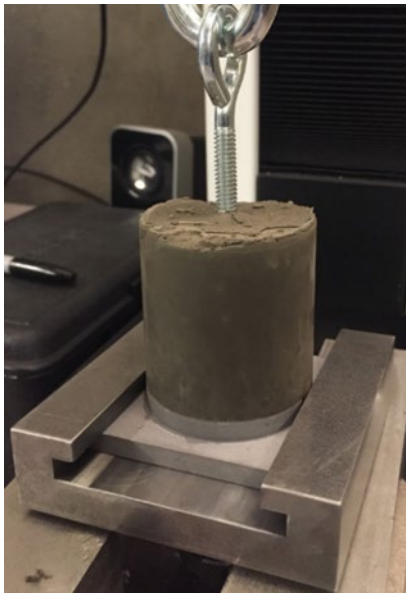

Figure 20: Tensile bond strength sample prepared and seated in sample holder.

Figure 21: Initial anchoring design for tensile bond testing.

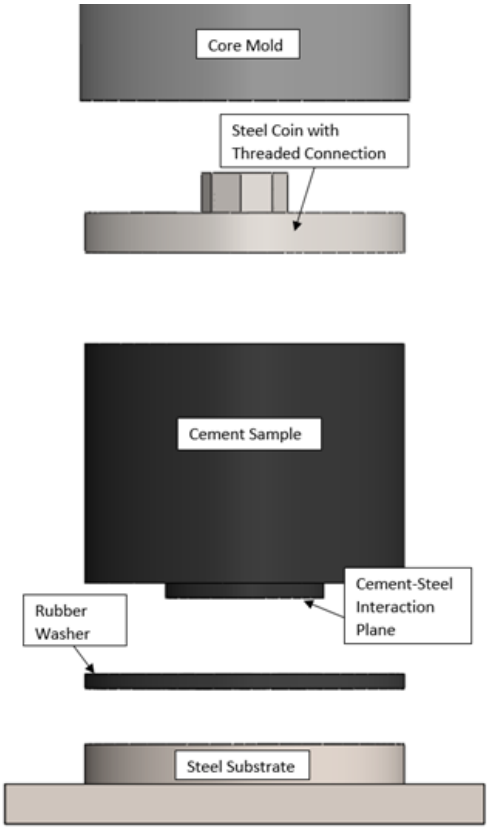

Figure 22: Visualization of the final tensile bond strength sample design.

Figure 23: Steel substrate after testing with indications of failure other than debonding.

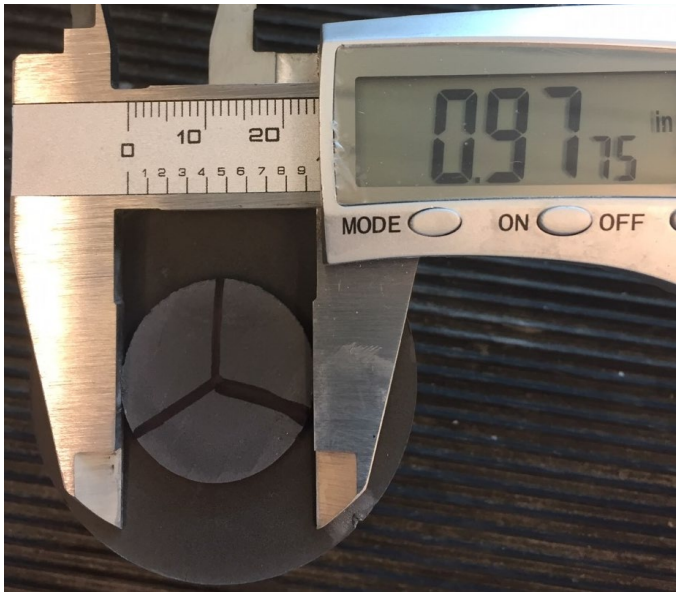

Figure 24: The bonded plane being measured for diameter after testing in order to calculate the bond strength seen there.

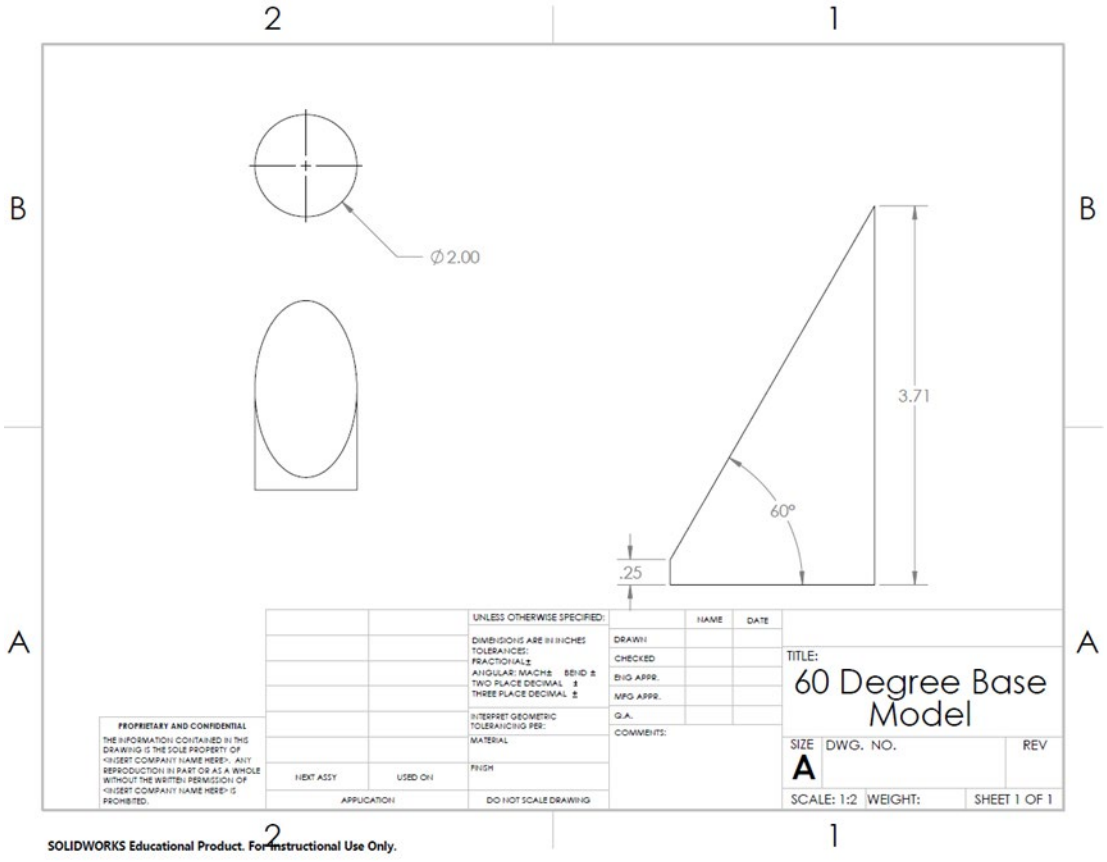

Figure 25: Sketch of the initial steel substrate for shear bond testing.

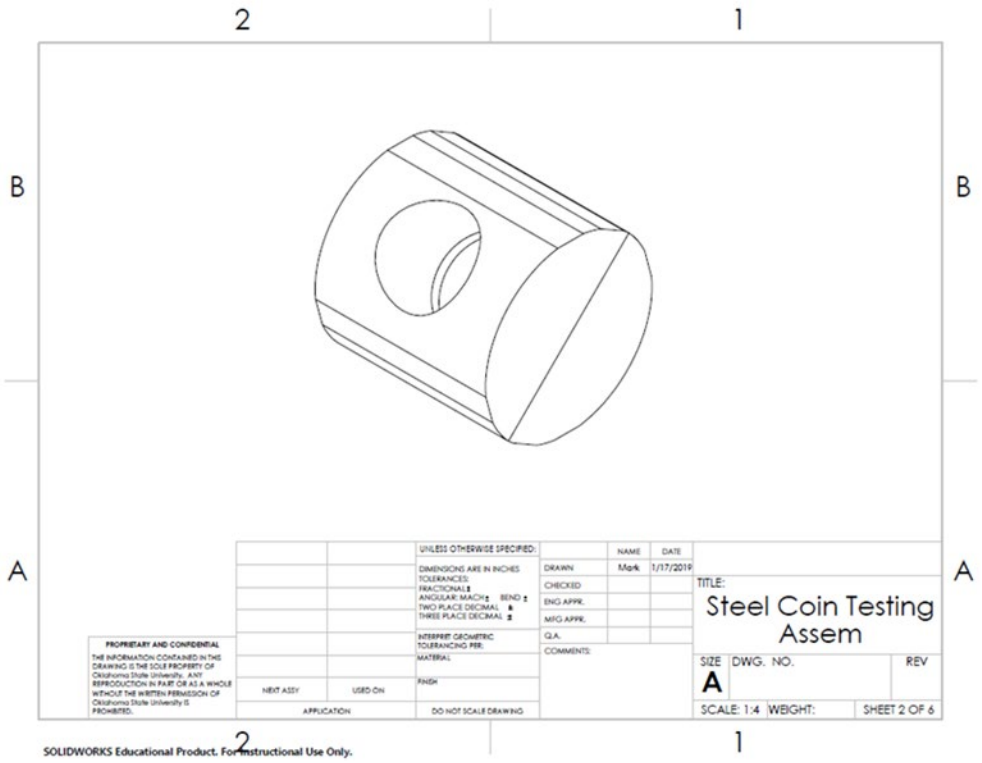

Figure 26: Sketch of the shear bond testing apparatus concept.

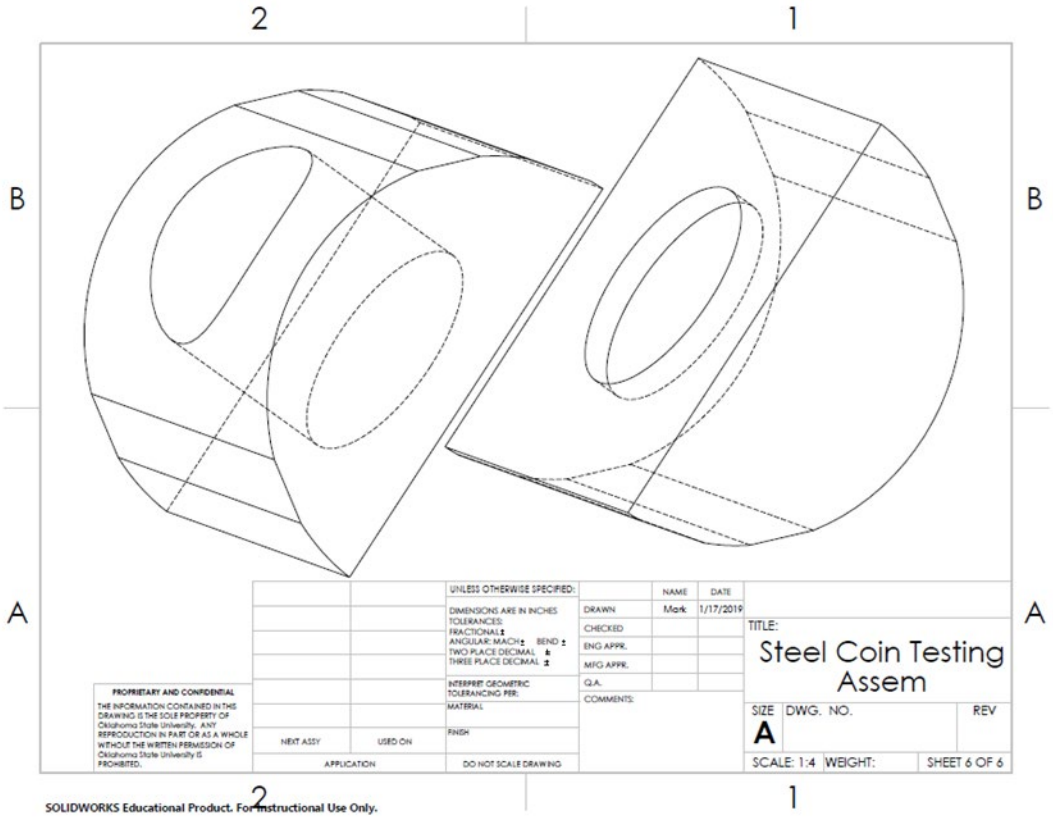

Figure 27: Exploded view of the shear bond testing apparatus concept.

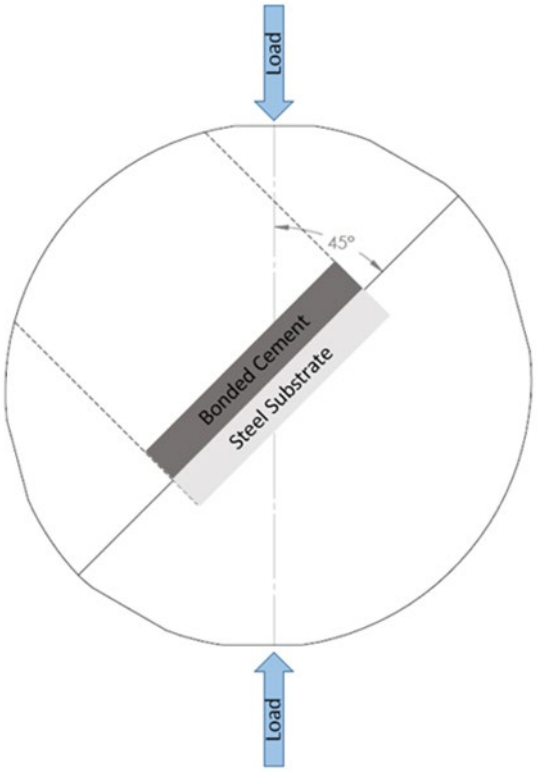

Figure 28: Working principles of the shear bond testing apparatus.

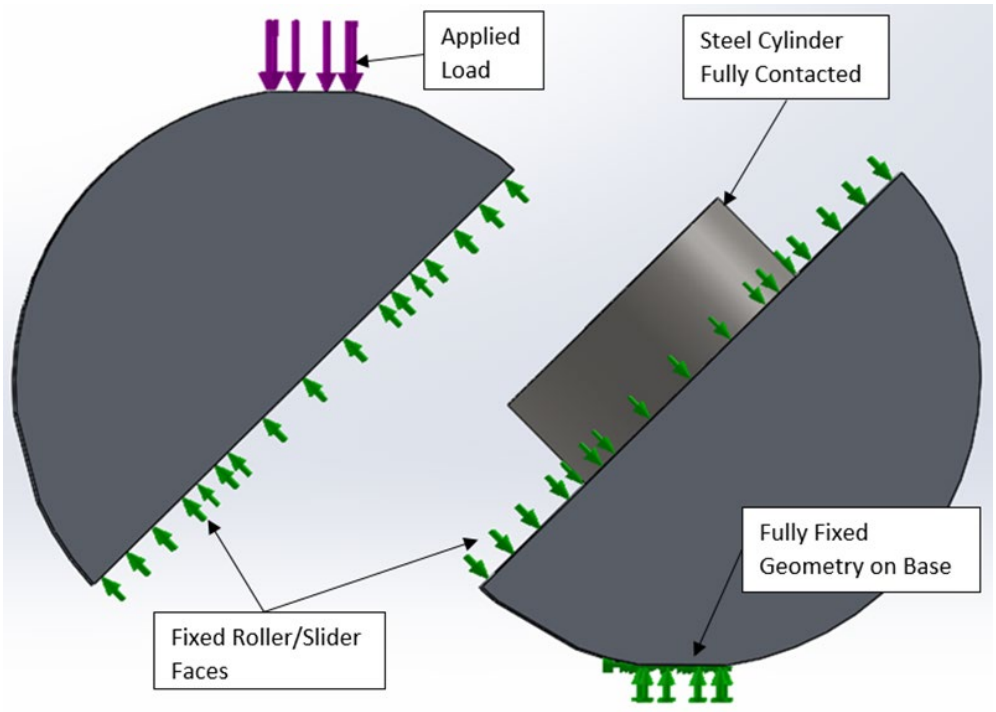

Figure 29: Annotated visualization of the load simulations.

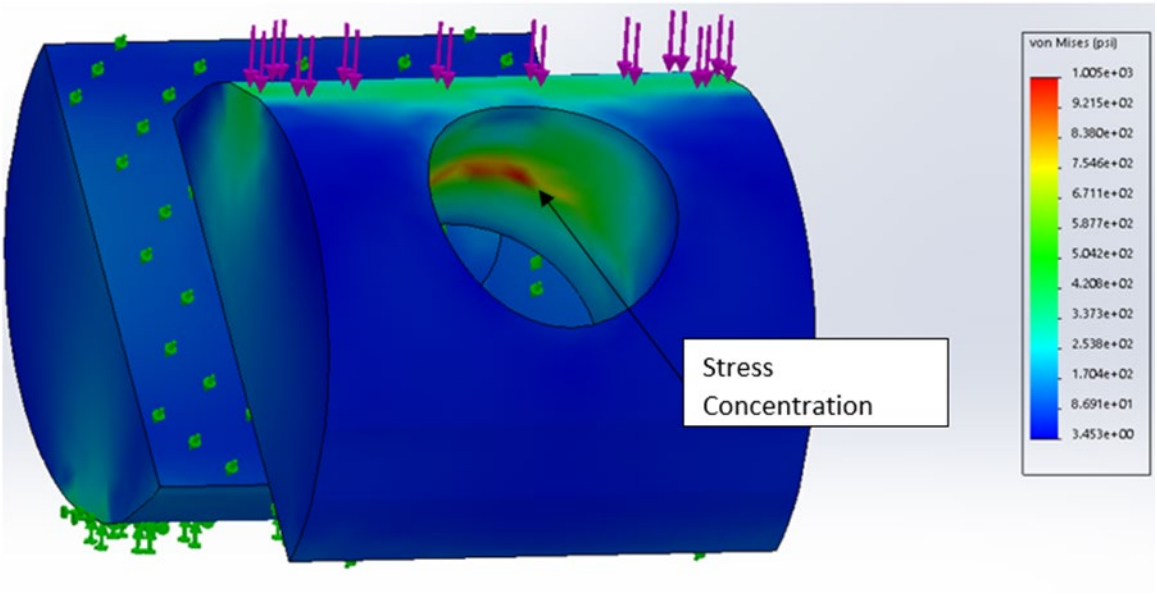

Figure 30: Von Mises stress model of apparatus under 1100 lbf load showing that the stress concentration under the max load does not approach the yield point for 6061 alloy aluminum.

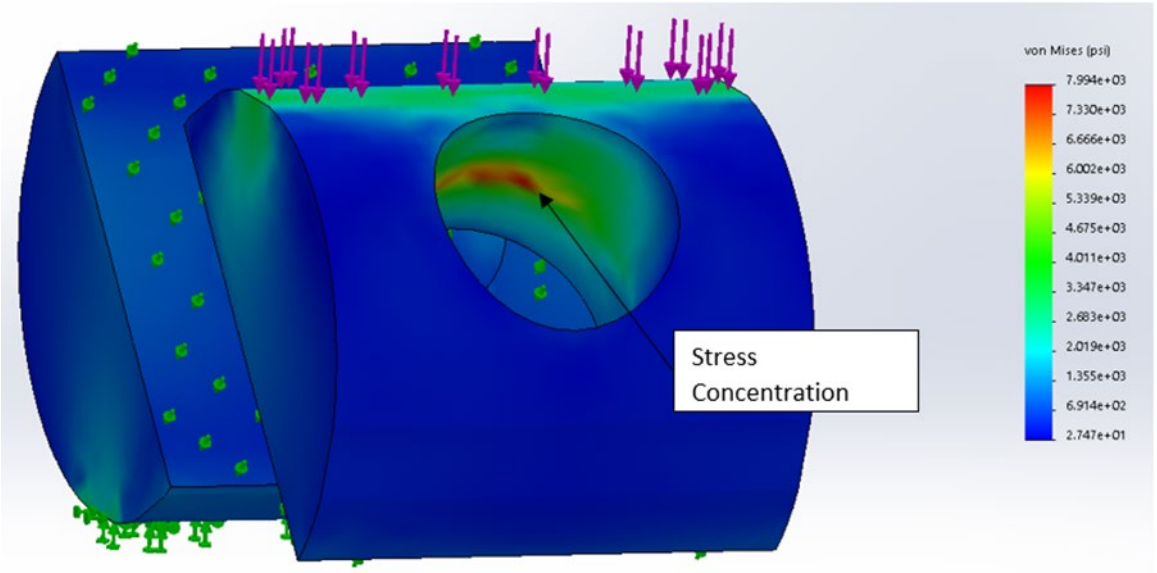

Figure 31: Von Mises stress model of apparatus under 8750 lbf load.

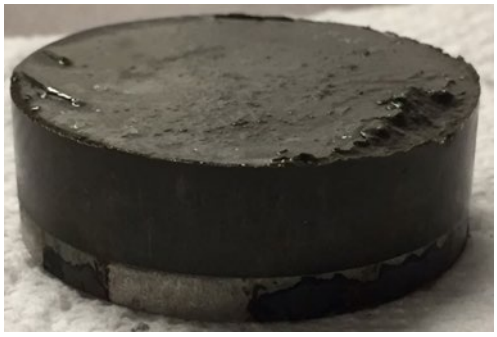

Figure 32: Shear bond strength sample.

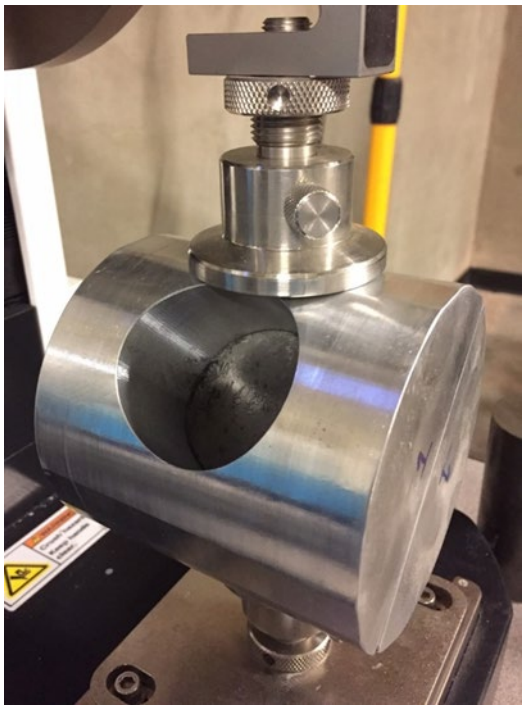

Figure 33: Shear bond testing apparatus with sample at 45° alignment on Mark-10 load frame.

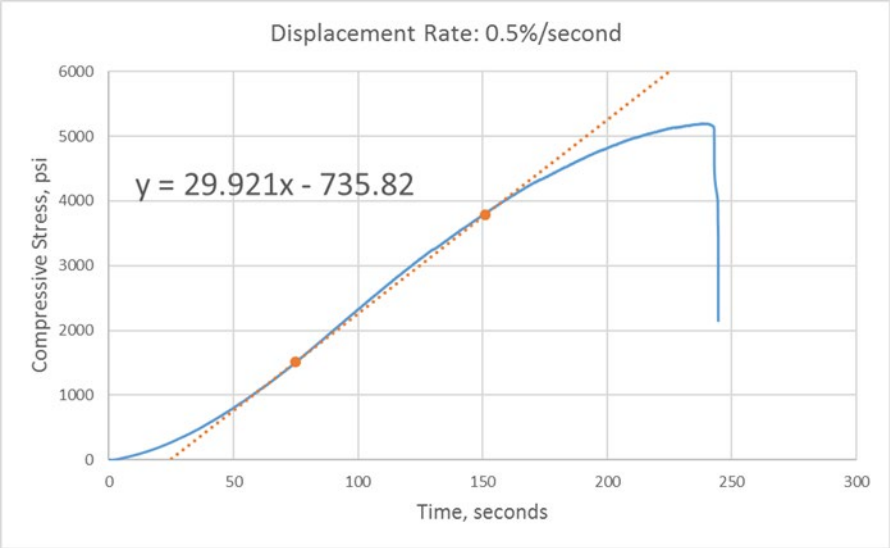

Figure 34: Compressive stress and time plotted to determine a displacement rate that would yield a stressing rate of 35±7psi/s.

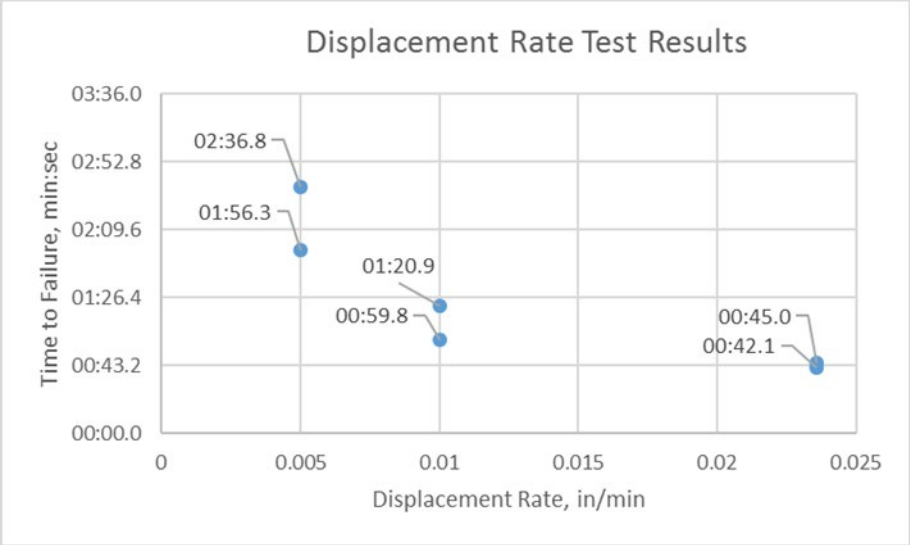

Figure 35: Brazilian tensile testing displacement rate trials.

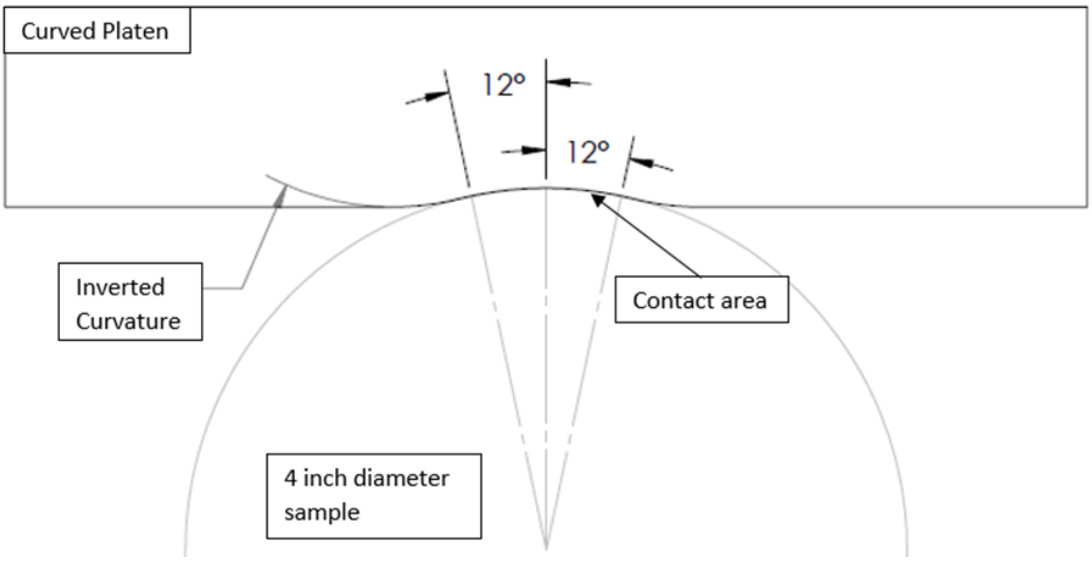

Figure 36: Detailed sketch of Brazilian loading platen design.

Figure 37: OFI Testing Equipment high pressure, high temperature fluid loss tester.

Figure 38: Fann 35A Rheology tester.

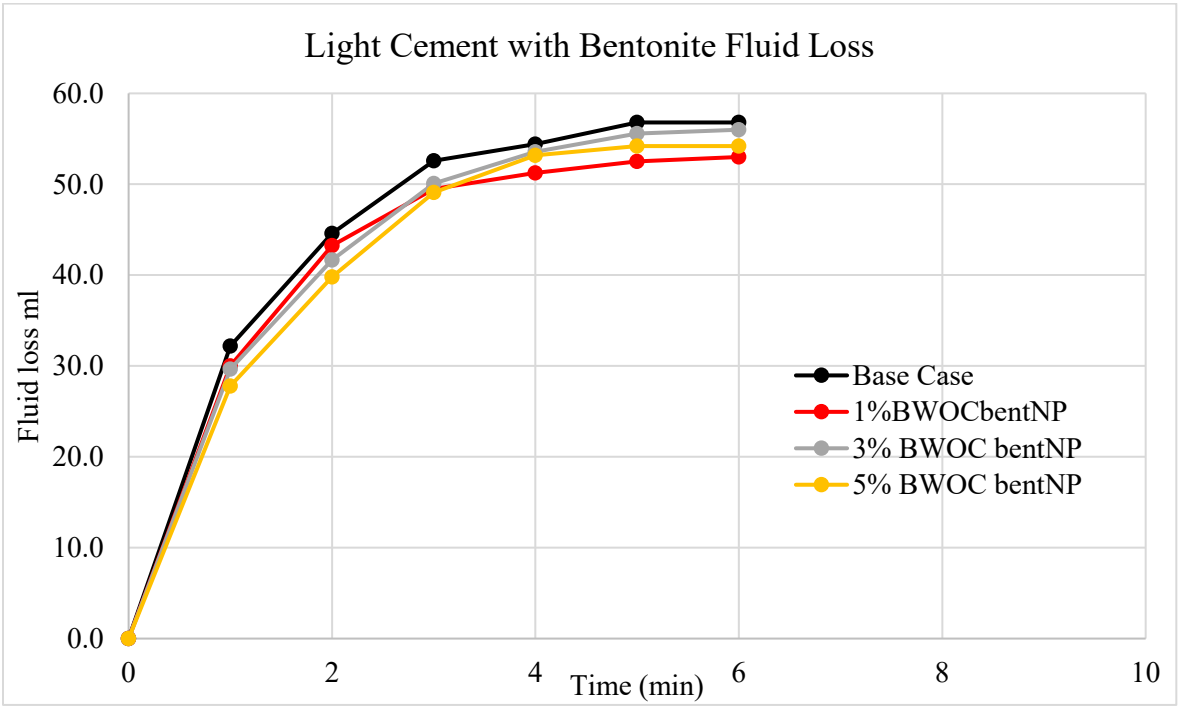

Figure 39: Fluid loss results for light cement with bentonite nanoparticles.

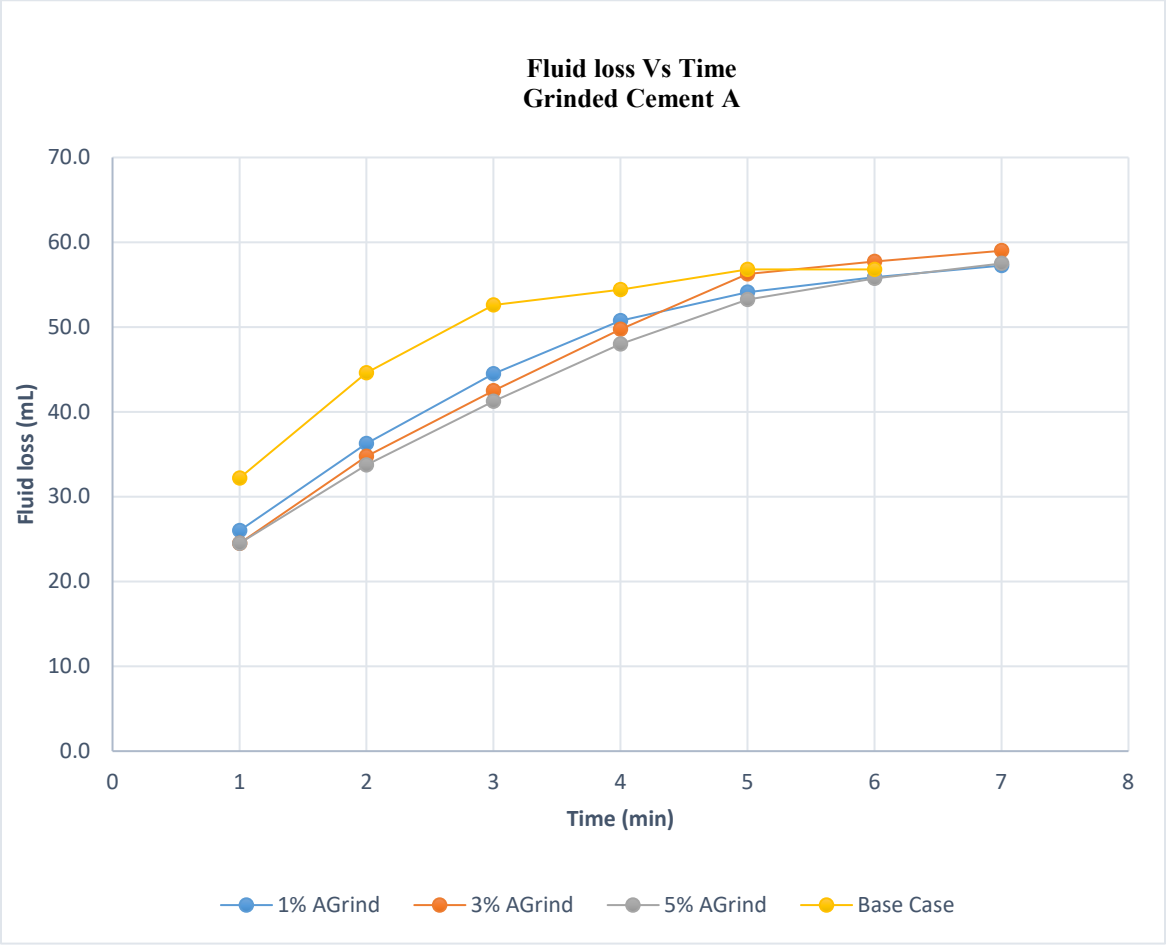

Figure 40: Fluid loss results for light cement with light cement nanoparticles.

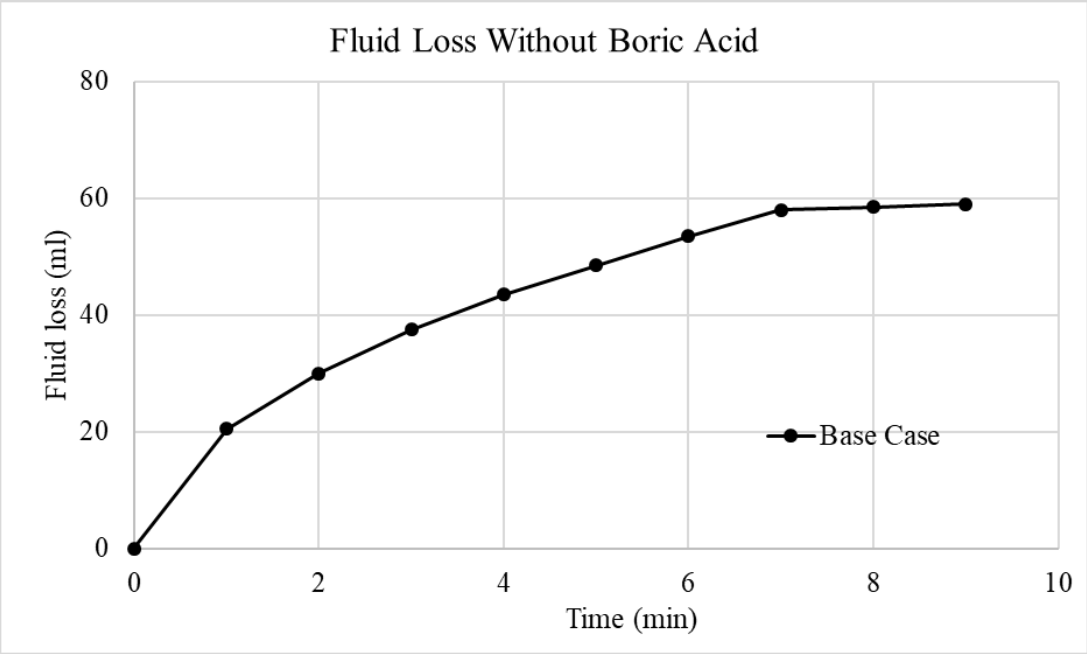

Figure 41: Fluid loss results for light cement base case.

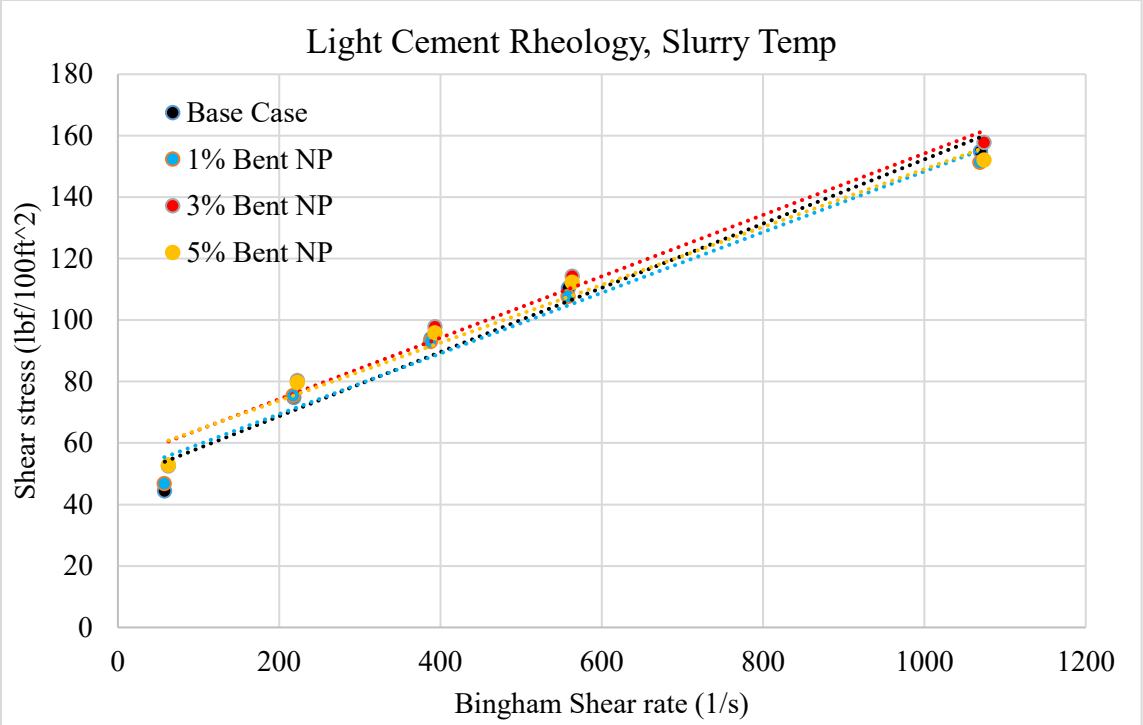

Figure 42: Rheology result for light cement base case with bentonite nanoparticles.

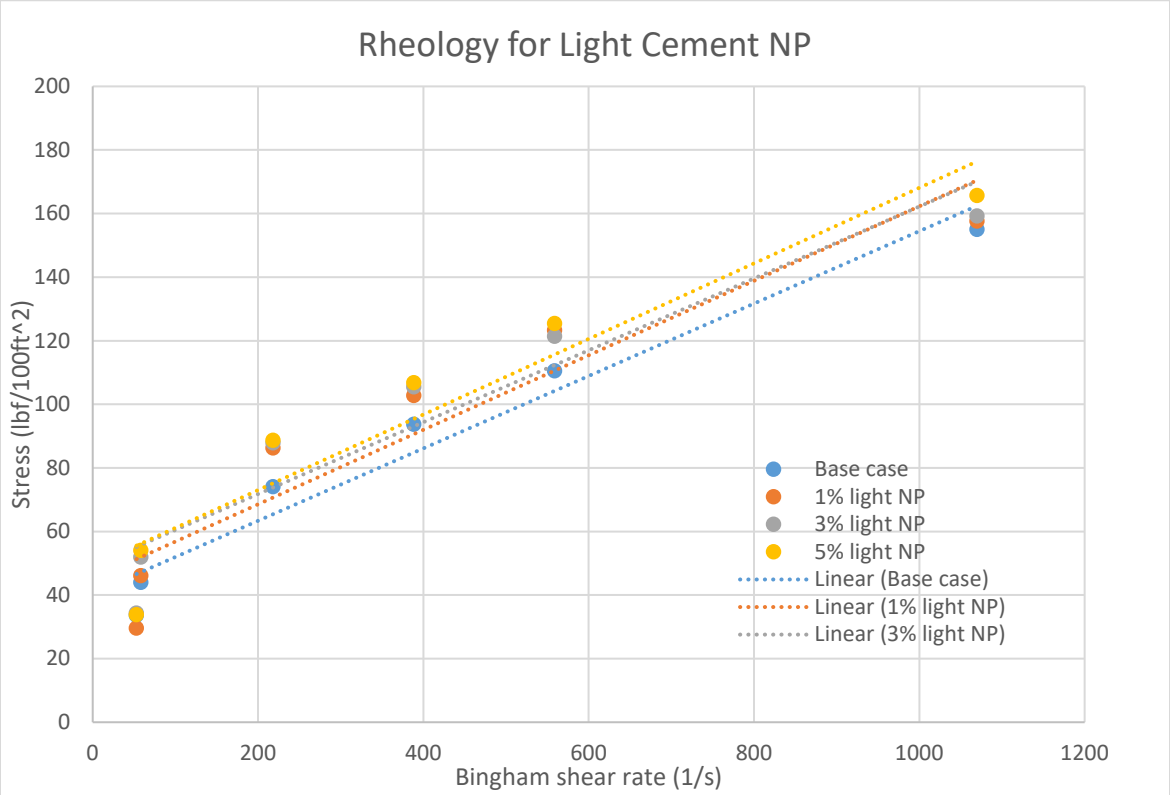

Figure 43: Rheology result for light cement with light cement nanoparticles.

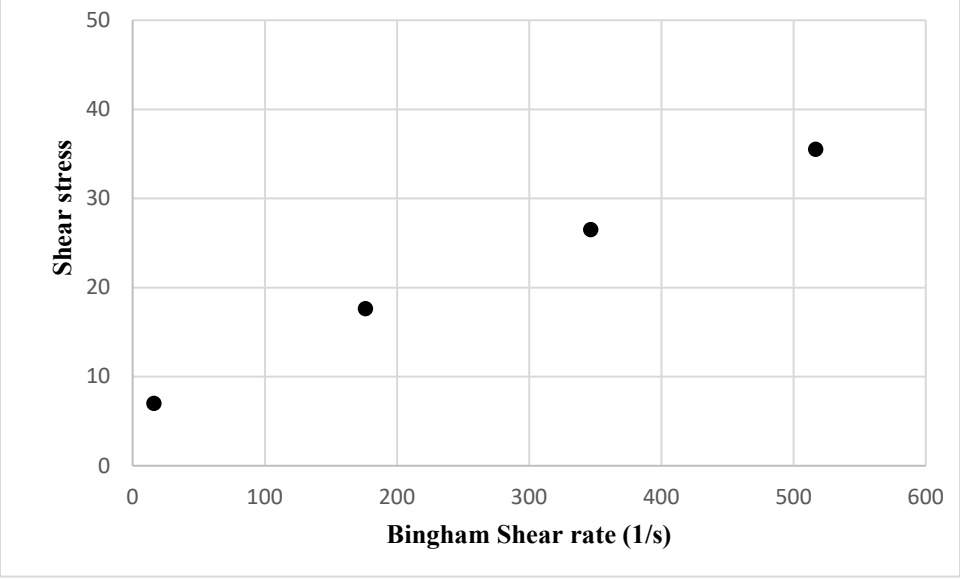

Figure 44: Rheology result for light cement base case with bentonite nanoparticles.

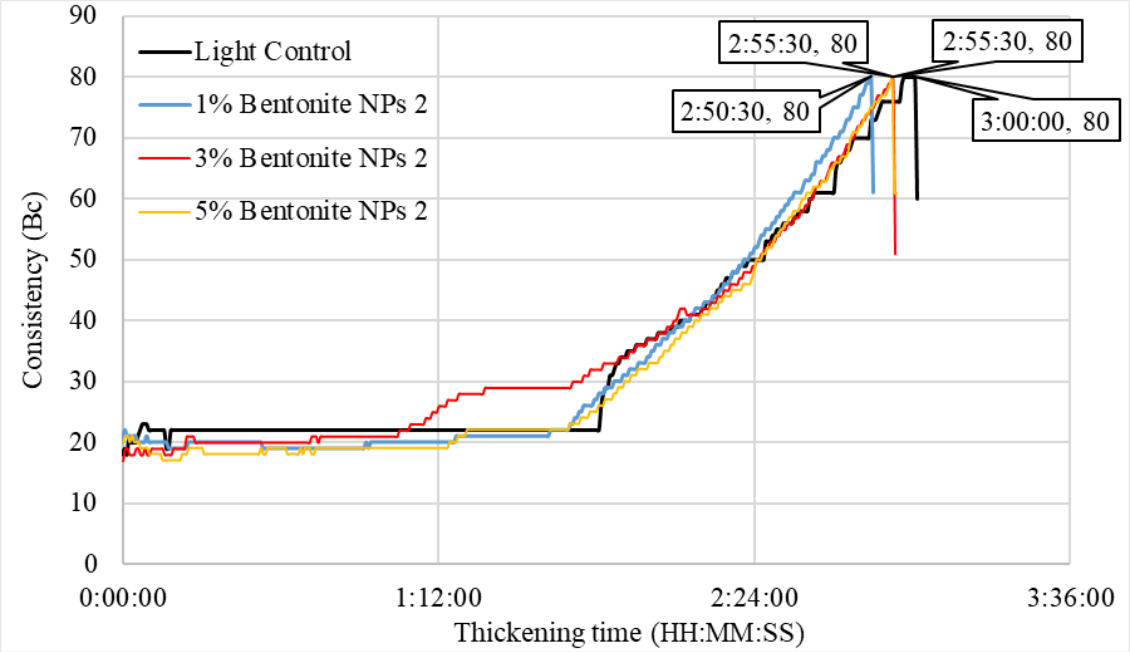

Figure 45: Round 1 Light base case with (1%, 3%, and 5% BWOC) bentonite nanoparticles.

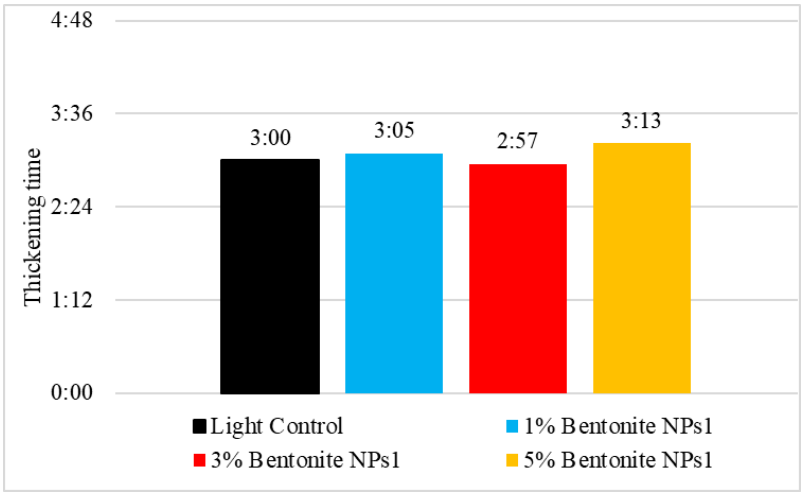

Figure 46: Round 1 Light base case with (1%, 3%, and 5% BWOC) bentonite nanoparticles.

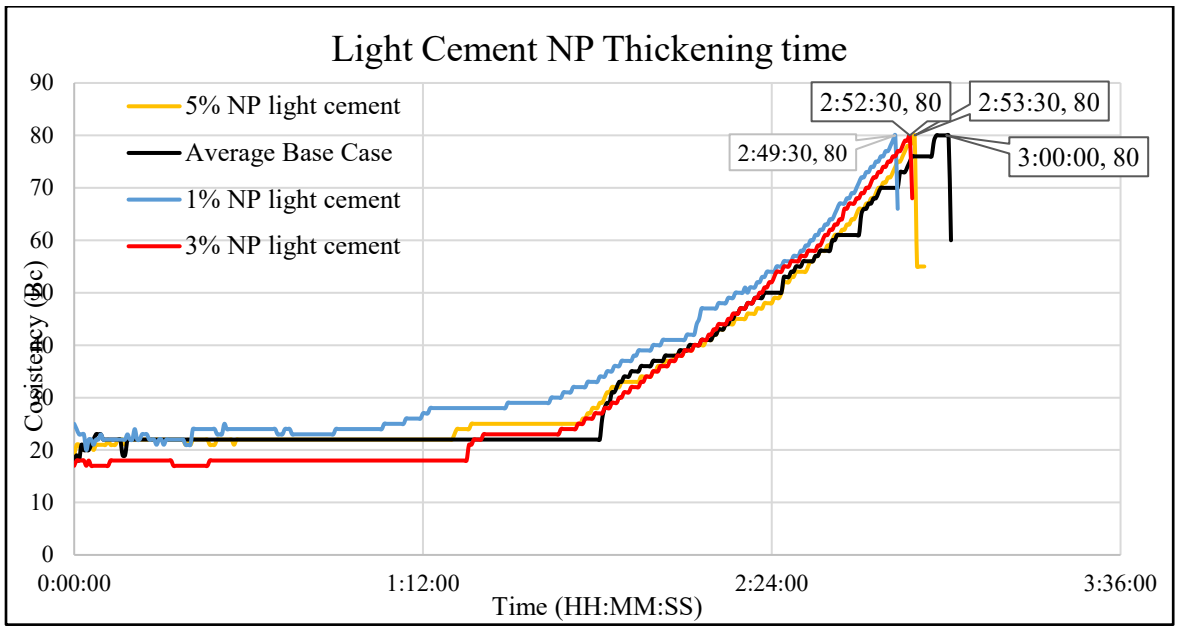

Figure 47: Light cement base case with (1%, 3%, and 5% BWOC) light cement nanoparticles.

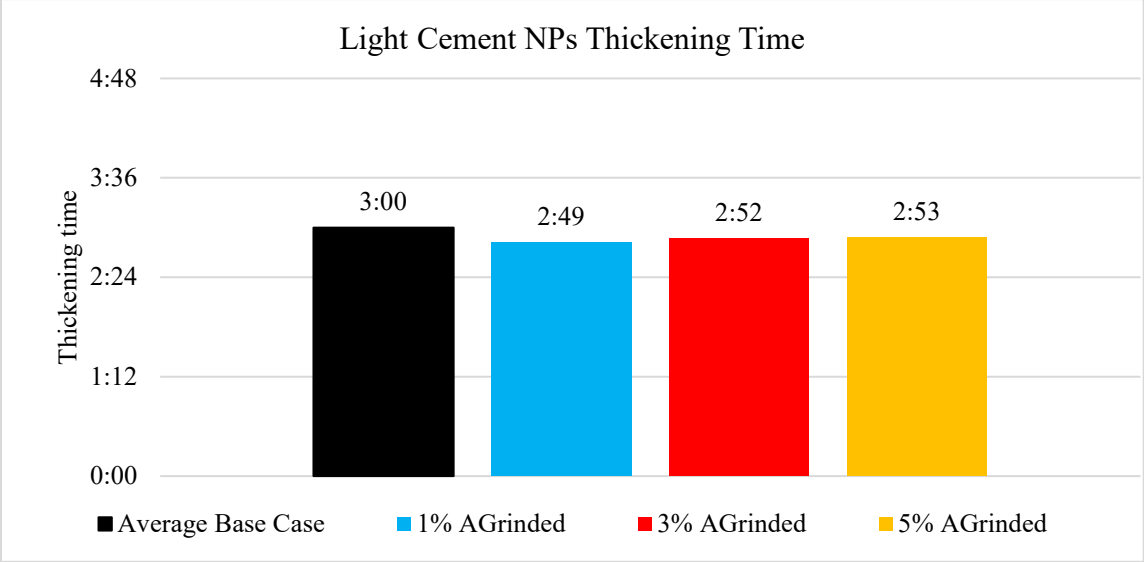

Figure 48: Light base case with (1%, 3%, and 5% BWOC) light cement nanoparticles.

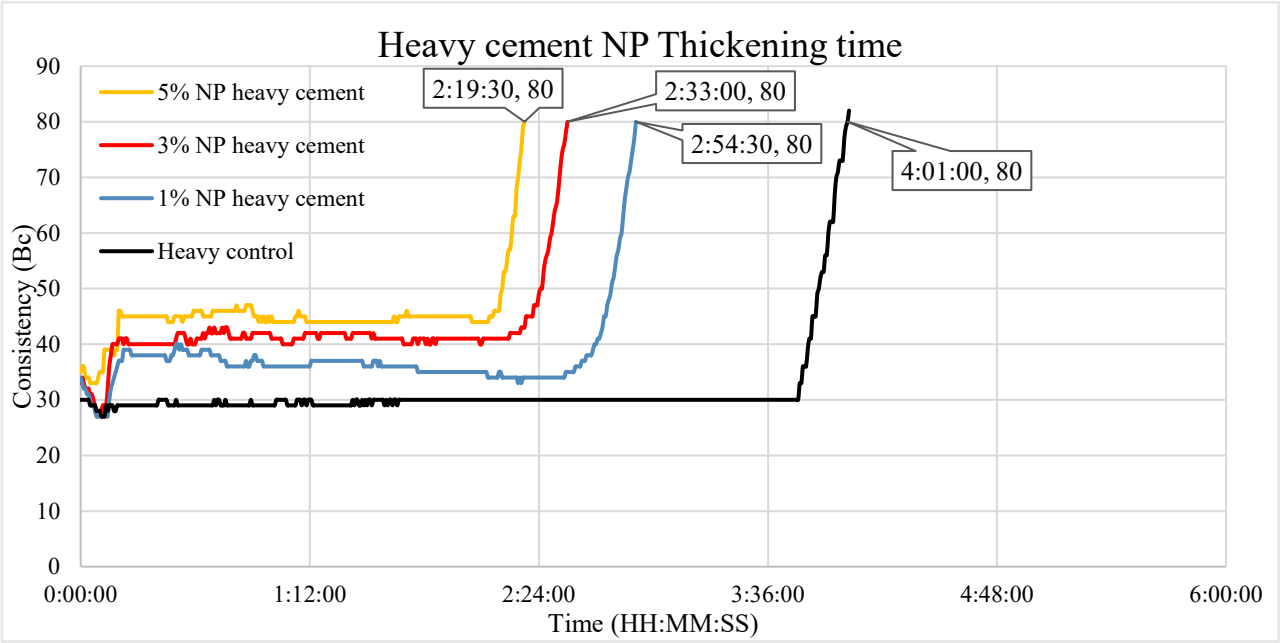

Figure 49: Heavy base case with (1%, 3%, and 5% BWOC) heavy cement nanoparticles.

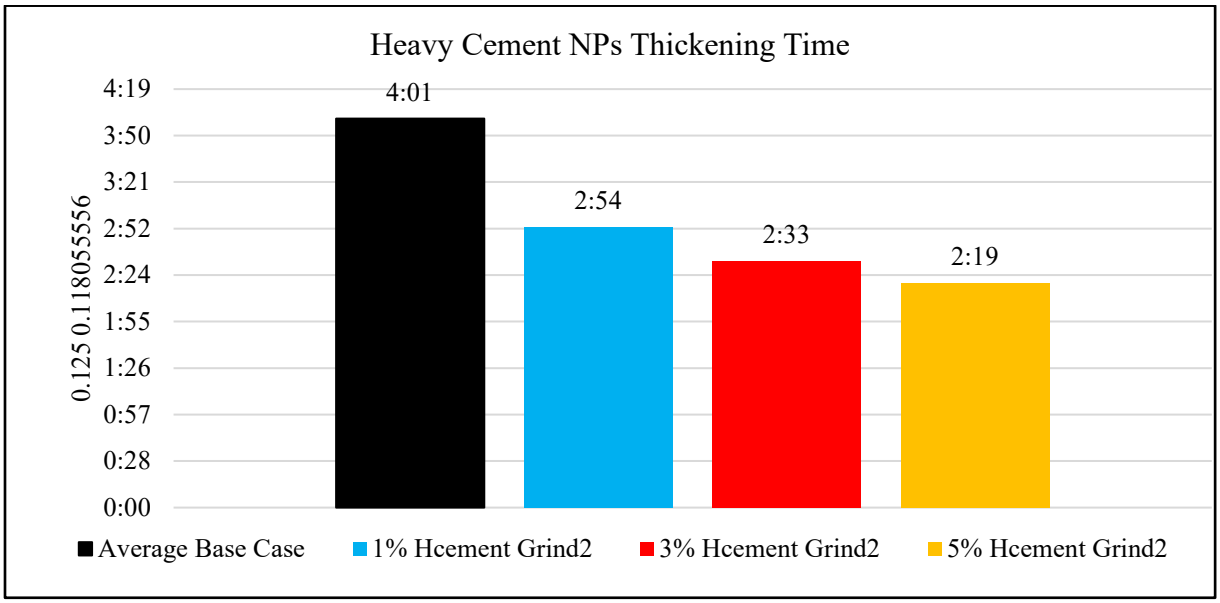

Figure 50: Heavy base case with (1%, 3%, and 5% BWOC) heavy cement nanoparticles.

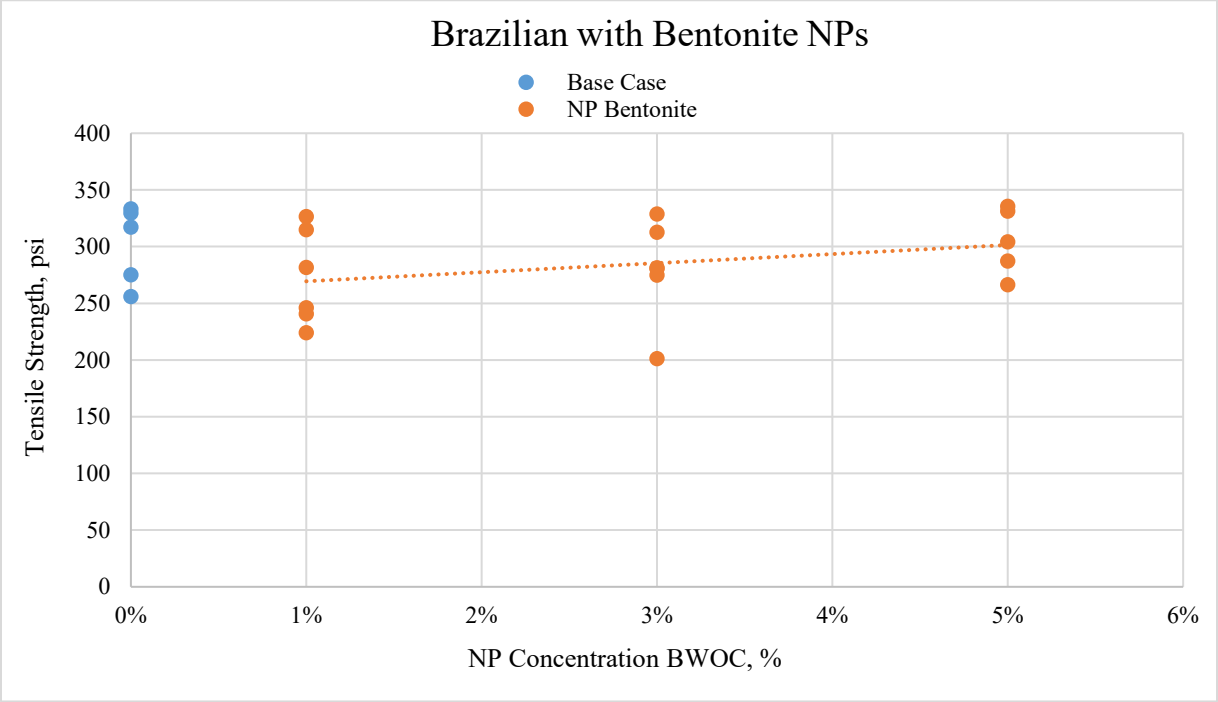

Figure 51: Average tensile strengths seen for Bentonite nanoparticles.

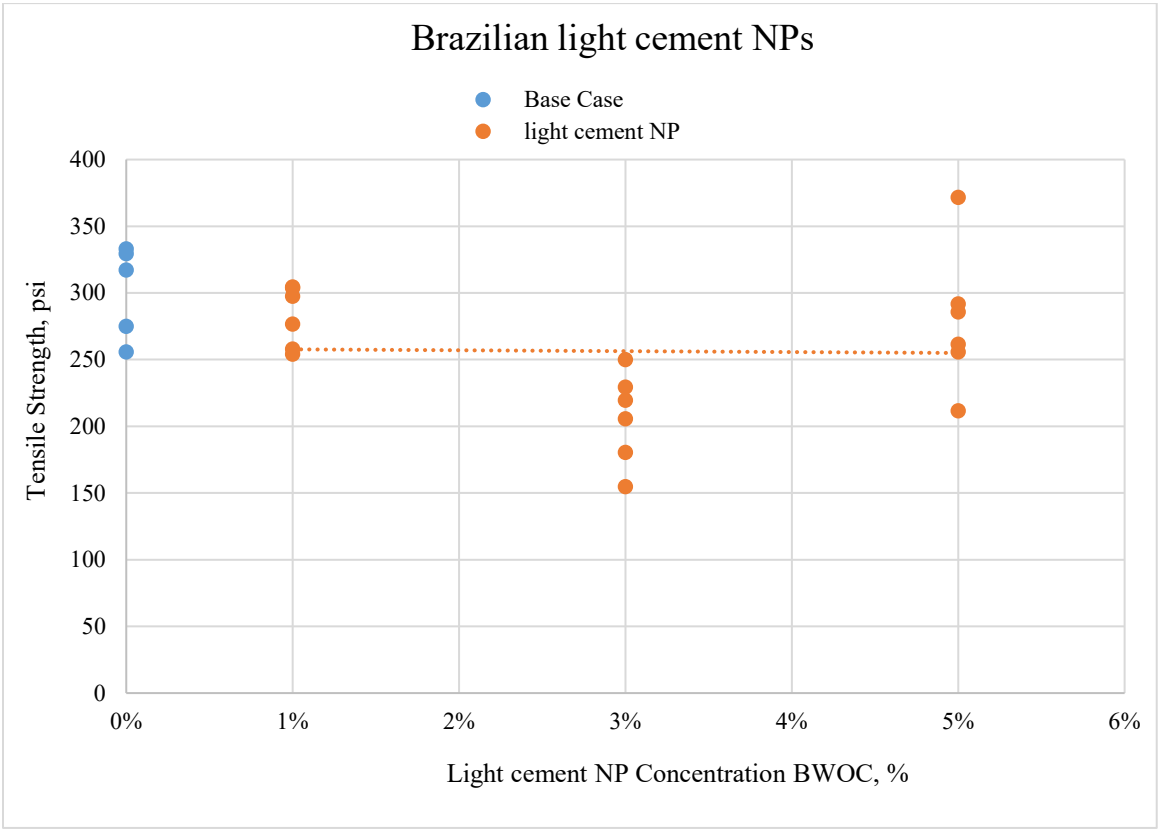

Figure 52: Average tensile strengths seen for light cement nanoparticles.

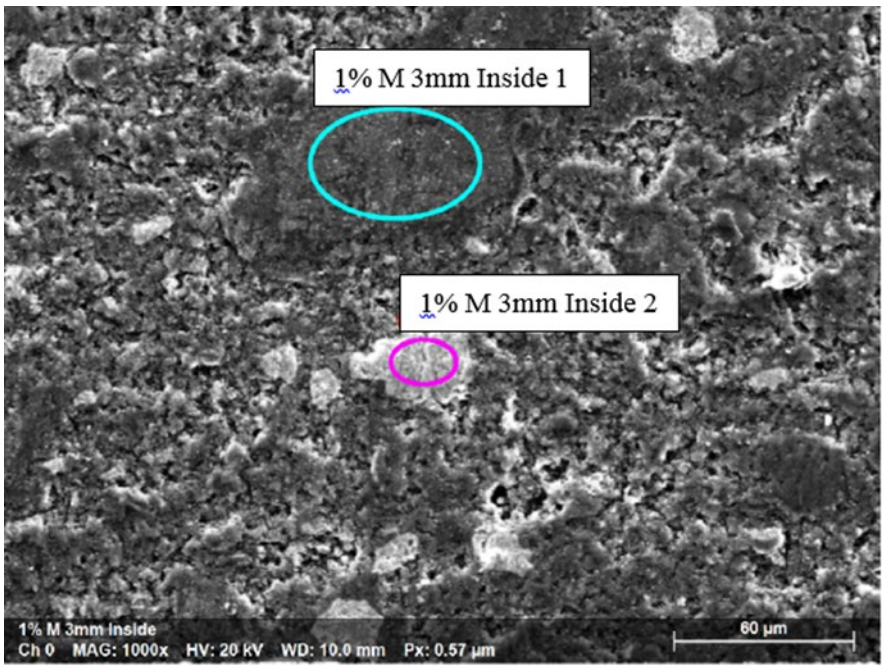

Figure 53: Pocket of barite observed (point 2) through scanning electron microscope roughly 3mm from the core wall of a 1% nanoparticle magnetite sample.

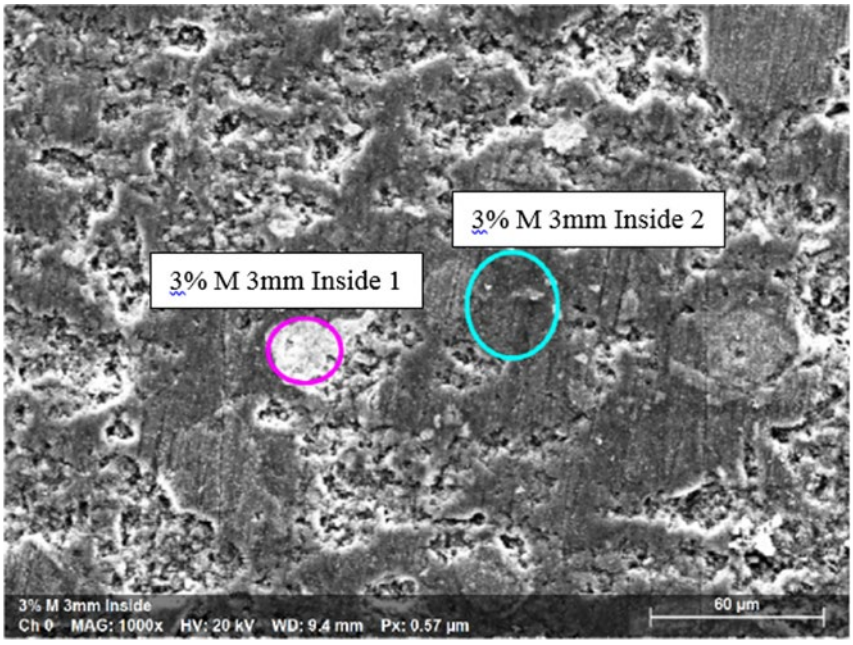

Figure 54: Pocket of barite observed (point 1) through scanning electron microscope roughly 3mm from the core wall of a 1% nanoparticle magnetite sample.

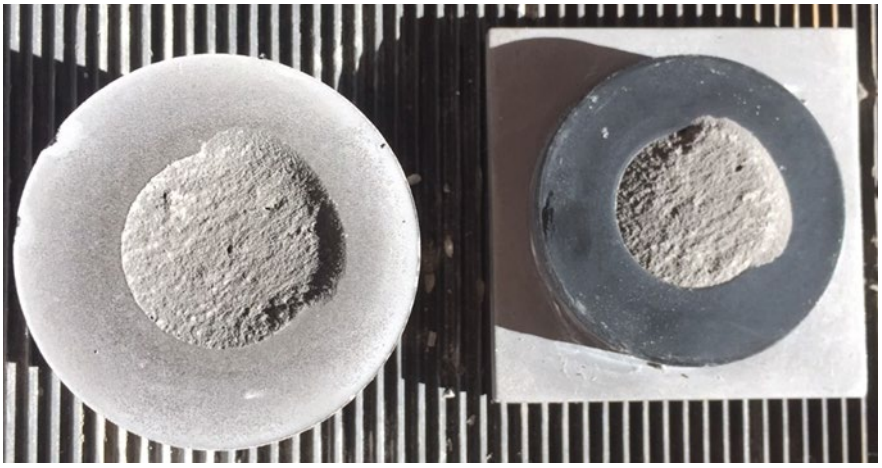

Figure 55: Tensile failure seen within the cement body after tensile bond testing.

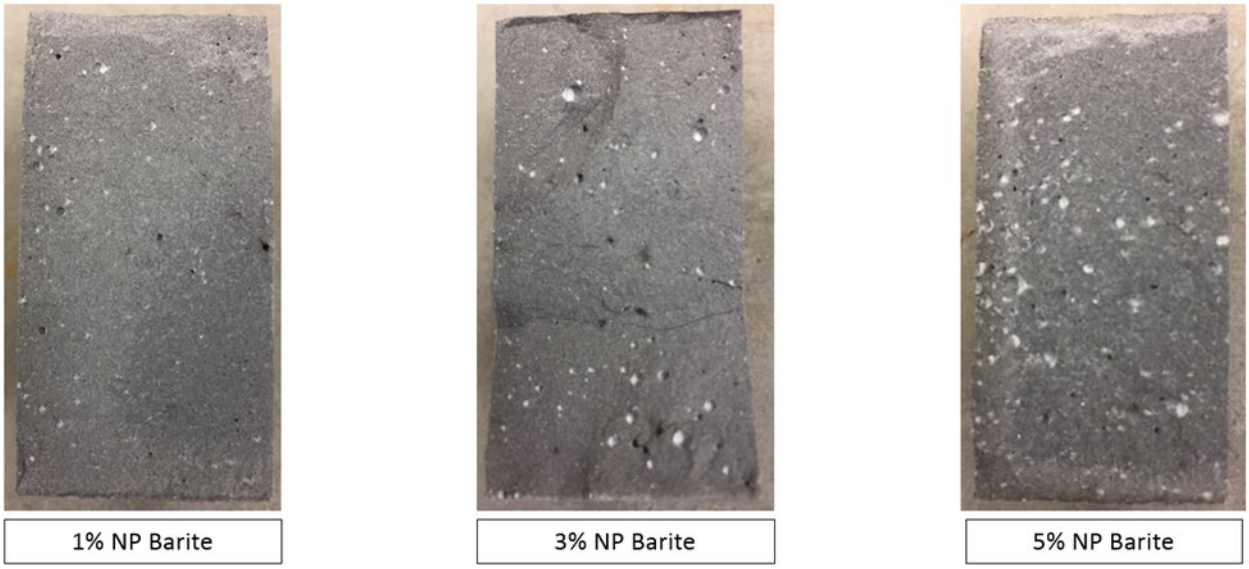

Figure 56: Cross sectional views of nanoparticle barite samples. Note the increasing frequency and size of the pores with the increasing nanoparticle concentrations.

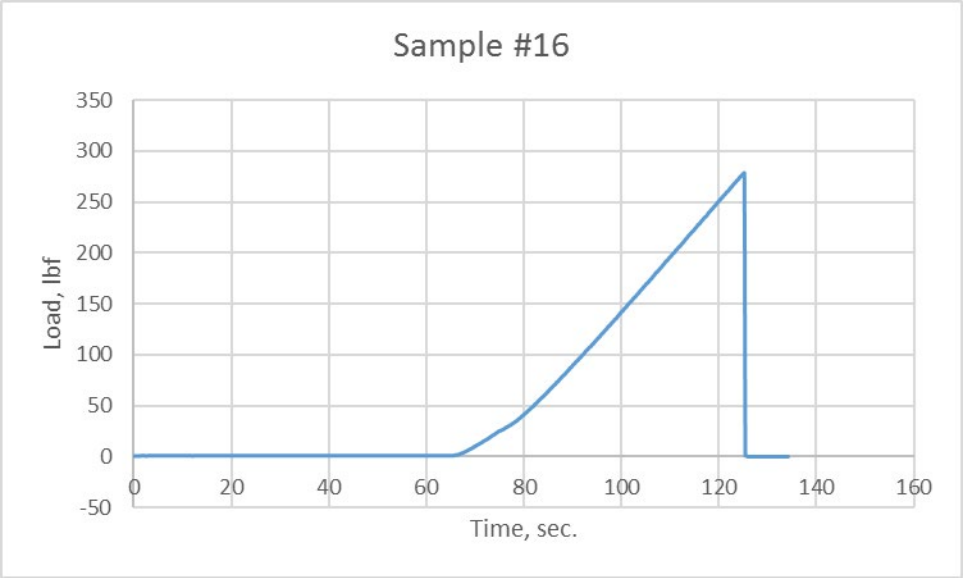

Figure 57: Loading plot of a completely bonded shear bond strength sample.

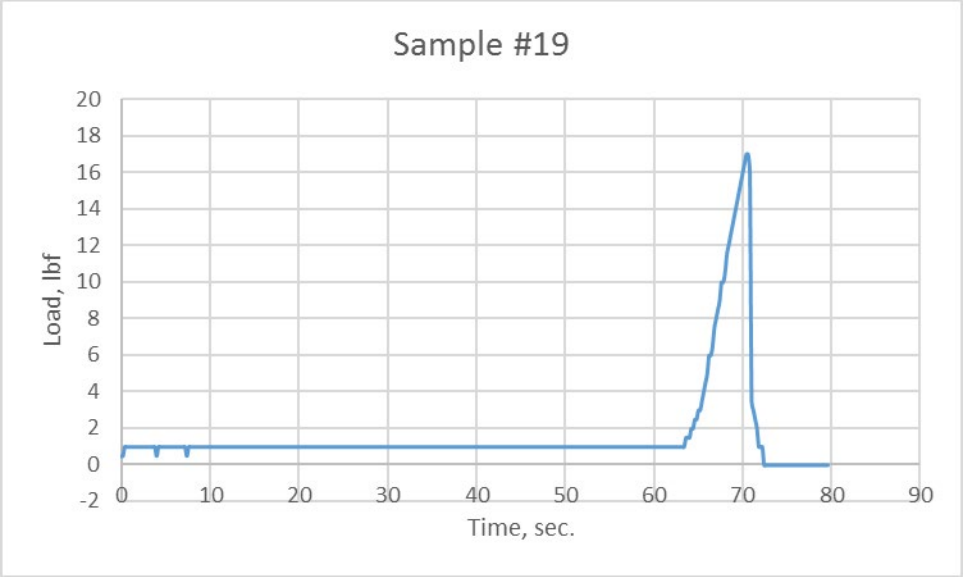

Figure 58: Loading plot of a partially bonded shear bond strength sample.

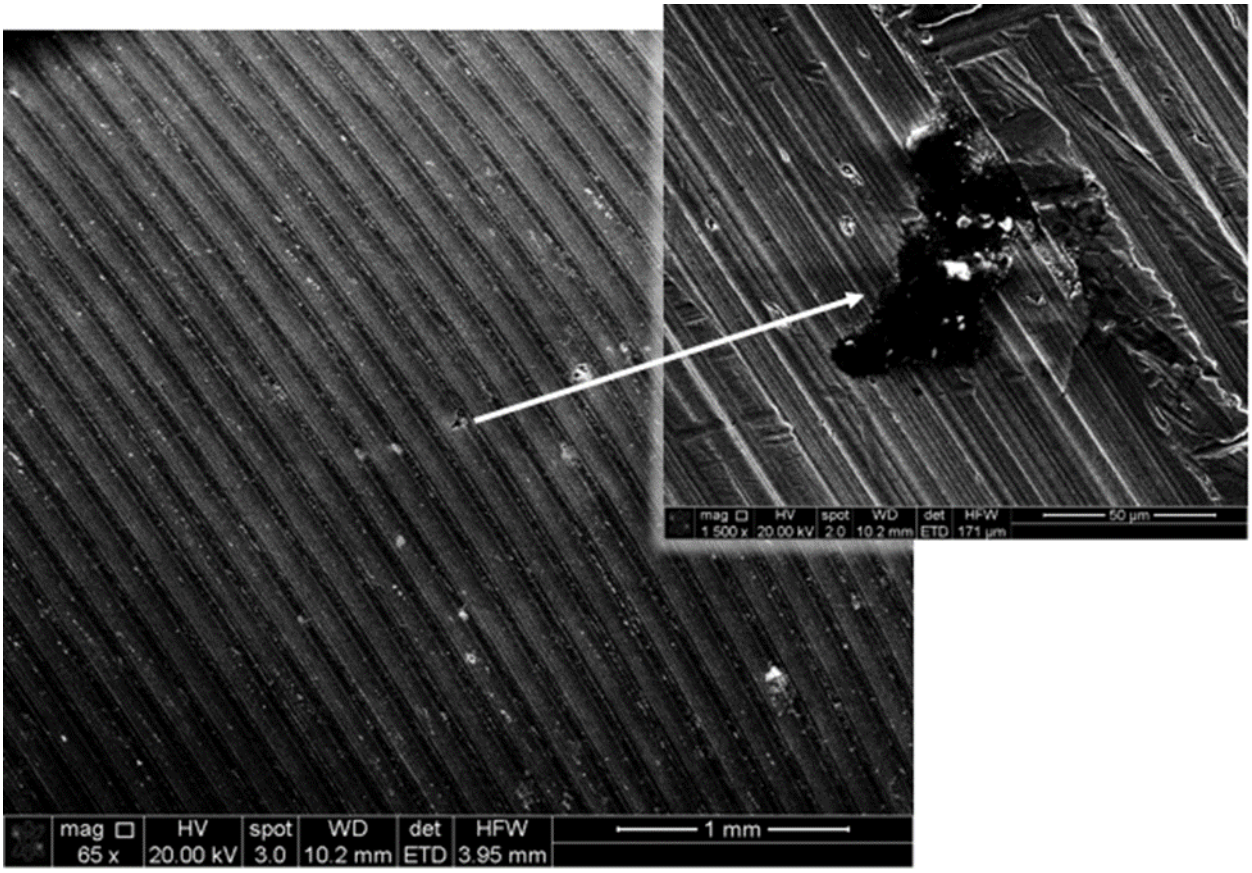

Figure 59: Scanning electron microscope view of residual cement deposits on steel substrate surface.

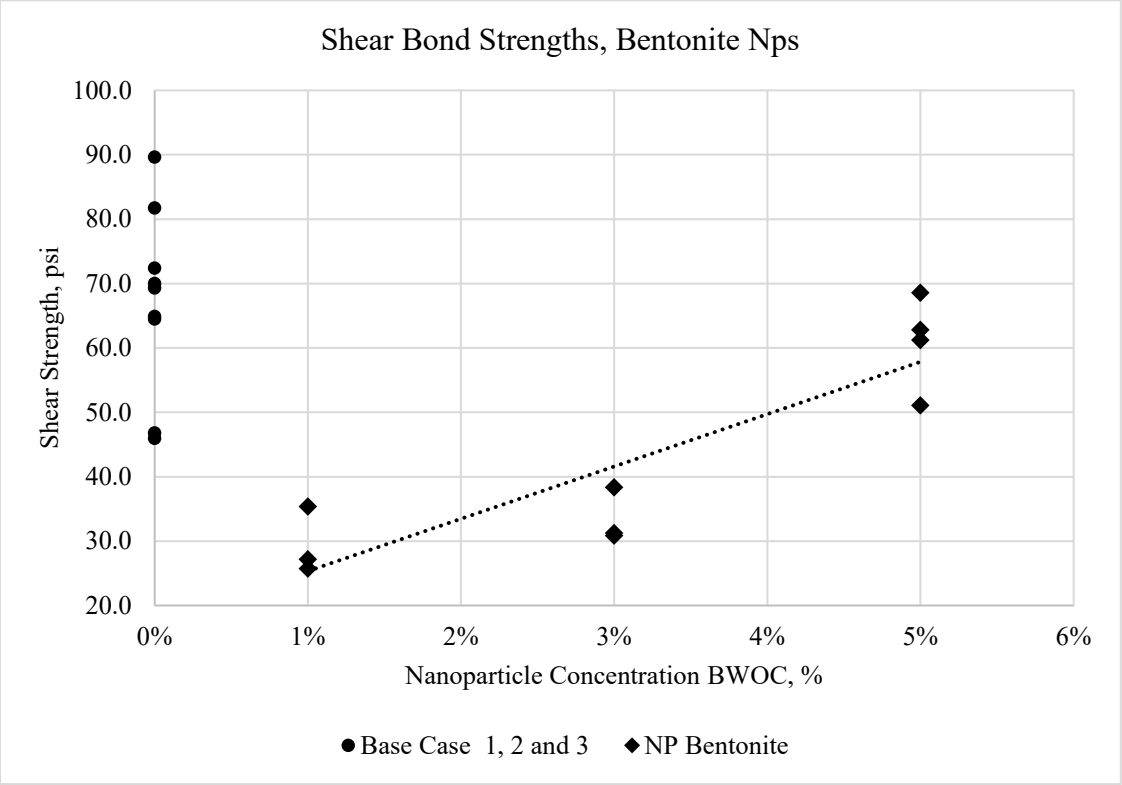

Figure 60: Observed shear strengths plotted with concentrations of nanoparticle bentonite.

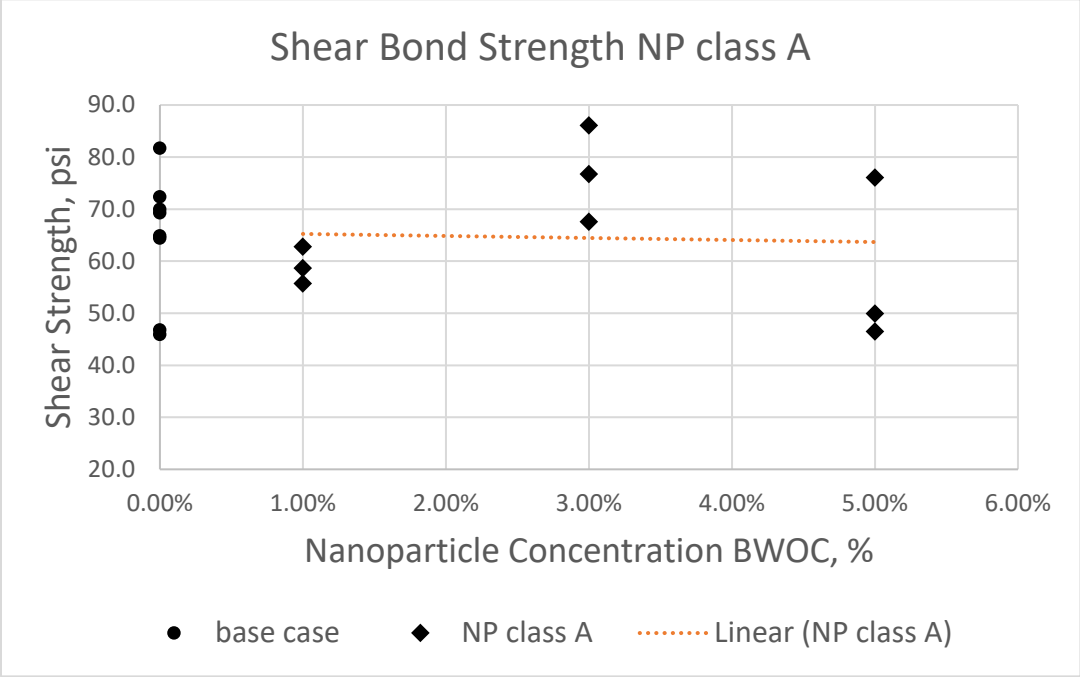

Figure 61: Observed shear strengths plotted with concentrations of nanoparticle cement class A.

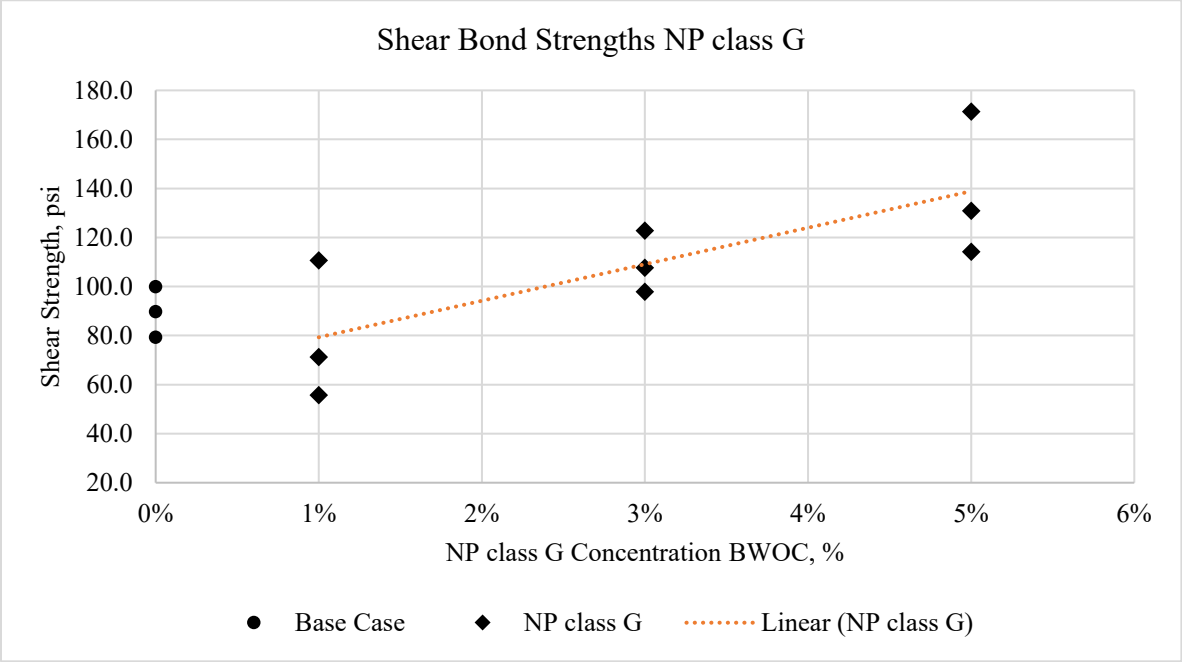

Figure 62: Observed shear strengths plotted with concentrations of nanoparticle cement class G.

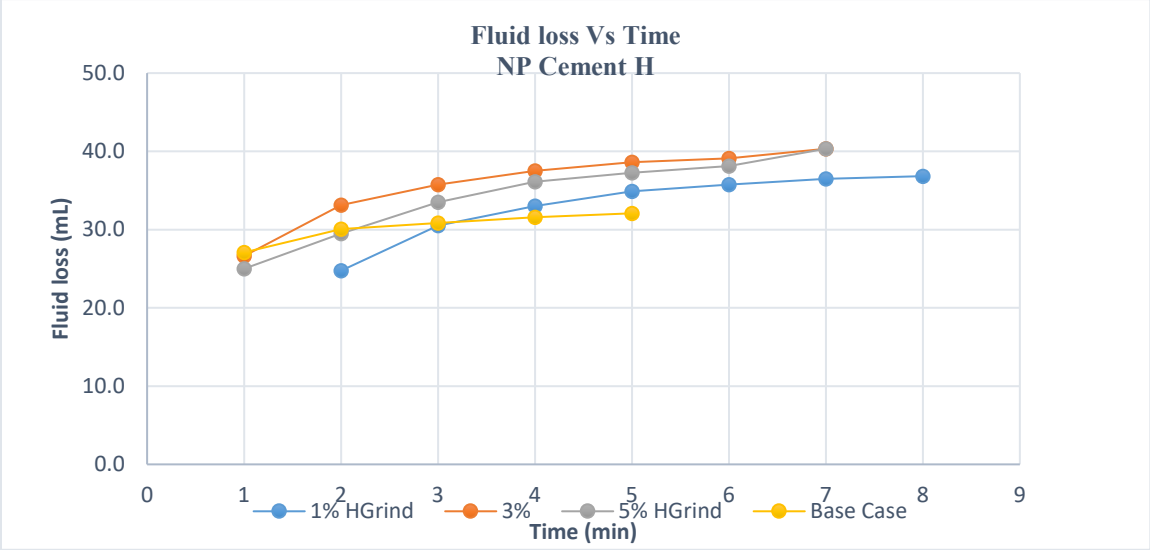

Figure 63: Fluid loss results for heavy cement base case with light cement nanoparticles.

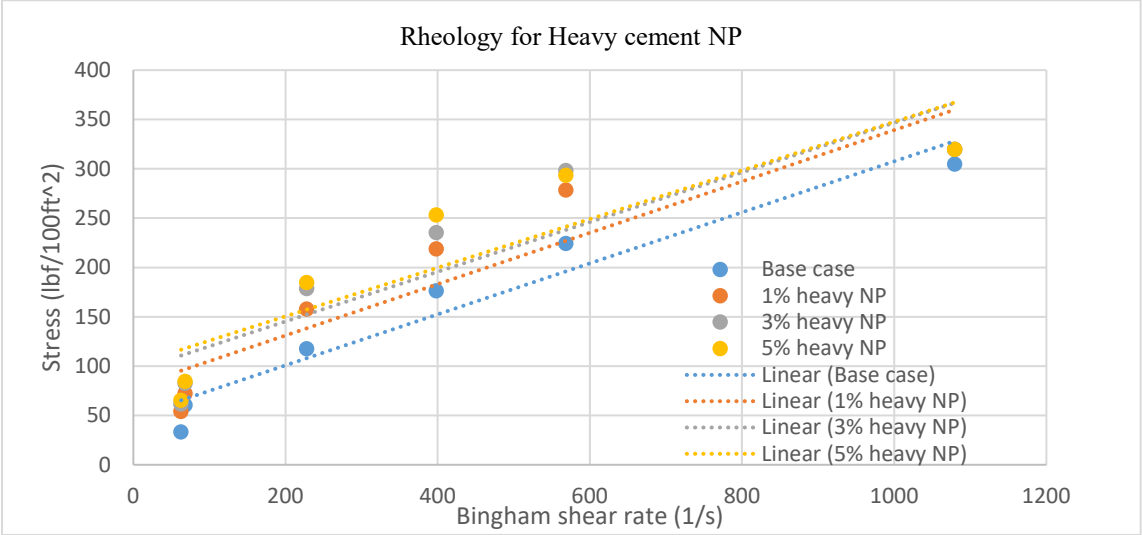

Figure 64: Rheology result for heavy cement base case with bentonite nanoparticles.

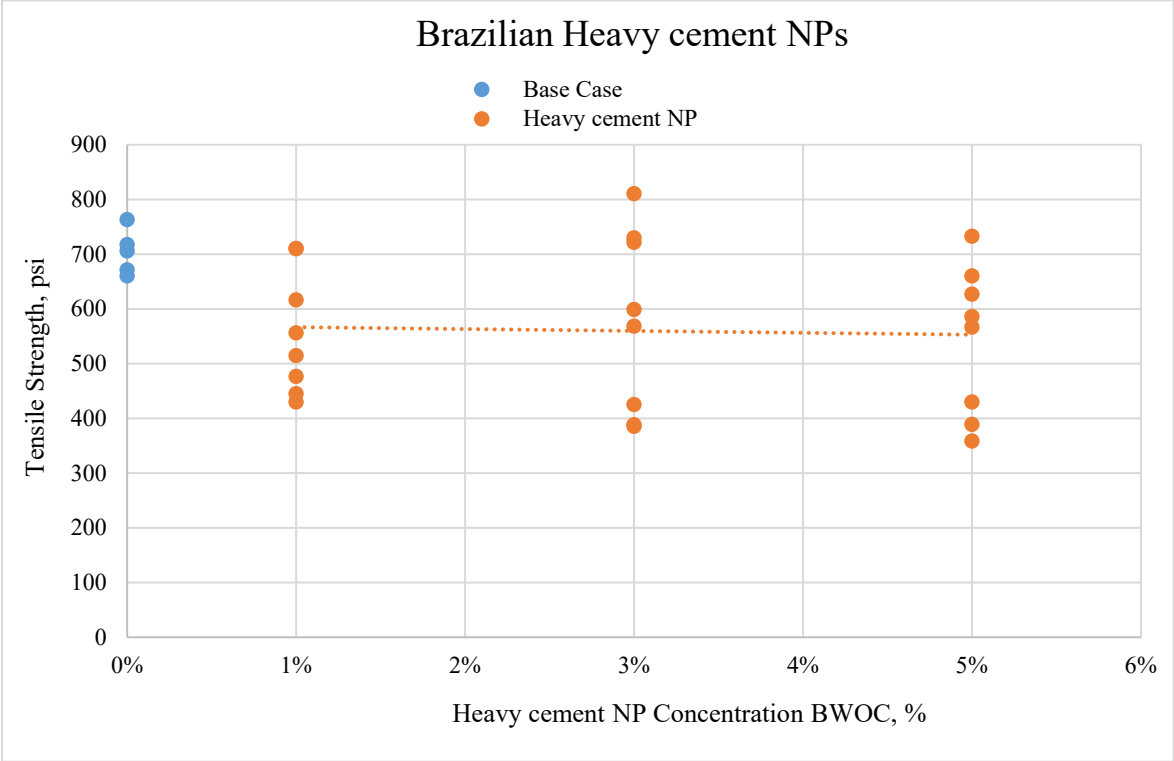

Figure 65: Average tensile strengths seen for heavy cement nanoparticles.

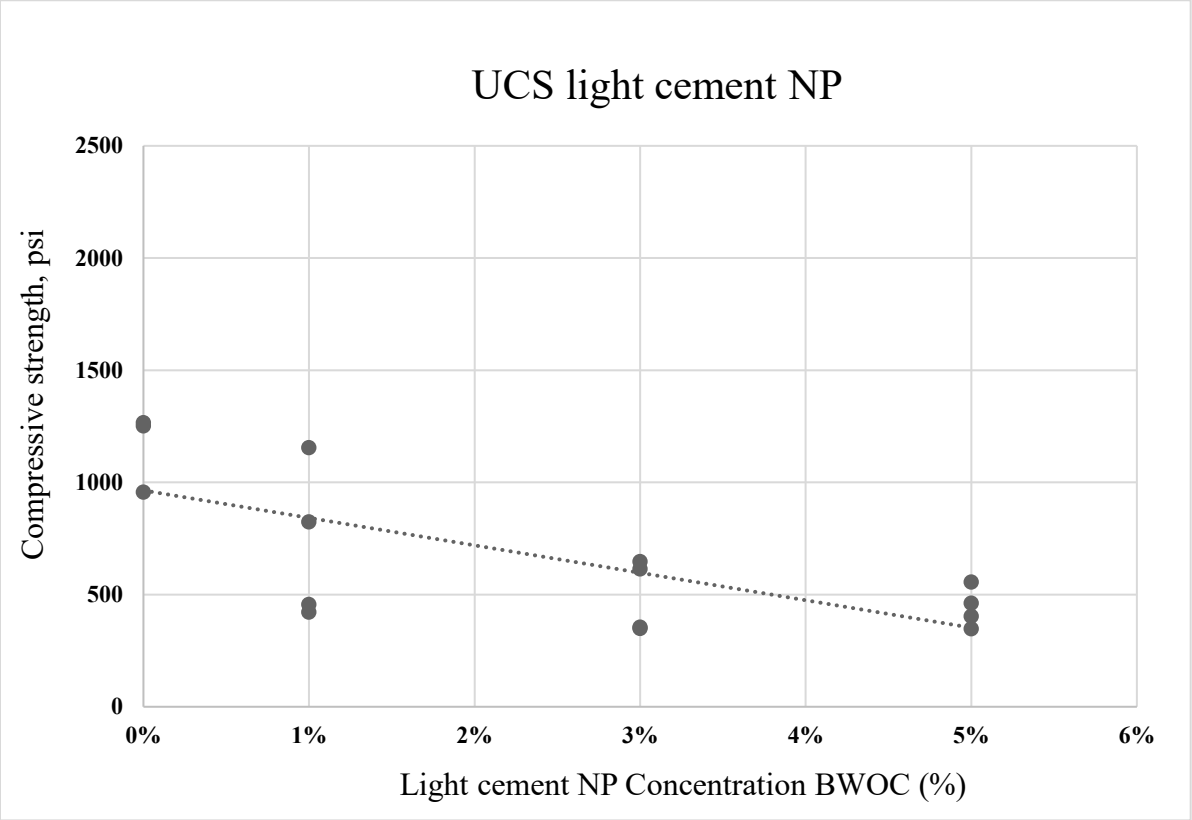

Figure 66: Unconfined compressive strength results for light cement nanoparticles.

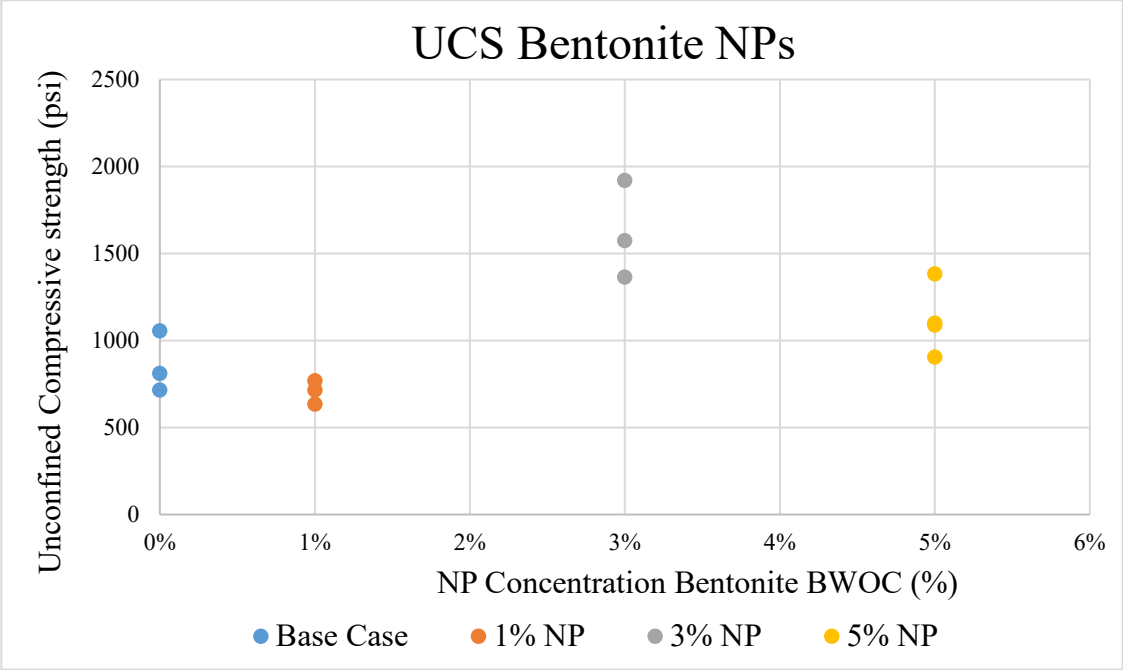

Figure 67: Unconfined compressive strength results for bentonite nanoparticles.

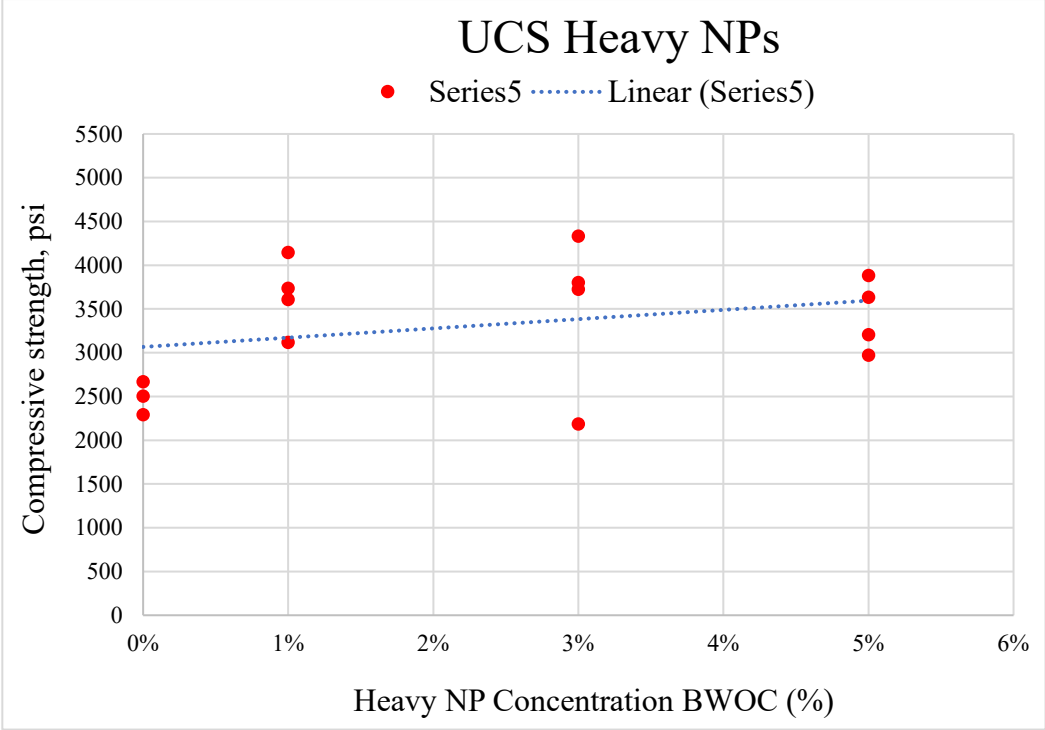

Figure 68: Unconfined compressive strength results for heavy cement nanoparticles.

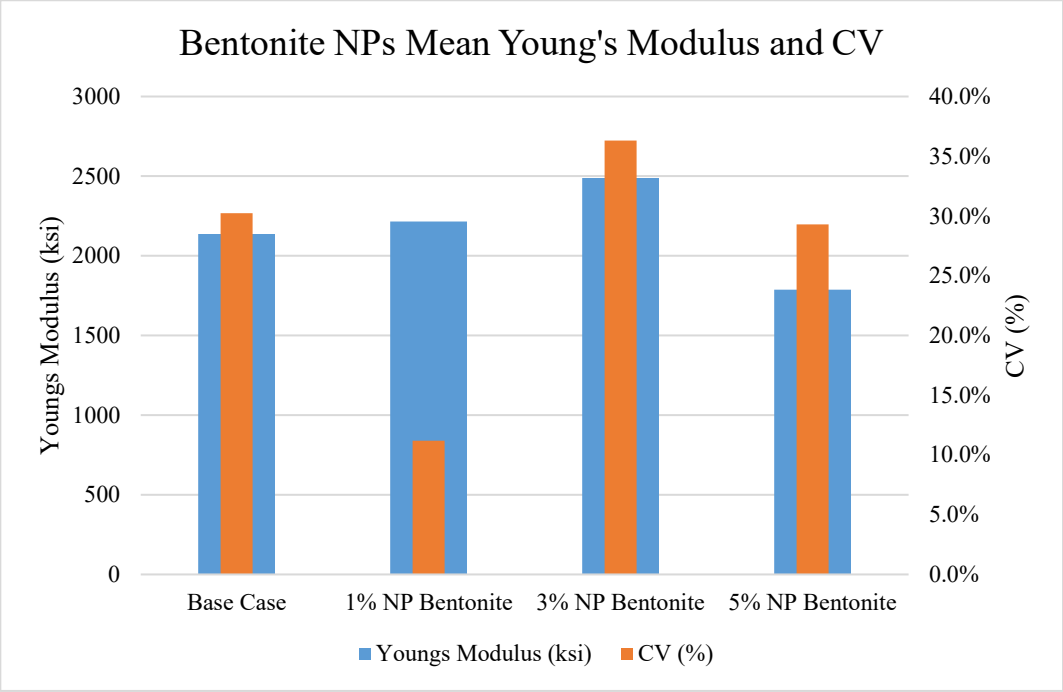

Figure 69: Mean Young's modulus and Variation results for base case and bentonite nanoparticles.

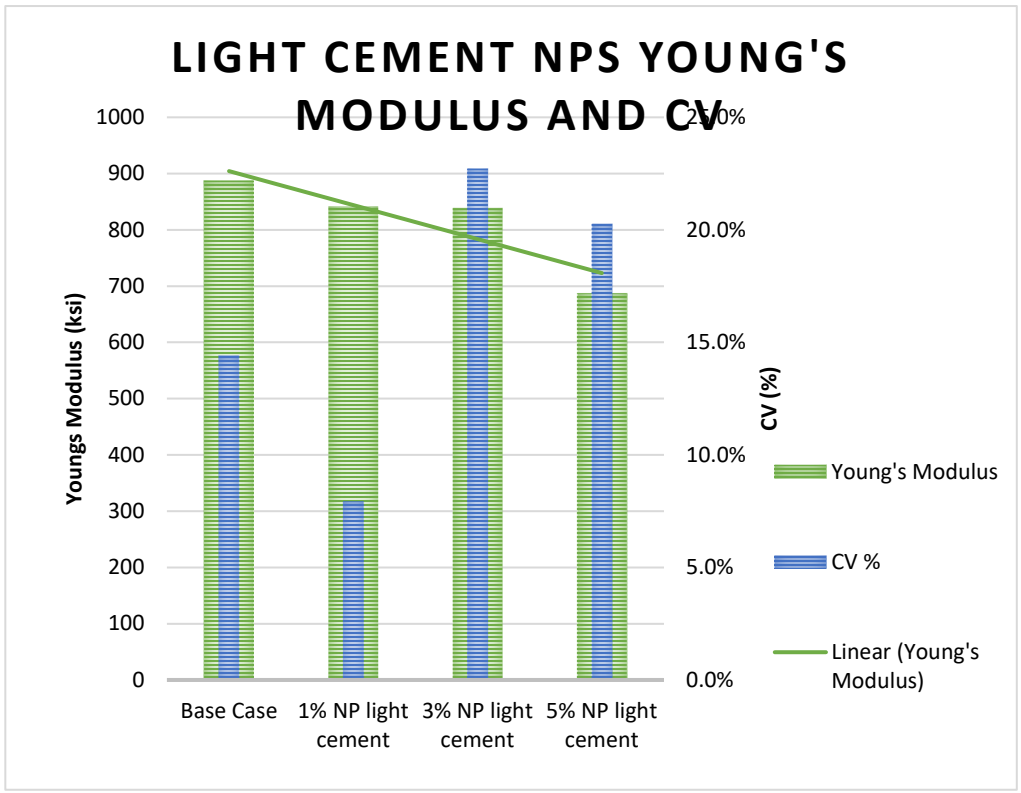

Figure 70: Mean Young's modulus and variation results for base case and light cement nanoparticles.

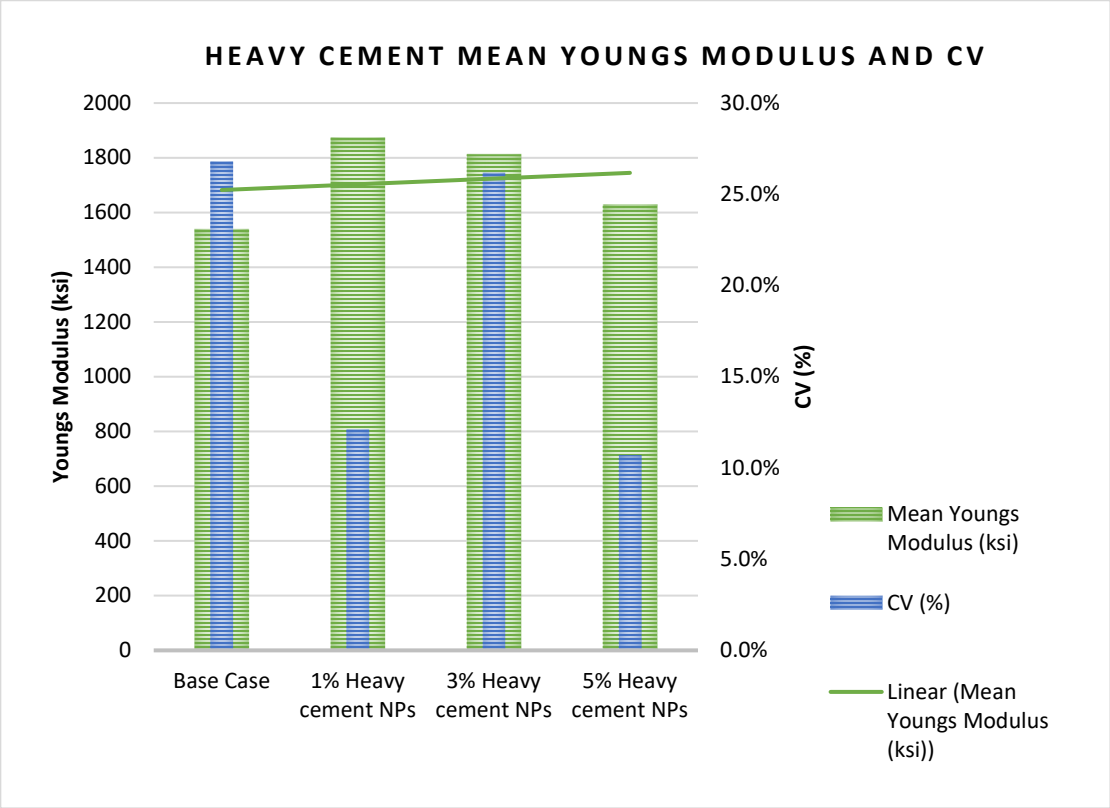

Figure 71: Mean Young's modulus and variation results for base case and heavy cement nanoparticles.

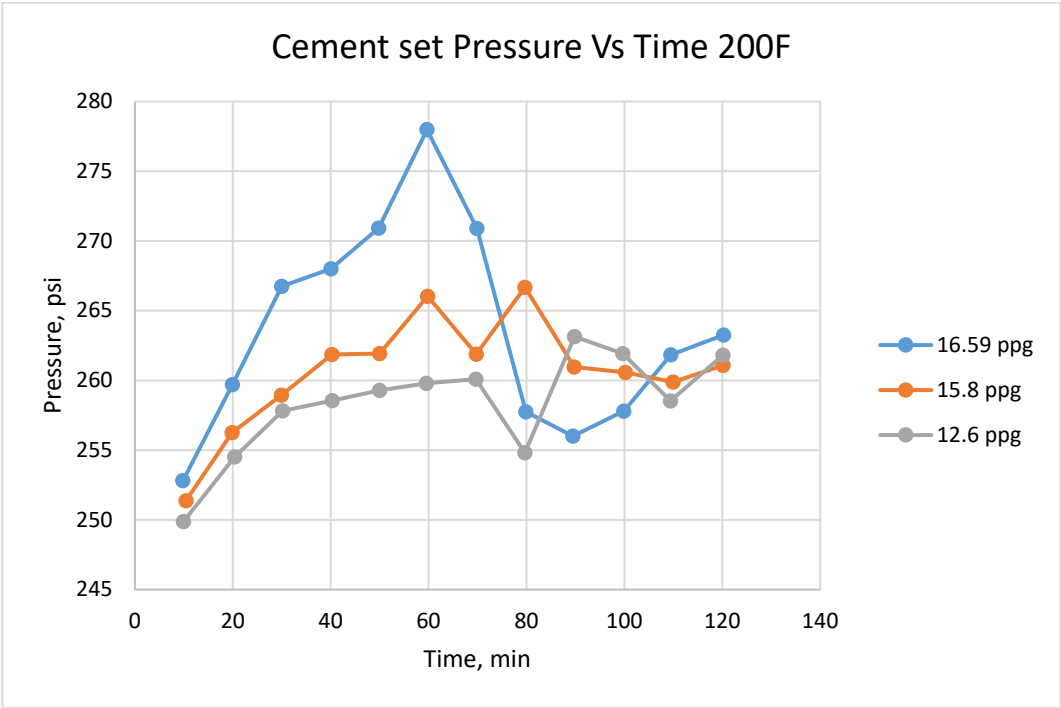

Figure 72: Cement Setting Pressure Vs Time.

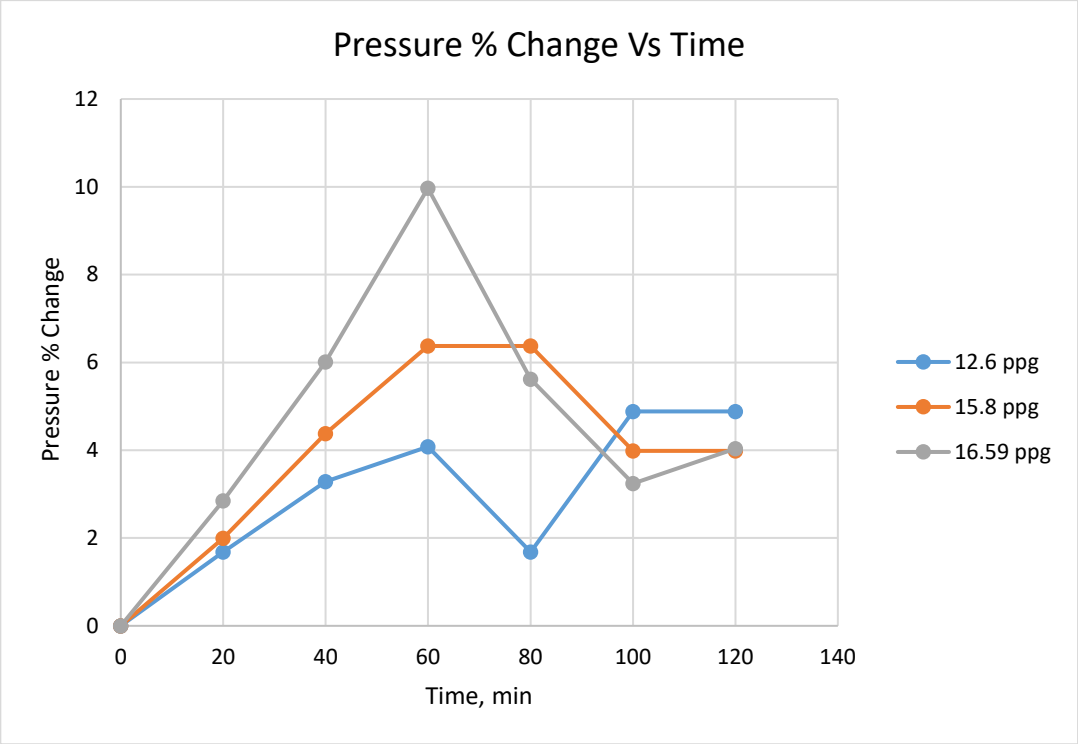

Figure 73: Pressure % change Vs Time.

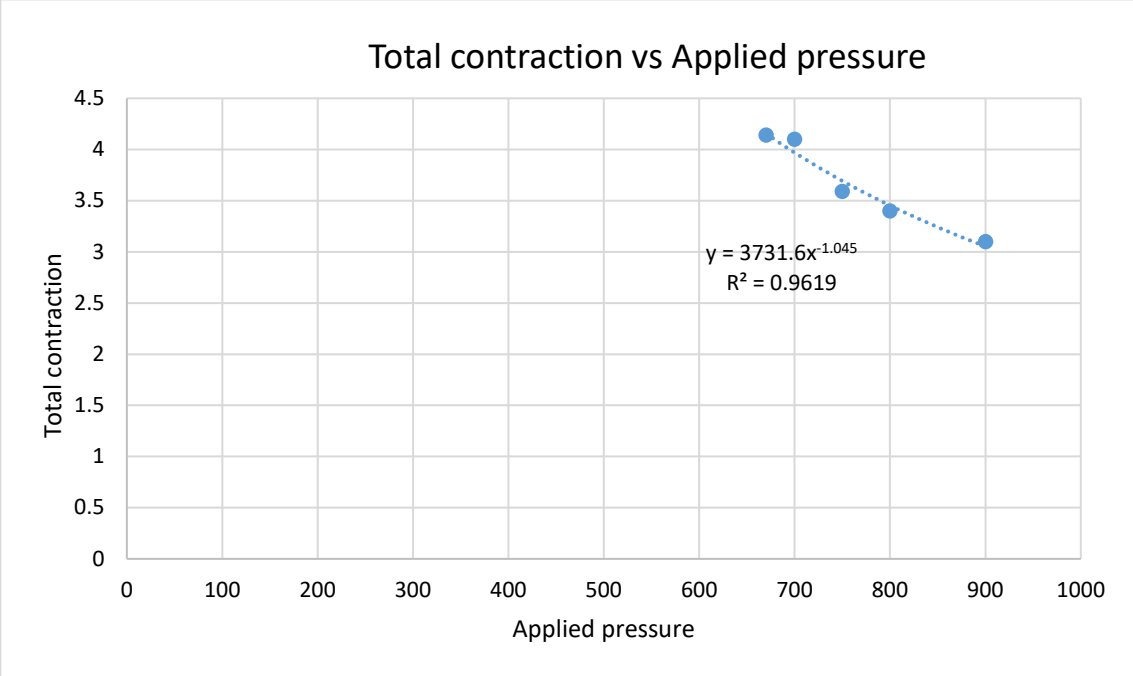

Figure 74: Total Contraction Vs Applied Pressure.

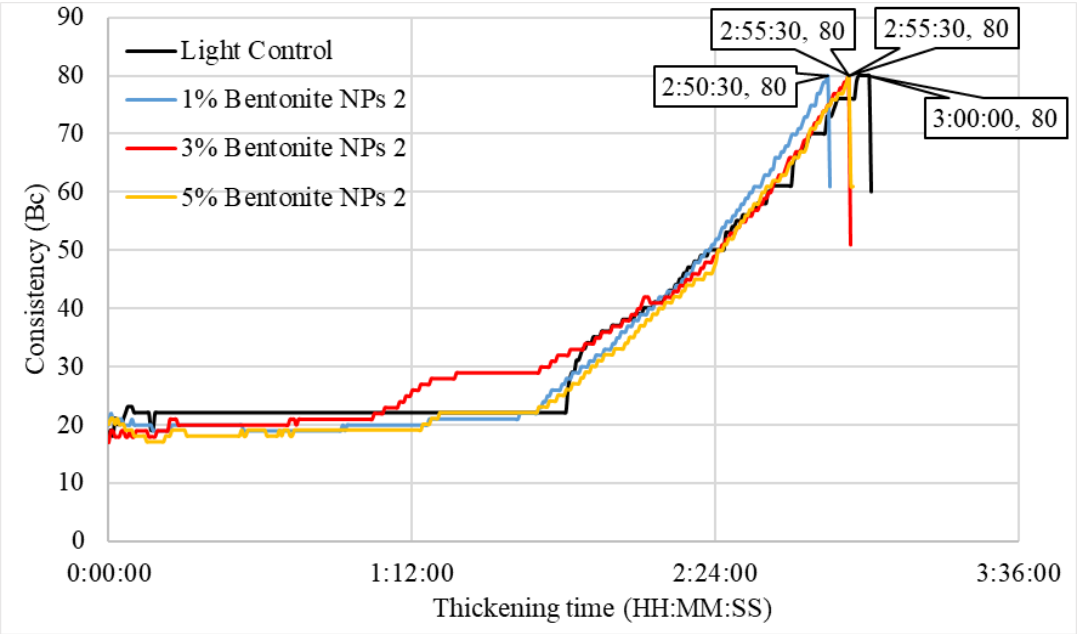

Figure 75: Round 2 light cement with bentonite nanoparticles at temperature 100°F and pressure 3000 psi.

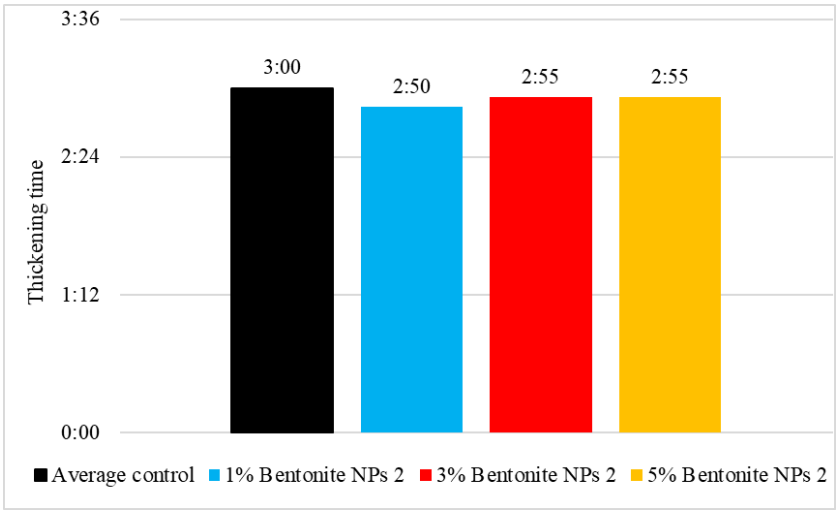

Figure 76: Round 2, light cement with bentonite nanoparticles at temperature 100°F and pressure 3000 psi.

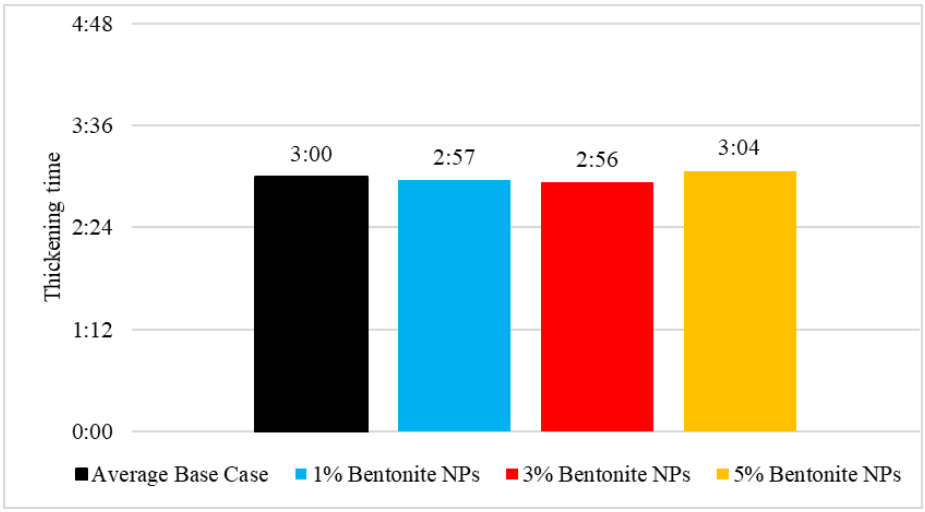

Figure 77: The combined average thickening time for Cement A containing bentonite nanoparticles.

Figure 78: Samples of heavy and light control cases for porosity and permeability tests.

Figure 79: PERG-200 Permeability test.

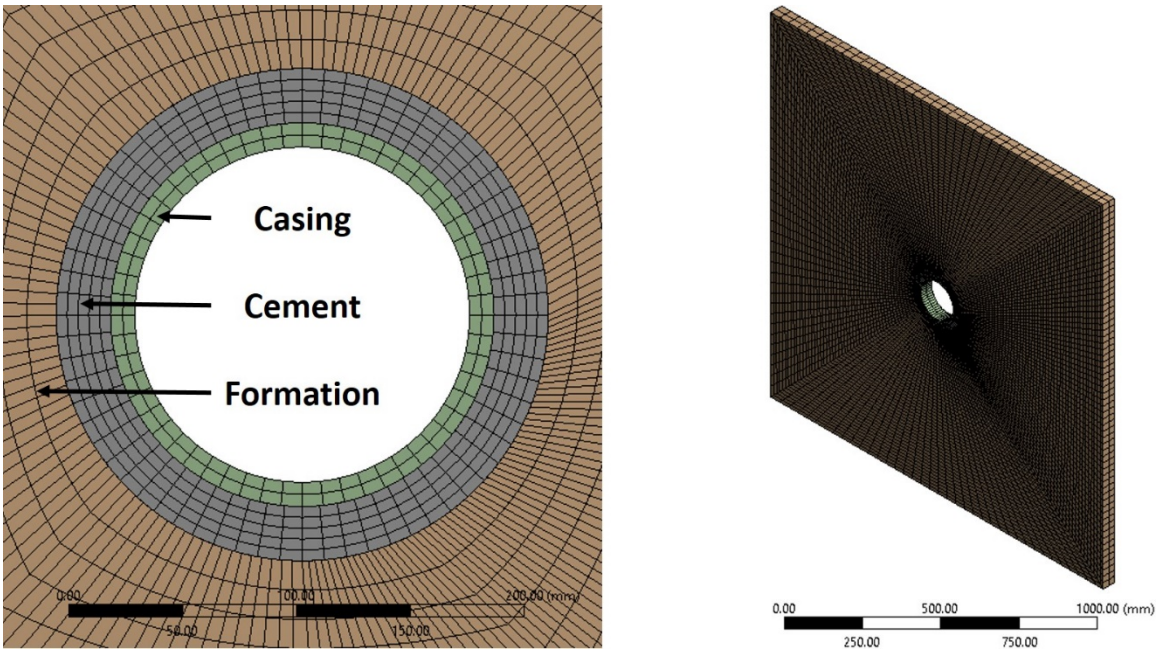

Figure 80: 2D (left) and 3D (right) view of the gridded finite element model.

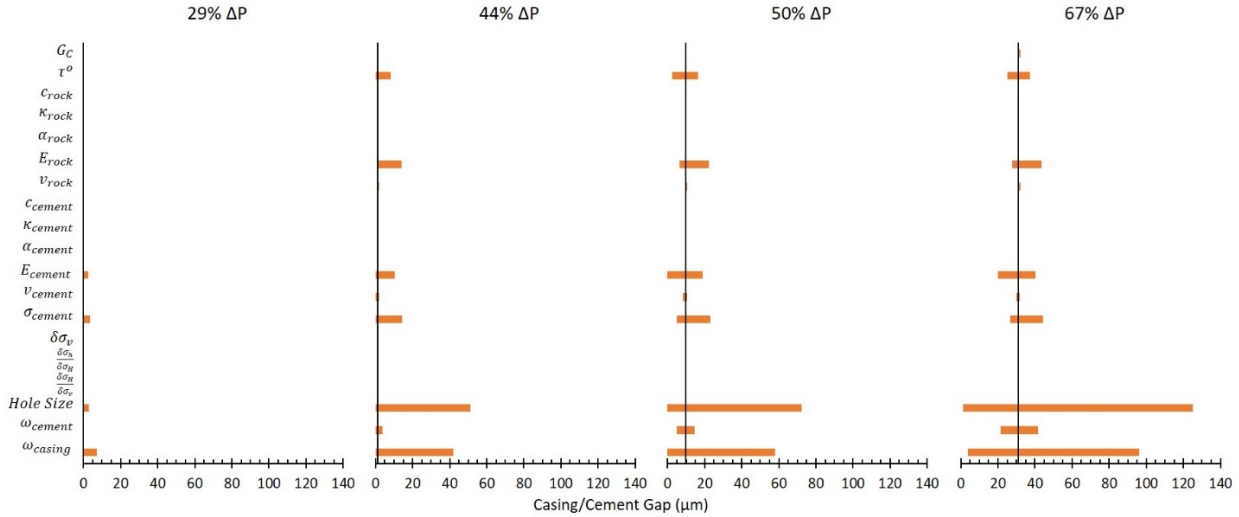

Figure 81: Parametric analysis of the maximum and minimum variables tested for change in wellbore pressures (***ΔP***) of 29%, 44%, 50%, and 67%. Variances in the hole size and casing thickness have the largest change in resulting gap magnitudes.

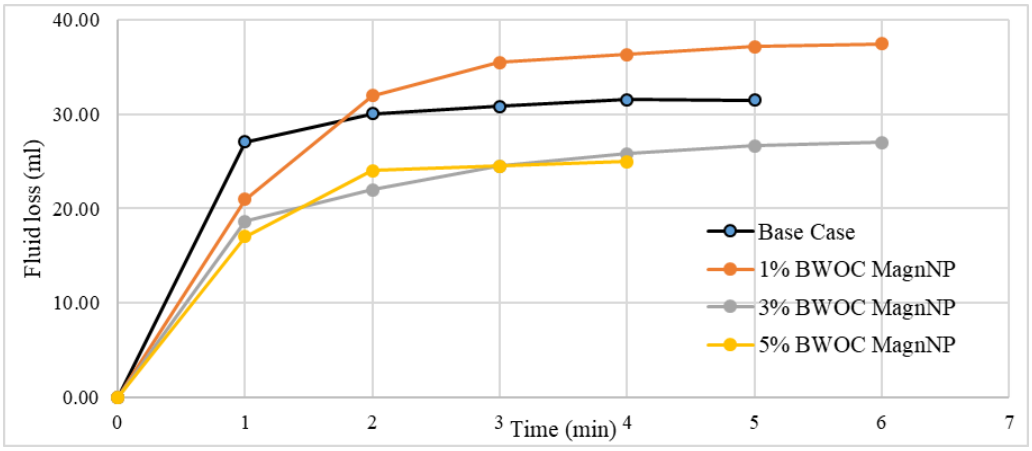

Figure 82: Fluid loss results for heavy cement with magnetite nanoparticles.

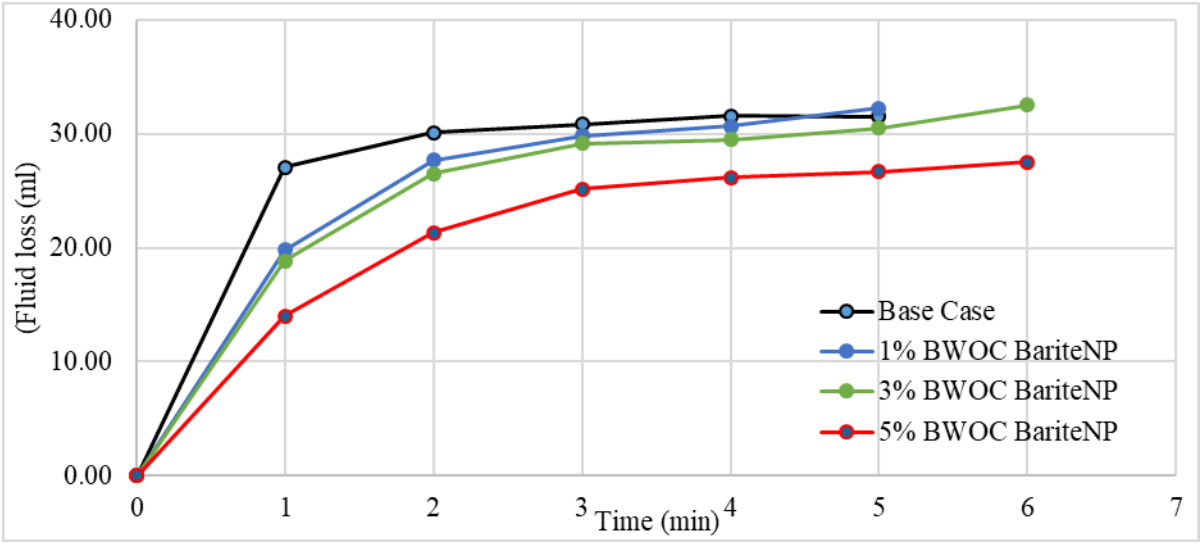

Figure 83: Fluid loss results for heavy cement with barite nanoparticles.

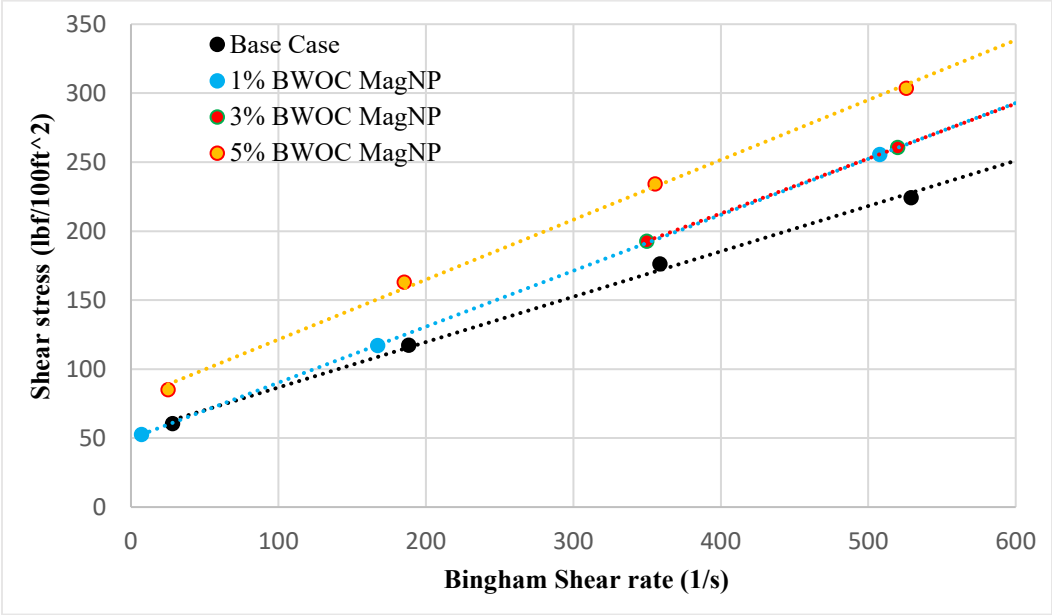

Figure 84: Rheology result for heavy cement base case with magnetite nanoparticles.

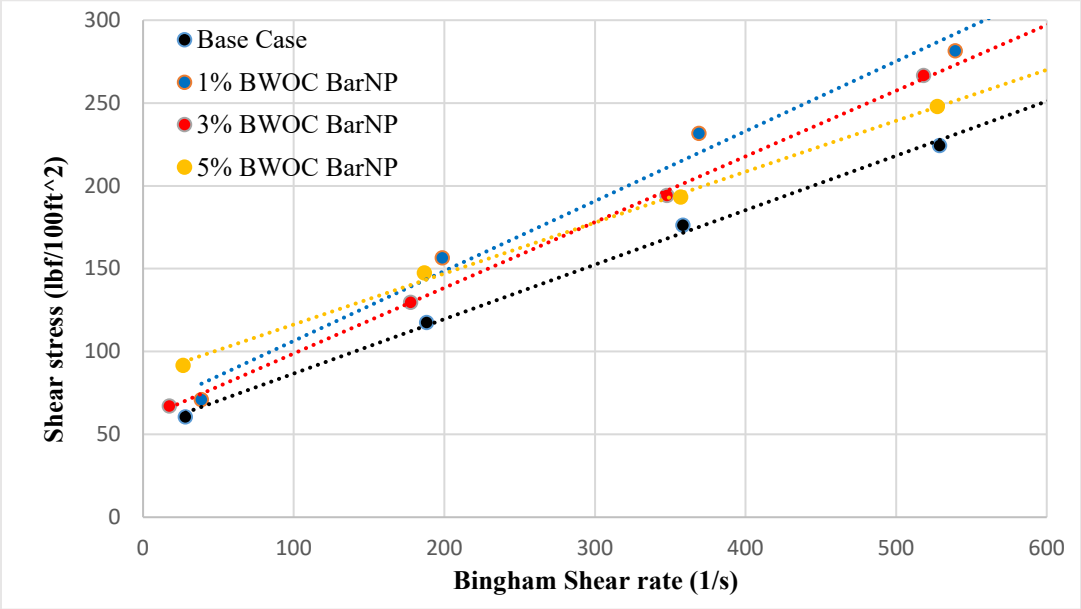

Figure 85: Rheology result for heavy cement base case with barite nanoparticles.

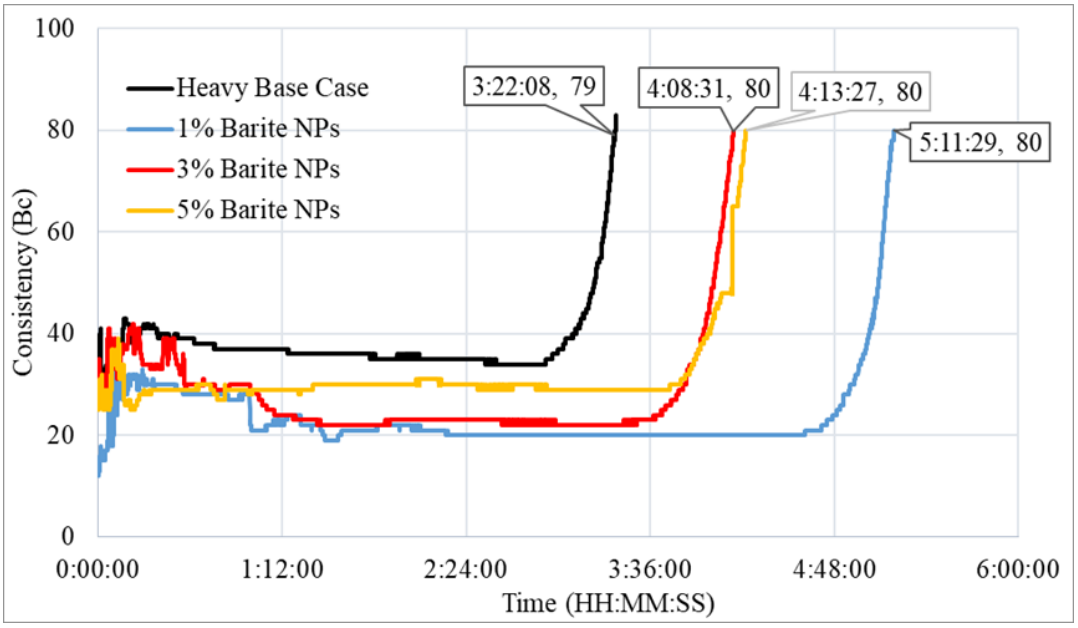

Figure 86: Heavy base case with (1%, 3%, and 5% BWOC) barite nanoparticles with higher amount of seawater in the nanoparticles than base case (Test 1).

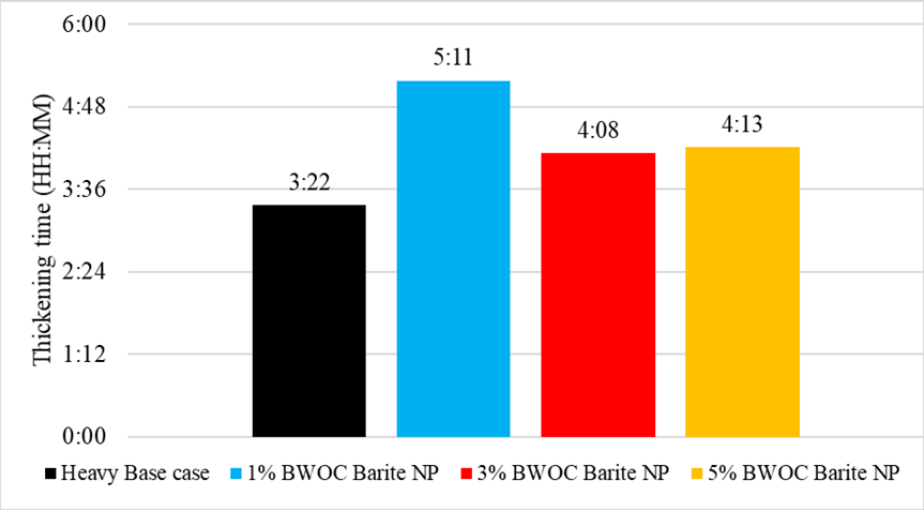

Figure 87: Heavy base case with (1%, 3%, and 5% BWOC) barite nanoparticles with higher amount of seawater in the nanoparticles than base case (Test 1).

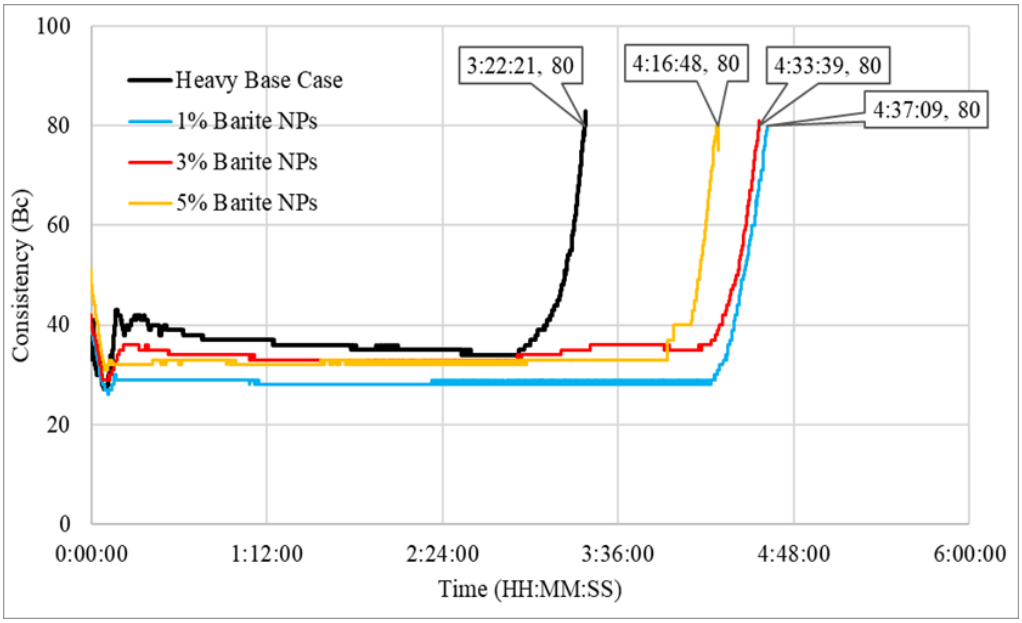

Figure 88: The Repeated heavy base case with (1%, 3%, and 5% BWOC) barite nanoparticles, but now with same amount of seawater in the nanoparticles as in base case (Test 2).

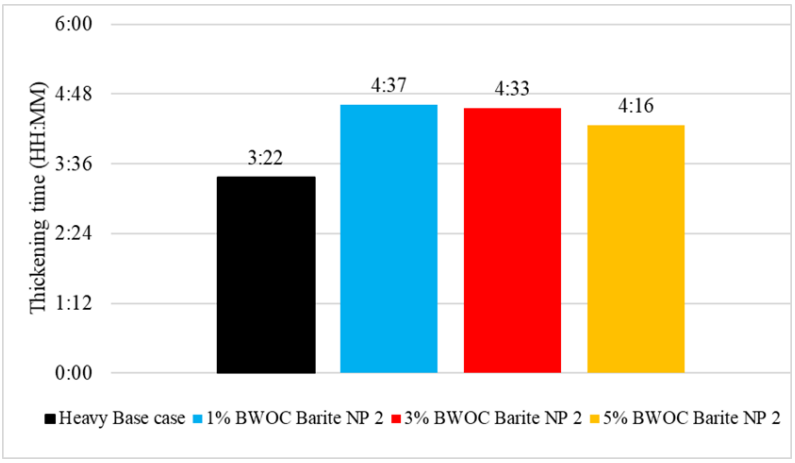

Figure 89: Heavy barite nanoparticles with same amount of seawater in the nanoparticles as in the final base case (Test 2).

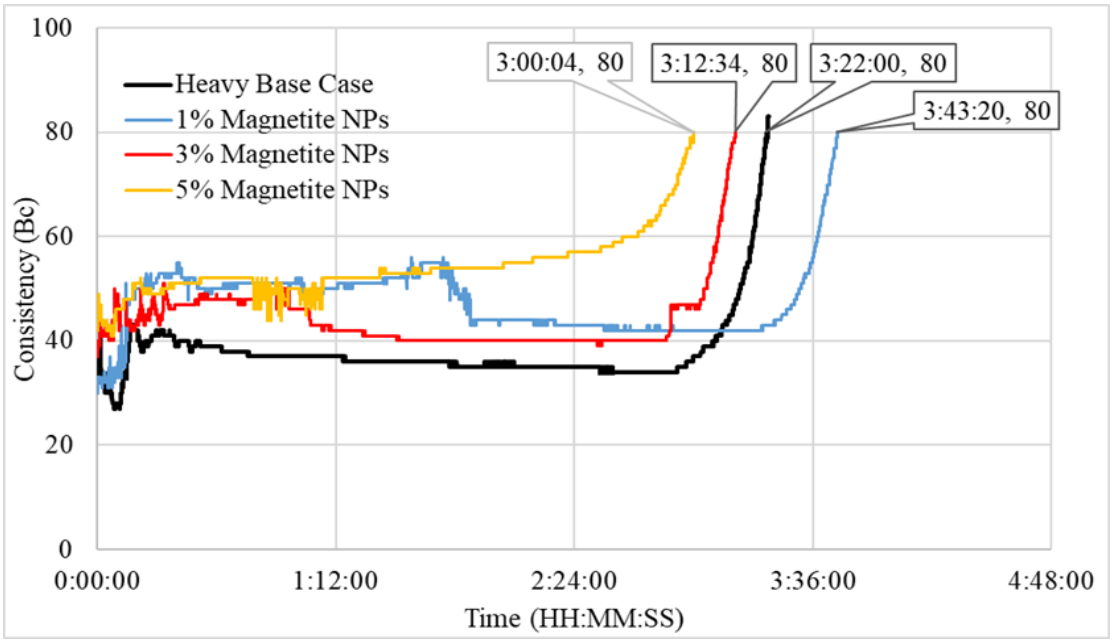

Figure 90: Heavy Magnetite nanoparticles with same amount of seawater in the nanoparticles as in base case.

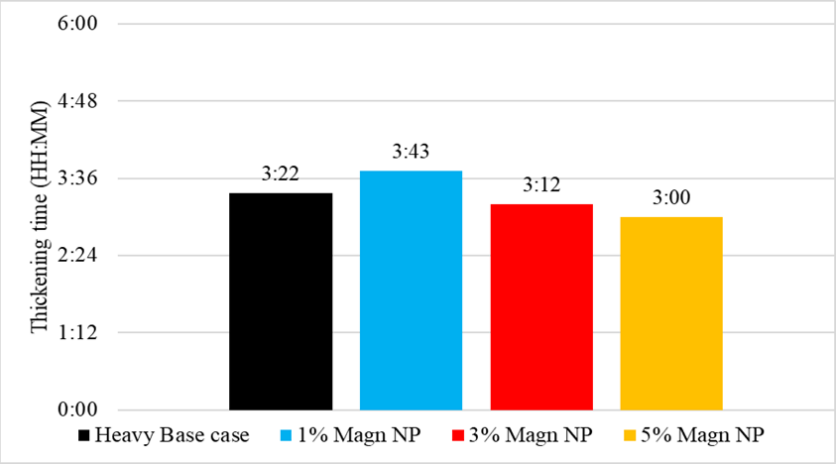

Figure 91: Heavy magnetite nanoparticles with same amount of seawater in the nanoparticles as in base case.

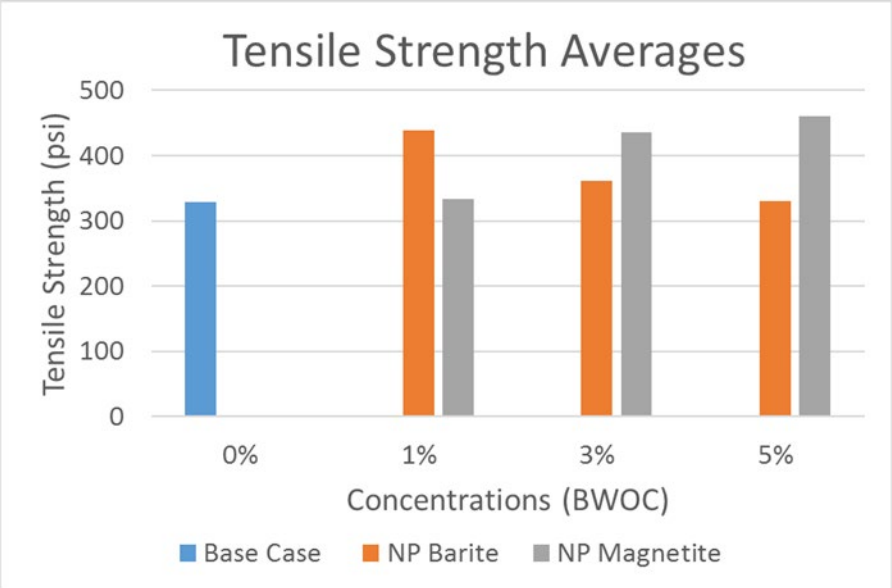

Figure 92: Average tensile strengths seen in the first round of samples.

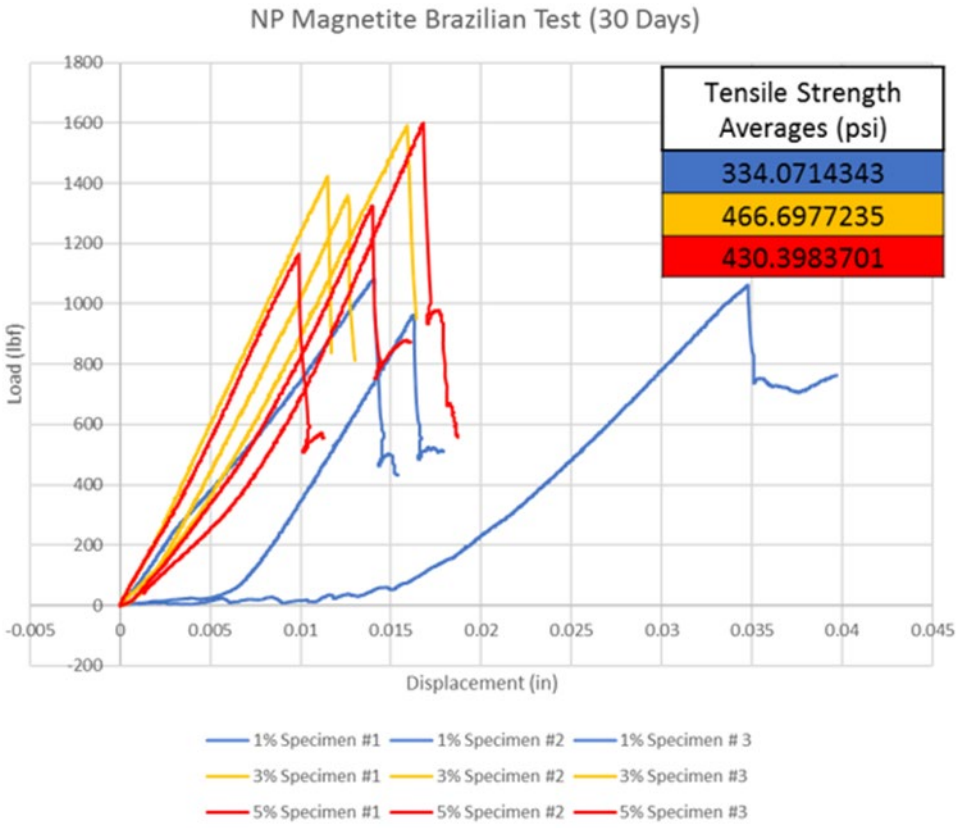

Figure 93: Load vs. displacement curves for the first round of tensile strength samples.

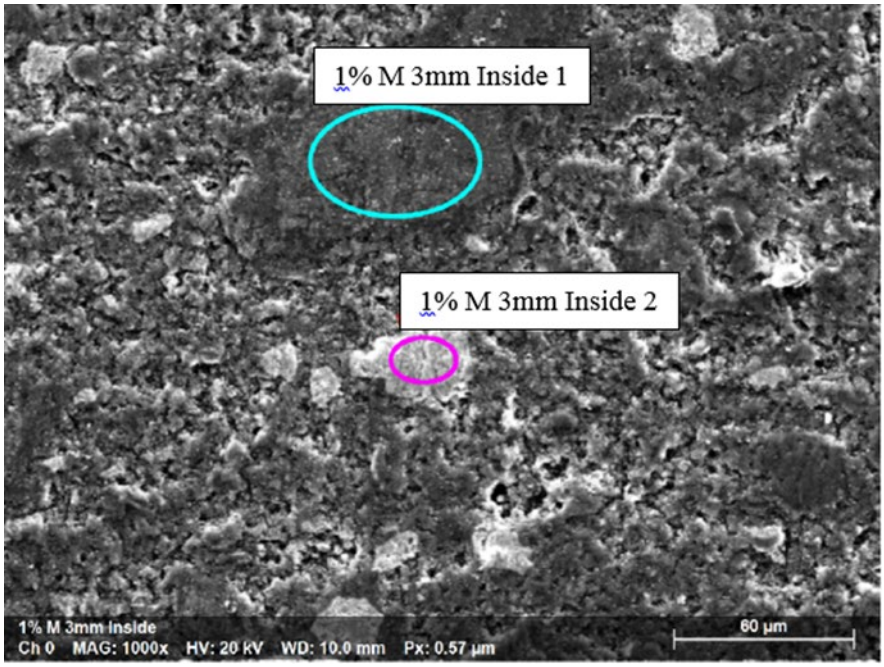

Figure 94: Pocket of barite observed (point 2) through SEM roughly 3mm from the core wall of a 1% nanoparticle magnetite sample.

Equations

$$\sigma_{Tensile\ Bond} = \frac{P}{(\frac{\pi}{4} * D_{avg}{}^{2})}$$

Equation 1: Formula used to find the tensile bond strength where D_avg is the average diameter of the bonded plane and P is the tensile load at failure.

$$F_f = \cos(\theta) * F * \mu_s$$

Equation 2: Formula used to determine the shear load caused by friction.

$$F_\tau = \sin(\theta) * F$$

Equation 3: Formula used to find the total shear load.

$$\tau = \frac{(F_\tau - F_f)}{A}$$

Equation 4: Formula used to find the shear bond strength.

Shear Stress τ lb/100 ft^2 1"Fann = 1.065 lb/100 ft^2

Equation 5: Formula used to find shear stress of slurry.

$$\dot{\gamma} = N * 1.703 + 479 * \tau_y/\mu_p(\frac{3.174}{1.7245^2} - 1) \quad \text{unit (1/s)}$$

Equation 6: Formula used to find the shear rate of the slurry.

$$\mu_p = \frac{300}{N_2 - N_1}(\theta_{N2} - \theta_{N1}) \quad \text{or} \quad \mu_p = \theta_{600} - \theta_{300}, \quad \text{unit (cP)}$$

Equation 7: Formula used to find the plastic viscosity of the slurry.

$$\tau_y = \theta_{N1} - \mu_p \frac{N1}{300} \quad \text{or} \quad \tau_y = \theta_{300} - \mu_p \quad \text{unit (lb/100 ft}^2\text{)}$$

Equation 8: Formula used to find the yield point of the slurry.

$$\Delta Psetting = 0.04 * Phydrostatic * \frac{3731.6 Phydrostatic^{-1.045}}{6.129}$$

Equation 9: Formula used to find the setting pressure of cement at a given hydrostatic pressure.

Bibliography

Archer, S., & Rasouli, V. (2012). A log based analysis to estimate mechanical properties and in-situ stresses in a shale gas well in North Perth Basin. *WIT Transactions on Engineering Sciences*, *81*, 163–174. https://doi.org/10.2495/pmr120151

Bois, A. P., Vu, M. H., Ghabezloo, S., Sulem, J., Garnier, A., & Laudet, J. B. (2013). Cement Sheath Integrity for CO_2 Storage – An Integrated Perspective. *Energy Procedia*, *37*, 5628–5641. https://doi.org/10.1016/j.egypro.2013.06.485

Bois, A. P., Garnier, A., Galdiolo, G., & Laudet, J. B. (2012). Use of a Mechanistic Model To Forecast Cement-Sheath Integrity. *SPE Drilling & Completion*, *27*(02), 303–314. https://doi.org/10.2118/139668-pa

Bois, A. P., Garnier, A., Rodot, F., Saint-Marc, J., & Aimard, N. (2011). How To Prevent Loss of Zonal Isolation Through a Comprehensive Analysis of Microannulus Formation. *SPE Drilling & Completion*, *26*(01), 13–31. https://doi.org/10.2118/124719-pa

Bosma, M., Ravi, K., van Driel, W., & Schreppers, G. J. (1999, October). Design Approach to Sealant Selection for the Life of the Well. In *SPE Annual Technical Conference and Exhibition*. Houston, TX. SPE-56536-MS. https://doi.org/10.2118/56536-ms

Breckels, I. M., & van Eekelen, H. A. M. (1982). Relationship Between Horizontal Stress and Depth in Sedimentary Basins. *Journal of Petroleum Technology*, *34*(09), 2191–2199. SPE-10336-PA. https://doi.org/10.2118/10336-pa

Bureau of Safety and Environmental Enforcement (BSEE). (2018). *Borehole Online Query*. Retrieved September 13, 2021, from https://www.data.bsee.gov/Well/Borehole/Default.aspx

Celia, M. A., Bachu, S., Nordbotten, J. M., Gasda, S. E., & Dahle, H. K. (2005, September). Quantitative estimation of CO_2 leakage from geological storage: Analytical models, numerical models, and data needs. *Greenhouse Gas Control Technologies 7*, 663–671. https://doi.org/10.1016/b978-008044704-9/50067-7

Crain, D., Zhang, W., and Eckert, A. (2018, June). Numerical Simulation of Micro-Annuli Attributes Imposed by Stress Regime and Elastic Contrast. In *52nd US Rock Mechanics/Geomechanics Symposium*. Seattle, WA. ARMA-2018-1026.

De Andrade, J., Fagerås, S., and Sangesland, S. (2019, March). A Novel Mechanical Tool for Annular Cement Verification. In *SPE/IADC International Drilling Conference and Exhibition*. The Hague, Netherlands. SPE-194135-MS. https://doi.org/10.2118/194135-MS

De Andrade, J., Sangesland, S., Skorpa, R., Todorovic, J., & Vrålstad, T. (2016). Experimental Laboratory Setup for Visualization and Quantification of Cement-Sheath Integrity. *SPE Drilling & Completion*, *31*(04), 317–326. SPE-173871-PA. https://doi.org/10.2118/173871-pa

Deshpande, A., Jones, P., Jadhav, R., Pangu, G. & Mishra, V. (2019, March). Comparative Study of the Mechanical Properties of Reduced Density Cements. In *SPE Middle East Oil and Gas Show and Conference*. Manama, Bahrain. SPE-194918-MS. https://doi.org/10.2118/194918-MS

Feng, Y., Li, X., & Gray, K. E. (2017). Development of a 3D numerical model for quantifying fluid-driven interface debonding of an injector well. *International Journal of Greenhouse Gas Control*, *62*, 76–90. https://doi.org/10.1016/j.ijggc.2017.04.008

Finkbeiner, T., Stump, B. B., Zoback, M. D., & Flemings, P. B. (1996). *Pressure (Pp), overburden (Sv), and minimum horizontal stress (SHMIN) in Eugene Island Block 330, offshore Gulf of Mexico. Topical report, April 1-July 1, 1996*. Office of Scientific and Technical Information, U.S. Department of Energy. https://www.osti.gov/biblio/442326

Fjaer, E., Holt, R. M., Horsrud, P., Raaen, A. M., & Risnes, R. (2008). *Petroleum Related Rock Mechanics* (1st ed., Vol. 33). Elsevier.

Fourmaintraux, D. M., Bois, A. P., Fraboulet, B., & Brossolllet, P. (2005, June). Efficient Wellbore Cement Sheath Design Using the SRC (System Response Curve) Method. In *SPE Europe/EAGE Annual Conference*. Madrid, Spain. SPE-94176-MS. https://doi.org/10.2118/94176-MS

García, V., Márquez, C., Zúñiga-Suárez, A., Zuñiga-Torres, B. and Villalta-Granda, L. (2017). Brazilian Test of Concrete Specimens Subjected to Different Loading Geometries: Review and New Insights. *International Journal of Concrete Structures and Materials*, 11(2), 343–363. https://doi.org/10.1007/s40069-017-0194-7

Goodwin, K. J., & Crook, R. J. (1992). Cement Sheath Stress Failure. *SPE Drilling Engineering*, *7*(04), 291–296. https://doi.org/10.2118/20453-pa

Gray, K. E., Podnos, E., & Becker, E. (2009). Finite-Element Studies of Near-Wellbore Region During Cementing Operations: Part I. *SPE Drilling & Completion*, *24*(01), 127–136. SPE-106998-PA. https://doi.org/10.2118/106998-pa

Greenberg, M. L., & Castagna, J. P. (1992). Shear-Wave Velocity Estimation in Porous Rocks: Theoretical Formulation, Preliminary Verification and Applications. *Geophysical Prospecting*, *40*(2), 195–209. https://doi.org/10.1111/j.1365-2478.1992.tb00371.x

Hillerborg, A., Modéer, M., & Petersson, P. E. (1976). Analysis of crack formation and crack growth in concrete by means of fracture mechanics and finite elements. *Cement and Concrete Research*, *6*(6), 773–781. https://doi.org/10.1016/0008-8846(76)90007-7

Ichim, A. & Teodoriu, C. (2017, March). Development of a Cement Repository to Improve the Understanding of Well Integrity Behavior with Time. In *SPE Oklahoma City Oil and Gas Symposium*. Oklahoma City, OK. SPE-185089-MS. https://doi.org/10.2118/185089-MS

Jaeger, J. C., Cook, N. G. W., & Zimmerman, R. W. (2007). *Fundamentals of Rock Mechanics* (4th ed.). Wiley-Blackwell.

James, S. G. & Boukhelifa, L. (2006, November). Zonal Isolation Modelling and Measurements-Past Myths and Todays Realities. In *Abu Dhabi International Petroleum Exhibition and Conference*. Abu Dhabi, UAE. SPE-101310-MS. https://doi.org/10.2118/101310-MS

Jasiczak, J., Kulczewski, P., & Borowski, P. (2017). Laboratory Tests of Adhesion of Steel Bars to Ordinary and Frozen Concrete. *IOP Conference Series: Materials Science and Engineering*, *245*, 032043. https://doi.org/10.1088/1757-899x/245/3/032043

Kiran, R., Teodoriu, C., Dadmohammadi, Y., Nygaard, R., Wood, D., Mokhtari, M., & Salehi, S. (2017). Identification and evaluation of well integrity and causes of failure of well integrity barriers (A review). *Journal of Natural Gas Science and Engineering*, *45*, 511–526. https://doi.org/10.1016/j.jngse.2017.05.009

Lavrov, A., Todorovic, J., and Torsæter, M. (2015, July). Numerical study of tensile thermal stresses in a casing-cement-rock system with heterogeneities. In *49th US Rock Mechanics/Geomechanics Symposium*. San Francisco, CA. ARMA-2015-110.

Le Roy-Delage, S., Baumgarte, C., Thiercelin, M. & Vidick, B. (2000, February). New Cement Systems for Durable Zonal Isolation. In *IADC/SPE Drilling Conference*. New Orleans, LA. SPE-59132-MS. https://doi.org/10.2118/59132-MS

Li, Y., & Nygaard, R. (2017). A numerical study on the feasibility of evaluating CO_2 injection wellbore integrity through casing deformation monitoring. *Greenhouse Gases: Science and Technology*, *8*, 51–62. https://doi.org/10.1002/ghg.1733

Li, Y., Cheng, B., Zhu, W., Xiao, H., & Nygaard, R. (2017). Development and evaluation of the coaxial cable casing imager: a cost-effective solution to real-time downhole monitoring for CO_2 sequestration wellbore integrity. *Greenhouse Gases: Science and Technology*, *7*(5), 927–941. https://doi.org/10.1002/ghg.1691

Loiseau, A. (2014, September). Thermal Expansion of Cement and Well Integrity of Heavy Oil Wells. In *SPE Heavy and Extra Heavy Oil Conference: Latin America*. Medellin, Colombia. SPE-171066-MS. https://doi.org/10.2118/171066-MS

McDaniel, J., Watters, L. & Combs, N.K. (2014, August). Zonal Isolation Assurance: Relating Cement Mechanical Properties to Mechanical Durability. In *SPE/AAPG/SEG 2nd Unconventional Resources Technology Conference*. Denver, CO. URTEC-1913405-MS. https://doi.org/10.15530/URTEC-2014-1913405

Meng, J., Pashin, J. C., Nygaard, R., & Chandra, A. (2018). Analysis of the stress field in the DeSoto canyon Salt Basin for ensuring safe offshore carbon storage. *International Journal of Greenhouse Gas Control*, *79*, 279–288. https://doi.org/10.1016/j.ijggc.2018.11.006

Morris, W., Criado, M.A., Robles, J. & Bianchi, G. (2003, April). Design of High Toughness Cement for Effective Long Lasting Well Isolations. In *SPE Latin American and Caribbean Petroleum Engineering Conference*. Port-of-Spain, Trinidad and Tobago. SPE-81001-MS. https://doi.org/10.2118/81001-MS

Nelson, E., & Guillot, D. (2006). *Well Cementing* (2nd Edition). Schlumberger.

Standards Norway. (2004, August). *D-010 Well integrity in drilling and well operations (Rev. 4, June 2013)* (NORSOK D-010:2013). https://www.standard.no/pagefiles/1315/d-010r3.pdf

Nygaard, R., Salehi, S., Weideman, B., & Lavoie, R. G. (2014). Effect of Dynamic Loading on Wellbore Leakage for the Wabamun Area CO2-Sequestration Project. *Journal of Canadian Petroleum Technology*, *53*(01), 69–82. https://doi.org/10.2118/146640-pa

Patel, H., & Salehi, S. (2019). Development of an Advanced Finite Element Model and Parametric Study to Evaluate Cement Sheath Barrier. *Journal of Energy Resources Technology*, *141*(9), 092902. https://doi.org/10.1115/1.4043137

Pattillo, P. D., & Kristiansen, T. G. (2002, October). Analysis of horizontal casing integrity in the Valhall field. In *SPE/ISRM Rock Mechanics Conference*. Irving, TX. SPE-78204-MS. https://doi.org/10.2118/78204-MS

Philippacopoulos, A.J., & Berndt, M.L. (2002, September-October). Mechanical Response and Characterization of Well Cements. In *SPE Annual Technical Conference and Exhibition*. San Antonio, TX, USA. SPE-77755-MS. https://doi.org/10.2118/77755-MS

Ravi, K., Bosma, M., & Gastebled, O. (2002a, February). Improve the economics of oil and gas wells by reducing the risk of cement failure. In *IADC/SPE Drilling Conference*. Dallas, TX. SPE-74497-MS. https://doi.org/10.2118/74497-MS

Ravi, K., Bosma, M., & Gastebled, O. (2002b, April). Safe and economic gas wells through cement design for life of the well. In *SPE Gas Technology Symposium*. Calgary, Alberta, Canada. SPE-75700-MS. https://doi.org/10.2118/75700-MS

U.S. Government Accountability Office (GAO). (2015, December). *Actions Needed to Better Protect Against Billions of Dollars in Federal Exposure to Decommissioning Liabilities* (GAO-16-40). https://www.gao.gov/products/gao-16-40

Saint-Marc, J., Garnier, A., & Bois, A. P. (2008, September). Initial State of Stress: The Key to Achieving Long-Term Cement-Sheath Integrity. In *SPE Annual Technical Conference and Exhibition*. Denver, CO. SPE-116651-MS. https://doi.org/10.2118/116651-MS

Salehi, S., & Nygaard, R. (2015). Full Fluid–Solid Cohesive Finite-Element Model to Simulate Near Wellbore Fractures. *Journal of Energy Resources Technology*, *137*(1), 012903. https://doi.org/10.1115/1.4028251

Stormont, J. C., Fernandez, S. G., Taha, M. R., & Matteo, E. N. (2018). Gas flow through cement-casing microannuli under varying stress conditions. *Geomechanics for Energy and the Environment*, *13*, 1–13. https://doi.org/10.1016/j.gete.2017.12.001

Turon, A., Dávila, C. G., Camanho, P. P., & Costa, J. (2007). An engineering solution for mesh size effects in the simulation of delamination using cohesive zone models. *Engineering Fracture Mechanics*, *74*(10), 1665–1682. https://doi.org/10.1016/j.engfracmech.2006.08.025

Vrålstad, T., Saasen, A., Fjær, E., Øia, T., Ytrehus, J. D., & Khalifeh, M. (2019). Plug & abandonment of offshore wells: Ensuring long-term well integrity and cost-efficiency. *Journal of Petroleum Science and Engineering*, *173*, 478–491. https://doi.org/10.1016/j.petrol.2018.10.049

Vrålstad, T., Skorpa, R., Opedal, N., & De Andrade, J. (2015, November). Effect of thermal cycling on cement sheath integrity: Realistic experimental tests and simulation of resulting leakages. In *SPE Thermal Well Integrity and Design Symposium*. Banff, Alberta, Canada. SPE-178467-MS. https://doi.org/10.2118/178467-MS

Wang, H. F. (2017). *Theory of Linear Poroelasticity with Applications to Geomechanics and Hydrogeology*. Amsterdam University Press.

Wang, W., & Taleghani, A. D. (2014). Three-dimensional analysis of cement sheath integrity around Wellbores. *Journal of Petroleum Science and Engineering*, *121*, 38–51. https://doi.org/10.1016/j.petrol.2014.05.024

Watson, T. L., & Bachu, S. (2009). Evaluation of the potential for gas and CO_2 leakage along wellbores. *SPE Drilling & Completion*, *24*(01), 115-126. SPE-106817-PA. https://doi.org/10.2118/106817-PA

Wehling, P. 2008. Wellbore Cement Integrity Testing [M.S. Thesis]. *Technical University of Clausthal, Clausthal-Zellerfeld, Germany*.

Weideman, B., & Nygaard, R. (2014, April). How cement operations affect your cement sheath short and long term integrity. In *American Association of Drilling Engineers Fluids Technical Conference and Exhibition.* Houston, TX. AADE-14-FTCE-20

Weideman, B. L. (2014). Investigation of cased wellbore integrity in the Wabamun area sequestration project [M.S. Thesis]. *Missouri University of Science and Technology*. https://scholarsmine.mst.edu/masters_theses/7284/

Wise, J., Nygaard, R., & Hareland, G. (2019, June). Numerical Analysis of Wellbore Integrity and Cement Sheath Debonding for Wells in the Eugene Island OPD, Gulf of Mexico. In *53rd US Rock Mechanics/Geomechanics Symposium*. New York City, NY. ARMA-2019-0439.

Wojtanowicz, A. K., Bourgoyne, A. T., Zhou, D., & Bender, K. (2000, December). *Strength and Fracture Gradients for Shallow Marine Sediments*. Minerals Management Service, US Department of Interior. https://www.bsee.gov/sites/bsee.gov/files/tap-technical-assessment-program/008dj.pdf

Won, J., Lee, D., Na, K., Lee, I. M., & Choi, H. (2015). Physical properties of G-class cement for geothermal well cementing in South Korea. *Renewable Energy*, *80*, 123–131. https://doi.org/10.1016/j.renene.2015.01.067

Zhang, M., & Bachu, S. (2011). Review of integrity of existing wells in relation to CO_2 geological storage: What do we know? *International Journal of Greenhouse Gas Control*, *5*(4), 826–840. https://doi.org/10.1016/j.ijggc.2010.11.006

Zhang, Z., Prud'homme, R. K., & Scherer, G. (2016, May). Adhesion and Bonding Between Steel Pipe and Cement/Spacer/Mud System. *9th International Conference on Fracture Mechanics of Concrete and Concrete Structures*. Berkeley, CA. https://doi.org/10.21012/FC9.313

Zhang, W., Eckert, A., and Liu, X. (2017, June). Numerical Simulation of Micro-Annuli Generation by Thermal Cycling. In *51st U.S. Rock Mechanics/Geomechanics Symposium*. San Francisco, CA. ARMA-2017-0354.

Data Report

DataType	DigitalResourceType	Title	FileName	Creators	Point of Contact	Publication Year	Repository Name	DOI or Persistent URL	Keywords	Publications
Engineering	Tabular/Spreadsheet	Grinder Barite DLS Tests	DLS Barite SizeTimeModel (PR1-Fig15).xls	Amin Asashnezhad	Geir Hareland, geir.hareland@okstate.edu 405-744-9113	2018	Task2/Nanoparticle Preparation	gulf-cement-project.oucreate.com/Task2/Nanoparticle Preparation/DLS Barite SizeTimeModel (PR1-Fig15).xls	Barite NP, high speed grinder	TBD
Engineering	Tabular/Spreadsheet	Grinder Bentonite DLS Tests	DLS Bentonite (PR1-Fig14).xls	Mark Ritchie	Geir Hareland, geir.hareland@okstate.edu 405-744-9113	2018	Task2/Nanoparticle Preparation	gulf-cement-project.oucreate.com/Task2/Nanoparticle Preparation/DLS Bentonite (PR1-Fig14).xls	Bentonite NP, high speed grinder	TBD
Engineering	Tabular/Spreadsheet	Barite NPs Cement Fluid Loss Tests	BariteNPs Cement Fluid Loss(PR1-Fig30&31).xls	Amin Asashnezhad	Geir Hareland, geir.hareland@okstate.edu 405-744-9113	2018	Task3/Fluid Loss Tests	gulf-cement-project.oucreate.com/BariteNPs Cement Fluid Loss(PR1-Fig30&31).xls	Barite NP, Fluid Loss	TBD
Engineering	Tabular/Spreadsheet	Consistometer HEC Test	Consistometer HEC (PR1-Fig35).xls	Amin Asashnezhad	Geir Hareland, geir.hareland@okstate.edu 405-744-9113	2018	Task4/Consistometer Tests	gulf-cement-project.oucreate.com/Task4/Consistometer Tests/Consistometer HEC (PR1-Fig35).xls	Class A Cement, HEC Tests	TBD
Engineering	Tabular/Spreadsheet	Consistometer Salt Test	Consistometer Salt(PR1-Fig32).xls	Amin Asashnezhad	Geir Hareland, geir.hareland@okstate.edu 405-744-9113	2018	Task4/Consistometer Tests	gulf-cement-project.oucreate.com/Task4/Consistometer Tests/Consistometer Salt(PR1-Fig32).xls	Class A Cement, Salt Tests	TBD
Engineering	Tabular/Spreadsheet	Consistometer Cement NP tests	Consitometer Cement NP(PR1-Fig34).xls	Amin Asashnezhad	Geir Hareland, geir.hareland@okstate.edu 405-744-9113	2018	Task4/Consistometer Tests	gulf-cement-project.oucreate.com/Task4/Consistometer Tests/Consitometer Cement NP(PR1-Fig34).xls	Class A Cement, Cement NP Tests	TBD
Engineering	Text	Model Input "Life of Well"	PR1-FEA_Model_Input(Fig4)	Jarrett Wise	Geir Hareland, geir.hareland@okstate.edu 405-744-9113	2018	Task1/FEA_vs_Analytical	gulf-cement-project.oucreate.com/Task1/FEA_vs_Analytical/PR1-FEA_Model_Input(Fig4).txt	FEA Model Input	Wise et al. 2019
Engineering	Text	Model Output "Life of Well"	PR1-FEA_model_Output(Fig4)	Jarrett Wise	Geir Hareland, geir.hareland@okstate.edu 405-744-9113	2018	Task1/FEA_vs_Analytical	gulf-cement-project.oucreate.com/Task1/FEA_vs_Analytical/PR1-FEA_model_Output(Fig4).txt	FEA Model Output	Wise et al. 2019
Engineering	Tabular/Spreadsheet	Model Results "Life of Well"	PR1-FEA_vs_analytical(Fig4)	Jarrett Wise	Geir Hareland, geir.hareland@okstate.edu 405-744-9113	2019	Task1/FEA_vs_Analytical	gulf-cement-project.oucreate.com/Task1/FEA_vs_Analytical/PR1-FEA_vs_analytical(Fig4).xlsx	FEA Model vs Analytical Output Results and Plot	Wise et al. 2019
Engineering	Tabular/Spreadsheet	Barite Concentration Testing	Barite Concentration Testing.xlsx	Mark Ritcie	Geir Hareland, geir.hareland@okstate.edu 405-744-9113	2018	Task2/Nanoparticle Preparation	gulf-cement-project.oucreate.com/Task2/Nanoparticle Preparation/Barite Concentration Testing.xlsx	Nanoparticles, high speed grinder, DLS	
Engineering	Tabular/Spreadsheet	Barite DLS Results for new grinding procedure	Barite ~New Procedure.xlsx	Mark Ritcie	Geir Hareland, geir.hareland@okstate.edu 405-744-9113	2018	Task2/Nanoparticle Preparation	gulf-cement-project.oucreate.com/Task2/Nanoparticle Preparation/Barite ~New Procedure.xlsx	Nanoparticles, high speed grinder, DLS	
Engineering	Tabular/Spreadsheet	Barite DLS Results 1	Barite DLS.xlsx	Mark Ritchie	Geir Hareland, geir.hareland@okstate.edu 405-744-9113	2018	Task2/Nanoparticle Preparation	gulf-cement-project.oucreate.com/Task2/Nanoparticle Preparation/Barite DLS.xlsx	Nanoparticles, high speed grinder, DLS	
Engineering	Tabular/Spreadsheet	Bentonite Concentration Testing	Bentonite Concentration Testing.xlsx	Mark Ritchie	Geir Hareland, geir.hareland@okstate.edu 405-744-9113	2018	Task2/Nanoparticle Preparation	gulf-cement-project.oucreate.com/Task2/Nanoparticle Preparation/Bentonite Concentration Testing.xlsx	Nanoparticles, high speed grinder, DLS	
Engineering	Tabular/Spreadsheet	Bentonite DLS Results	Bentonite DLS.xlsx	Mark Ritchie	Geir Hareland, geir.hareland@okstate.edu 405-744-9113	2018	Task2/Nanoparticle Preparation	gulf-cement-project.oucreate.com/Task2/Nanoparticle Preparation/Bentonite DLS.xlsx	Nanoparticles, high speed grinder, DLS	
Engineering	Tabular/Spreadsheet	Silicon DLS Results	Silicon DLS Testing.xlsx	Mark Ritchie	Geir Hareland, geir.hareland@okstate.edu 405-744-9113	2018	Task2/Nanoparticle Preparation	gulf-cement-project.oucreate.com/Task2/Nanoparticle Preparation/Silicon DLS Testing.xlsx	Nanoparticles, high speed grinder, DLS	
Engineering	Tabular/Spreadsheet	7-23 Spot Check Results (1% and 3% NP Mag.)	7-23 Spot Check Results (1% and 3% NP Mag.).xlsx	Mark Ritchie	Geir Hareland, geir.hareland@okstate.edu 405-744-9113	2019	Task 5/Brazilian Testing	gulf-cement-project.oucreate.com/Task 5/Brazilian Testing/7-23 Spot Check Results (1% and 3% NP Mag.).xlsx	Tensile Testing, Brazilian Data	Ritchie et. al
Engineering	Tabular/Spreadsheet	30 Day Base Case Brazilian Round 1 Data	30 Day Base Case Brazilian Round 1 Data	Mark Ritchie	Geir Hareland, geir.hareland@okstate.edu 405-744-9113	2019	Task 5/Brazilian Testing	gulf-cement-project.oucreate.com/Task 5/Brazilian Testing/30 Day Base Case Brazilian Round 1 Data.xlsx	Tensile Testing, Brazilian Data	Ritchie et. al
Engineering	Tabular/Spreadsheet	30 Day Base Case Brazilian Round 2 Data	30 Day Base Case Brazilian Round 2 Data.xlsx	Mark Ritchie	Geir Hareland, geir.hareland@okstate.edu 405-744-9113	2019	Task 5/Brazilian Testing	gulf-cement-project.oucreate.com/Task 5/Brazilian Testing/30 Day Base Case Brazilian Round 2 Data.xlsx	Tensile Testing, Brazilian Data	Ritchie et. al
Engineering	Tabular/Spreadsheet	30 Day Brazilian Base Case Round 3 Data	30 Day Brazilian Base Case Round 3 Data.xlsx	Mark Ritchie	Geir Hareland, geir.hareland@okstate.edu 405-744-9113	2019	Task 5/Brazilian Testing	gulf-cement-project.oucreate.com/Task 5/Brazilian Testing/30 Day Brazilian Base Case Round 3 Data.xlsx	Tensile Testing, Brazilian Data	Ritchie et. al
Engineering	Tabular/Spreadsheet	30 Day Brazilian NP Barite Data Round 1 Data	30 Day Brazilian NP Barite Data Round 1 Data.xlsx	Mark Ritchie	Geir Hareland, geir.hareland@okstate.edu 405-744-9113	2019	Task 5/Brazilian Testing	gulf-cement-project.oucreate.com/Task 5/Brazilian Testing/30 Day Brazilian NP Barite Round 1 Data.xlsx	Tensile Testing, Brazilian Data	Ritchie et. al
Engineering	Tabular/Spreadsheet	30 Day Brazilian NP Barite Round 3 Data	30 Day Brazilian NP Barite Round 3 Data.xlsx	Mark Ritchie	Geir Hareland, geir.hareland@okstate.edu 405-744-9113	2019	Task 5/Brazilian Testing	gulf-cement-project.oucreate.com/Task 5/Brazilian Testing/30 Day Brazilian NP Barite Round 3 Data.xlsx	Tensile Testing, Brazilian Data	Ritchie et. al
Engineering	Tabular/Spreadsheet	30 Day Brazilian NP Magnetite Round 1 Data	30 Day Brazilian NP Magnetite Round 1 Data.xlsx	Mark Ritchie	Geir Hareland, geir.hareland@okstate.edu 405-744-9113	2019	Task 5/Brazilian Testing	gulf-cement-project.oucreate.com/Task 5/Brazilian Testing/30 Day Brazilian NP Magnetite Round 1 Data.xlsx	Tensile Testing, Brazilian Data	Ritchie et. al
Engineering	Tabular/Spreadsheet	30 Day Brazilian NP Magnetite Round 3 Data	30 Day Brazilian NP Magnetite Round 3 Data.xlsx	Mark Ritchie	Geir Hareland, geir.hareland@okstate.edu 405-744-9113	2019	Task 5/Brazilian Testing	gulf-cement-project.oucreate.com/Task 5/Brazilian Testing/30 Day Brazilian NP Magnetite Round 3 Data.xlsx	Tensile Testing, Brazilian Data	Ritchie et. al
Engineering	Tabular/Spreadsheet	30 Day NP Barite Brazilian Round 2 Data	30 Day NP Barite Brazilian Round 2 Data.xlsx	Mark Ritchie	Geir Hareland, geir.hareland@okstate.edu 405-744-9113	2019	Task 5/Brazilian Testing	gulf-cement-project.oucreate.com/Task 5/Brazilian Testing/30 Day NP Barite Brazilian Round 2 Data.xlsx	Tensile Testing, Brazilian Data	Ritchie et. al
Engineering	Tabular/Spreadsheet	30 Day NP Magnetite Brazilian round 2 Data	30 Day NP Magnetite Brazilian round 2 Data.xlsx	Mark Ritchie	Geir Hareland, geir.hareland@okstate.edu 405-744-9113	2019	Task 5/Brazilian Testing	gulf-cement-project.oucreate.com/Task 5/Brazilian Testing30 Day NP Magnetite Brazilian round 2 Data.xlsx	Tensile Testing, Brazilian Data	Ritchie et. al
Engineering	Tabular/Spreadsheet	60 Day Brazilian Base Case Round 1 Data	60 Day Brazilian Base Case Round 1 Data.xlsx	Mark Ritchie	Geir Hareland, geir.hareland@okstate.edu 405-744-9113	2019	Task 5/Brazilian Testing	gulf-cement-project.oucreate.com/Task 5/Brazilian Testing/60 Day Brazilian Base Case Round 1 Data.xlsx	Tensile Testing, Brazilian Data	Ritchie et. al
Engineering	Tabular/Spreadsheet	60 Day Brazilian NP Barite Round 1 Data	60 Day Brazilian NP Barite Round 1 Data.xlsx	Mark Ritchie	Geir Hareland, geir.hareland@okstate.edu 405-744-9113	2019	Task 5/Brazilian Testing	gulf-cement-project.oucreate.com/Task 5/Brazilian Testing/60 Day Brazilian NP Barite Round 1 Data.xlsx	Tensile Testing, Brazilian Data	Ritchie et. al

Engineering	Tabular/Spreadsheet	60 Day Brazilian NP Magnetite Round 1 Data	60 Day Brazilian NP Magnetite Round 1 Data.xlsx	Mark Ritchie	Geir Hareland, geir.hareland@okstate.edu 405-744-9113	2019	Task 5/Brazilian Testing	gulf-cement-project.oucreate.com/Task 5/Brazilian Testing/60 Day Brazilian NP Magnetite Round 1 Data.xlsx	Tensile Testing, Brazilian Data	Ritchie et. al
Engineering	Tabular/Spreadsheet	Brazilian Testing Data	Brazilian Testing Data.xlsx	Mark Ritchie	Geir Hareland, geir.hareland@okstate.edu 405-744-9113	2019	Task 5/Brazilian Testing	gulf-cement-project.oucreate.com/Task 5/Brazilian Testing/Brazilian Testing Data.xlsx	Tensile Testing, Brazilian Data, Results	Ritchie et. al
Engineering	Tabular/Spreadsheet	Procedure Trials Data	Procedure Trials Data.xlsx	Mark Ritchie	Geir Hareland, geir.hareland@okstate.edu 405-744-9113	2019	Task 5/Brazilian Testing	gulf-cement-project.oucreate.com/Task 5/Brazilian Testing/Procedure Trials Data.xlsx	Tensile Testing, Brazilian Data	Ritchie et. al
Engineering	Images	Brazilian Test Sample Files	Brazilian Test Sample Files	Mark Ritchie	Geir Hareland, geir.hareland@okstate.edu 405-744-9113	2019	Task 5/Brazilian Testing	gulf-cement-project.oucreate.com/Task 5/Brazilian Testing/Brazilian Test Sample Files	Tensile Testing, Brazilian Data, Sample Images, Sample Files	Ritchie et. al
Engineering	Tabular/Spreadsheet	7-23 Spot Check Results (1% and 3% NP Mag.)	7-23 Spot Check Results (1% and 3% NP Mag.).xlsx	Mark Ritchie	Geir Hareland, geir.hareland@okstate.edu 405-744-9113	2019	Task 6/UCS Testing	gulf-cement-project.oucreate.com/Task 6/UCS Testing/7-23 Spot Check Results (1% and 3% NP Mag.).xlsx	UCS Testing/ UCS Results	Ritchie et. al
Engineering	Tabular/Spreadsheet	30 Day UCS Base Case Round 1	30 Day UCS Base Case Round 1.xlsx	Mark Ritchie	Geir Hareland, geir.hareland@okstate.edu 405-744-9113	2019	Task 6/UCS Testing	gulf-cement-project.oucreate.com/Task 6/UCS Testing/30 Day UCS Base Case Round 1.xlsx	UCS Testing/ UCS Results	Ritchie et. al
Engineering	Tabular/Spreadsheet	30 Day UCS Base Case Round 2	30 Day UCS Base Case Round 2.xlsx	Mark Ritchie	Geir Hareland, geir.hareland@okstate.edu 405-744-9113	2019	Task 6/UCS Testing	gulf-cement-project.oucreate.com/Task 6/UCS Testing/30 Day UCS Base Case Round 2.xlsx	UCS Testing/ UCS Results	Ritchie et. al
Engineering	Tabular/Spreadsheet	30 Day UCS Base Case Round 3	30 Day UCS Base Case Round 3.xlsx	Mark Ritchie	Geir Hareland, geir.hareland@okstate.edu 405-744-9113	2019	Task 6/UCS Testing	gulf-cement-project.oucreate.com/Task 6/UCS Testing/30 Day UCS Base Case Round 3.xlsx	UCS Testing/ UCS Results	Ritchie et. al
Engineering	Tabular/Spreadsheet	30 Day UCS NP Barite Round 1	30 Day UCS NP Barite Round 1.xlsx	Mark Ritchie	Geir Hareland, geir.hareland@okstate.edu 405-744-9113	2019	Task 6/UCS Testing	gulf-cement-project.oucreate.com/Task 6/UCS Testing/30 Day UCS NP Barite Round 1.xlsx	UCS Testing/ UCS Results	Ritchie et. al
Engineering	Tabular/Spreadsheet	30 Day UCS NP Barite Round 2	30 Day UCS NP Barite Round 2.xlsx	Mark Ritchie	Geir Hareland, geir.hareland@okstate.edu 405-744-9113	2019	Task 6/UCS Testing	gulf-cement-project.oucreate.com/Task 6/UCS Testing/30 Day UCS NP Barite Round 2.xlsx	UCS Testing/ UCS Results	Ritchie et. al
Engineering	Tabular/Spreadsheet	30 Day UCS NP Barite Round 3	30 Day UCS NP Barite Round 3.xlsx	Mark Ritchie	Geir Hareland, geir.hareland@okstate.edu 405-744-9113	2019	Task 6/UCS Testing	gulf-cement-project.oucreate.com/Task 6/UCS Testing/30 Day UCS NP Barite Round 3.xlsx	UCS Testing/ UCS Results	Ritchie et. al
Engineering	Tabular/Spreadsheet	30 Day UCS NP Magnetite Round 1	30 Day UCS NP Magnetite Round 1.xlsx	Mark Ritchie	Geir Hareland, geir.hareland@okstate.edu 405-744-9113	2019	Task 6/UCS Testing	gulf-cement-project.oucreate.com/Task 6/UCS Testing/30 Day UCS NP Magnetite Round 1.xlsx	UCS Testing/ UCS Results	Ritchie et. al
Engineering	Tabular/Spreadsheet	30 Day UCS NP Magnetite Round 2	30 Day UCS NP Magnetite Round 2.xlsx	Mark Ritchie	Geir Hareland, geir.hareland@okstate.edu 405-744-9113	2019	Task 6/UCS Testing	gulf-cement-project.oucreate.com/Task 6/UCS Testing/30 Day UCS NP Magnetite Round 2.xlsx	UCS Testing/ UCS Results	Ritchie et. al
Engineering	Tabular/Spreadsheet	30 Day UCS NP Magnetite Round 3	30 Day UCS NP Magnetite Round 3.xlsx	Mark Ritchie	Geir Hareland, geir.hareland@okstate.edu 405-744-9113	2019	Task 6/UCS Testing	gulf-cement-project.oucreate.com/Task 6/UCS Testing/30 Day UCS NP Magnetite Round 3.xlsx	UCS Testing/ UCS Results	Ritchie et. al
Engineering	Tabular/Spreadsheet	60 Day UCS Base Case Round 1	60 Day UCS Base Case Round 1.xlsx	Mark Ritchie	Geir Hareland, geir.hareland@okstate.edu 405-744-9113	2019	Task 6/UCS Testing	gulf-cement-project.oucreate.com/Task 6/UCS Testing/60 Day UCS Base Case Round 1.xlsx	UCS Testing/ UCS Results	Ritchie et. al
Engineering	Tabular/Spreadsheet	60 Day UCS NP Barite Round 1	60 Day UCS NP Barite Round 1.xlsx	Mark Ritchie	Geir Hareland, geir.hareland@okstate.edu 405-744-9113	2019	Task 6/UCS Testing	gulf-cement-project.oucreate.com/Task 6/UCS Testing/60 Day UCS NP Barite Round 1.xlsx	UCS Testing/ UCS Results	Ritchie et. al
Engineering	Tabular/Spreadsheet	60 Day UCS NP Magnetite Round 1	60 Day UCS NP Magnetite Round 1.xlsx	Mark Ritchie	Geir Hareland, geir.hareland@okstate.edu 405-744-9113	2019	Task 6/UCS Testing	gulf-cement-project.oucreate.com/Task 6/UCS Testing/60 Day UCS NP Magnetite Round 1.xlsx	UCS Testing/ UCS Results	Ritchie et. al
Engineering	Tabular/Spreadsheet	Displacement Rate Trials	Displacement Rate Trials.xlsx	Mark Ritchie	Geir Hareland, geir.hareland@okstate.edu 405-744-9113	2019	Task 6/UCS Testing	gulf-cement-project.oucreate.com/Task 6/UCS Testing/Displacement Rate Trials.xlsx	UCS Testing/ UCS Results	Ritchie et. al
Engineering	Tabular/Spreadsheet	Procedure Trials UCS	Procedure Trials UCS.xlsx	Mark Ritchie	Geir Hareland, geir.hareland@okstate.edu 405-744-9113	2019	Task 6/UCS Testing	gulf-cement-project.oucreate.com/Task 6/UCS Testing/Procedure Trials UCS.xlsx	UCS Testing/ UCS Results	Ritchie et. al
Engineering	Tabular/Spreadsheet	UCS Testing Data	UCS Testing Data.xlsx	Mark Ritchie	Geir Hareland, geir.hareland@okstate.edu 405-744-9113	2019	Task 6/UCS Testing	gulf-cement-project.oucreate.com/Task 6/UCS Testing/UCS Testing Data .xlsx	UCS Testing/ UCS Results	Ritchie et. al
Engineering	Images	UCS Sample Files	UCS Sample Files	Mark Ritchie	Geir Hareland, geir.hareland@okstate.edu 405-744-9113	2019	Task 6/UCS Testing	gulf-cement-project.oucreate.com/Task 6/UCS Testing/UCS Sample Files	UCS Individual Sample Files/ UCS Images	Ritchie et. al
Engineering	Tabular/Spreadsheet	Shear Bond Testing Data	Shear Bond Testing Data.xlsx	Mark Ritchie	Geir Hareland, geir.hareland@okstate.edu 405-744-9113	2019	Task 6/Shear Bond Testing	gulf-cement-project.oucreate.com/Task 6/Shear Bond TestingShear Bond Testing Data.xlsx	Shear Bond Testing/Shear Bond Test Results	Ritchie et. al
Engineering	Tabular/Spreadsheet	Shear Bond Sample Files	Shear Bond Sample Files	Mark Ritchie	Geir Hareland, geir.hareland@okstate.edu 405-744-9113	2019	Task 6/Shear Bond Testing	gulf-cement-project.oucreate.com/Task 6/Shear Bond Testing/Shear Bond Sample Files	Shear Bond Testing/Shear Bond Test Results/ Sample Files	Ritchie et. al
Engineering	Images	Shear Bond Apparatus Design	Shear Bond Apparatus Design (SW Files)	Mark Ritchie	Geir Hareland, geir.hareland@okstate.edu 405-744-9113	2019	Task 6/Shear Bond Testing	gulf-cement-project.oucreate.com/Task 2/Shear Bond Testing/Shear Bond Apparatus Design (SW Files)	Shear Bond Apparatus Design Files	Ritchie et. al
Engineering	Tabular/Spreadsheet	Tensile Bond Testing Data.xlsx	Tensile Bond Testing Data	Mark Ritchie	Geir Hareland, geir.hareland@okstate.edu 405-744-9113	2019	Task 5/Tesnile Bond Testing	gulf-cement-project.oucreate.com/Task 5/Tesnile Bond Testing/Tensile Bond Testing Data.xlsx	Tensile Bond Testing Data/ Tensile Bond Test Results	Ritchie et. al
Engineering	Tabular/Spreadsheet	Tensile Bond testing Sample Files	Tensile Bond testing Sample Files	Mark Ritchie	Geir Hareland, geir.hareland@okstate.edu 405-744-9113	2019	Task 5/Tesnile Bond Testing	gulf-cement-project.oucreate.com/Task 5/Tesnile Bond Testing/Tensile Bond Testing Sample Files	Tensile Bond Testing Data/ Tensile Bond Test Results/Sample Files	Ritchie et. al
Engineering	Images	Tensile Bond Test Images	Tensile Bond Test Images	Mark Ritchie	Geir Hareland, geir.hareland@okstate.edu 405-744-9113	2019	Task 5/Tesnile Bond Testing	gulf-cement-project.oucreate.com/Task 5/Tesnile Bond Testing/Tensile Bond Test Images	Tensile Bond Test Images/Anchor/ Steel substrate	Ritchie et. al
Engineering	Images	Cleaning by Sonication	Cleaning by Sonication	Mark Ritchie	Geir Hareland, geir.hareland@okstate.edu 405-744-9113	2019	Task 6/Shear Bond Testing	gulf-cement-project.oucreate.com/Task 2/Shear Bond Testing/Cleaning by Sonication	Sonicator/Sonicator Cleaning Solution	Ritchie et. al
Engineering	Images	Shear Bond Test Images	Shear Bond Test Images	Mark Ritchie	Geir Hareland, geir.hareland@okstate.edu 405-744-9113	2019	Task 6/Shear Bond Testing	gulf-cement-project.oucreate.com/Task 6/Shear Bond Testing/Shear Bond Test Images	Shear Bond Test Sample Images	Ritchie et. al

Engineering	Tabular/Spreadsheet	Shear Bond Test Friction Calculations	Friction Calculations	Mark Ritchie	Geir Hareland, geir.hareland@okstate.edu 405-744-9113	2019	Task 6/Shear Bond Testing	gulf-cement-project.oucreate.com/Task 6/Shear Bond Testing/Friction Calculations.xlsx	Shear Bond Friction Calculations	Ritchie et. al
Engineering	Tabular/Spreadsheet	Heavy Cement Design	Boric Acid Effect on Setting Time	Kjeldal, Vigleik Nicolai	Geir Hareland, geir.hareland@okstate.edu 405-744-9113	2019	Task 2/Cement Design Methodology and Storage	gulf-cement-project.oucreate.com/Task 2/Cement Design Methodology and Storage/Heavy Cement Design/Boric Acid Effect on Setting Time.xlsx	Boric Acid Effect on Setting Time	TBD
Engineering	Tabular/Spreadsheet	Heavy Cement Design	Heavy Cement Composition	Kjeldal, Vigleik Nicolai	Geir Hareland, geir.hareland@okstate.edu 405-744-9113	2019	Task 2/Cement Design Methodology and Storage	gulf-cement-project.oucreate.com/Task 2/Cement Design Methodology and Storage/Heavy Cement Design/Heavy Cement Composition.xlsx	Heavy Cement Composition	TBD
Engineering	Tabular/Spreadsheet	Light Cement Design	Boric Acid Effect on Setting Time	Kjeldal, Vigleik Nicolai	Geir Hareland, geir.hareland@okstate.edu 405-744-9113	2019	Task 2/Cement Design Methodology and Storage	gulf-cement-project.oucreate.com/Task 2/Cement Design Methodology and Storage/Light Cement Design/Boric Acid Effect on Setting Time.xlsx	Boric Acid Effect on Setting Time	TBD
Engineering	Tabular/Spreadsheet	Light Cement Design	Light Cement Composition	Kjeldal, Vigleik Nicolai	Geir Hareland, geir.hareland@okstate.edu 405-744-9113	2019	Task 2/Cement Design Methodology and Storage	gulf-cement-project.oucreate.com/Task 2/Cement Design Methodology and Storage/Light Cement Design/Light Cement Composition.xlsx	Light Cement Composition	TBD
Engineering	Images	Fluid Loss Testing Methodology	HPHT Fluid Loss Tester	Kjeldal, Vigleik Nicolai	Geir Hareland, geir.hareland@okstate.edu 405-744-9113	2019	Task 2/Fluid Loss Testing Methodology	gulf-cement-project.oucreate.com/Task 2/Fluid Loss Testing Methodology/HPHT Fluid Loss Tester.docx	Fluid Loss Testing Methodology	TBD
Engineering	Images	Rheology Testing Methodology	Viscometer	Kjeldal, Vigleik Nicolai	Geir Hareland, geir.hareland@okstate.edu 405-744-9113	2019	Task 2/Rheology Testing Methodology	gulf-cement-project.oucreate.com/Task 2/Rheology Testing Methodology/Viscometer.docx	Rheology Testing Methodology	TBD
Engineering	Images	Thickening Time Methodology	HPHT Consistometer	Kjeldal, Vigleik Nicolai	Geir Hareland, geir.hareland@okstate.edu 405-744-9113	2019	Task 2/Thickening Time Methodology	gulf-cement-project.oucreate.com/Task 2/Thickening Time Methodology/HPHT Consistometer.docx	Thickening Time Methodology	TBD
Engineering	Tabular/Spreadsheet	Cement Fluid Loss Testing	Heavy Cement Fluid Loss	Kjeldal, Vigleik Nicolai	Geir Hareland, geir.hareland@okstate.edu 405-744-9113	2019	Task 3/Cement Fluid Loss Testing	gulf-cement-project.oucreate.com/Task 3/Cement Fluid Loss Testing/Heavy Cement Fluid Loss.xlsx	Cement Fluid Loss Testing	TBD
Engineering	Tabular/Spreadsheet	Cement Fluid Loss Testing	Light Cement Fluid Loss	Kjeldal, Vigleik Nicolai	Geir Hareland, geir.hareland@okstate.edu 405-744-9113	2019	Task 3/Cement Fluid Loss Testing	gulf-cement-project.oucreate.com/Task 3/Cement Fluid Loss Testing/Light Cement Fluid Loss.xlsx	Cement Fluid Loss Testing	TBD
Engineering	Tabular/Spreadsheet	Cement Rheology Testing	Heavy Cement Rheology	Kjeldal, Vigleik Nicolai	Geir Hareland, geir.hareland@okstate.edu 405-744-9113	2019	Task 3/Cement Rheology Testing	gulf-cement-project.oucreate.com/Task 3/Cement Rheology Testing/Heavy Cement Rheology.xlsx	Cement Rheology Testing	TBD
Engineering	Tabular/Spreadsheet	Cement Rheology Testing	Light Cement Rheology	Kjeldal, Vigleik Nicolai	Geir Hareland, geir.hareland@okstate.edu 405-744-9113	2019	Task 3/Cement Rheology Testing	gulf-cement-project.oucreate.com/Task 3/Cement Rheology Testing/Light Cement Rheology.xlsx	Cement Rheology Testing	TBD
Engineering	Tabular/Spreadsheet	Cement Thickening Time Testing	Heavy Containing Barite NPs	Kjeldal, Vigleik Nicolai	Geir Hareland, geir.hareland@okstate.edu 405-744-9113	2019	Task 4/Cement Thickening Time Testing	gulf-cement-project.oucreate.com/Task 4/Cement Thickening Time Testing/Heavy Containing Barite NPs.xlsx	Cement Thickening Time Testing	TBD
Engineering	Tabular/Spreadsheet	Cement Thickening Time Testing	Heavy Containing Magnetite NPs	Kjeldal, Vigleik Nicolai	Geir Hareland, geir.hareland@okstate.edu 405-744-9113	2019	Task 4/Cement Thickening Time Testing	gulf-cement-project.oucreate.com/Task 4/Cement Thickening Time Testing/Heavy Containing Magnetite NPs.xlsx	Cement Thickening Time Testing	TBD
Engineering	Tabular/Spreadsheet	Cement Thickening Time Testing	Light Containing Bentonite NPs	Kjeldal, Vigleik Nicolai	Geir Hareland, geir.hareland@okstate.edu 405-744-9113	2019	Task 4/Cement Thickening Time Testing	gulf-cement-project.oucreate.com/Task 4/Cement Thickening Time Testing/Light Containing Bentonite NPs.xlsx	Cement Thickening Time Testing	TBD
Engineering	Text	Model Input "Life of Well"	PR3-FEA_Model_Input	Jarrett Wise	Geir Hareland, geir.hareland@okstate.edu 405-744-9113	2020	Task9/Model Validition	gulf-cement-project.oucreate.com/Task9/Model Validition/PR3-FEA_Model_Input.txt	FEA Model Input	TBD
Engineering	Text	Model Output "Life of Well"	PR3-FEA_Model_Output	Jarrett Wise	Geir Hareland, geir.hareland@okstate.edu 405-744-9113	2020	Task9/Model Validition	gulf-cement-project.oucreate.com/Task9/Model Validition/PR3-FEA_Model_Output.txt	FEA Model Output	TBD
Engineering	Tabular/Spreadsheet	Model Results "Life of Well"	PR3-FEA_Results	Jarrett Wise	Geir Hareland, geir.hareland@okstate.edu 405-744-9113	2020	Task9/Model Validition	gulf-cement-project.oucreate.com/Task9/Model Validition/PR3-FEA_Results.xlsx	FEA Model Output Results and Plot	TBD
Engineering	Tabular/Spreadsheet	Cement Thickening Time Testing	Light Containing Bentonite NPs	Kjeldal, Vigleik Nicolai	Geir Hareland, geir.hareland@okstate.edu 405-744-9113	2020	Task 4/Cement Thickening Time Testing	gulf-cement-project.oucreate.com/Task 4/Cement Thickening Time Testing/Light Containing Bentonite NPs New Tests.xlsx	Cement Thickening Time Testing	TBD
Engineering	Tabular/Spreadsheet	Cement Thickening Time Testing	Heavy Containing Ground Cement H	Kjeldal, Vigleik Nicolai	Geir Hareland, geir.hareland@okstate.edu 405-744-9113	2020	Task 4/Cement Thickening Time Testing	gulf-cement-project.oucreate.com/Task 4/Cement Thickening Time Testing/Heavy Containing Ground Cement H.xlsx	Cement Thickening Time Testing	TBD
Engineering	Tabular/Spreadsheet	Cement Thickening Time Testing	Light Containing Ground Cement A	Kjeldal, Vigleik Nicolai	Geir Hareland, geir.hareland@okstate.edu 405-744-9113	2020	Task 4/Cement Thickening Time Testing	gulf-cement-project.oucreate.com/Task 4/Cement Thickening Time Testing/Light Containing Ground Cement A.xlsx	Cement Thickening Time Testing	TBD
Engineering	Tabular/Spreadsheet	Cement Thickening Time Testing	Heavy Containing Barite NPs New Tests	Kjeldal, Vigleik Nicolai	Geir Hareland, geir.hareland@okstate.edu 405-744-9113	2020	Task 4/Cement Thickening Time Testing	gulf-cement-project.oucreate.com/Task 4/Cement Thickening Time Testing/Heavy Containing Barite NPs New Tests.xlsx	Cement Thickening Time Testing	TBD
Engineering	Tabular/Spreadsheet	Cement Thickening Time Testing	Heavy Containing Magnetite NPs New Tests	Kjeldal, Vigleik Nicolai	Geir Hareland, geir.hareland@okstate.edu 405-744-9113	2020	Task 4/Cement Thickening Time Testing	gulf-cement-project.oucreate.com/Task 4/Cement Thickening Time Testing/Heavy Containing Magnetite NPs New Tests.xlsx	Cement Thickening Time Testing	TBD
Engineering	Tabular/Spreadsheet	30 Day Base Case Brazilian	30 Day Brazilian Bentonite NPs	Kjeldal, Vigleik Nicolai	Geir Hareland, geir.hareland@okstate.edu 405-744-9113	2020	Task 5/Brazilian Testing	gulf-cement-project.oucreate.com/Task 5/Brazilian Testing/30 Day Brazilian Bentonite NPs.xlsx	Tensile Testing, Brazilian Data	TBD
Engineering	Tabular/Spreadsheet	30 Day Base Case UCS	30 Day UCS Bentonite NPs	Kjeldal, Vigleik Nicolai	Geir Hareland, geir.hareland@okstate.edu 405-744-9113	2020	Task 6/UCS Testing	gulf-cement-project.oucreate.com/Task 6/UCS Testing/30 Day UCS Bentonite NPs.xlsx	UCS Testing/ UCS Results	TBD

Engineering	Tabular/Spreadsheet	Cement Permeability	Cement Permeability	Kjeldal, Vigleik Nicolai	Geir Hareland, geir.hareland@okstate.edu 405-744-9113	2020	Task 8/Results	gulf-cement-project.oucreate.com/Task 8/Results/Cement Permeability.xlsx	Cement Permeability	TBD
Engineering	Tabular/Spreadsheet	Cement Porosity	Cement Porosity	Kjeldal, Vigleik Nicolai	Geir Hareland, geir.hareland@okstate.edu 405-744-9113	2020	Task 8/Results	gulf-cement-project.oucreate.com/Task 8/Results/Cement Porosity.xlsx	Cement Porosity	TBD
Engineering	Figure	PERG 200	PERG 201	Kjeldal, Vigleik Nicolai	Geir Hareland, geir.hareland@okstate.edu 405-744-9113	2020	Task 8	gulf-cement-project.oucreate.com/Task 8/PERG200.jpg	Permeability	TBD
Engineering	Tabular/Spreadsheet	Cement Setting pressure	Cement Setting pressure	Kjeldal, Vigleik Nicolai	Geir Hareland, geir.hareland@okstate.edu 405-744-9113	2020	Task 7	gulf-cement-project.oucreate.com/Task 7/Cement Setting pressure.xlsx	Cement Setting pressure	TBD
Engineering	Tabular/Spreadsheet	Cement Rheology Testing	Rheology Heavy Containing Ground H	Kjeldal, Vigleik Nicolai	Geir Hareland, geir.hareland@okstate.edu 405-744-9113	2020	Task 3/Cement Rheology Testing	gulf-cement-project.oucreate.com/Task 3/Cement Rheology Testing/Rheology Heavy Containing Ground H.xlsx	Cement Rheology Testing	TBD
Engineering	Tabular/Spreadsheet	Cement Rheology Testing	Rheology Light Containing Ground A	Kjeldal, Vigleik Nicolai	Geir Hareland, geir.hareland@okstate.edu 405-744-9113	2020	Task 3/Cement Rheology Testing	gulf-cement-project.oucreate.com/Task 3/Cement Rheology Testing/Rheology Heavy Containing Ground A.xlsx	Cement Rheology Testing	TBD
Engineering	Tabular/Spreadsheet	Cement Rheology Testing	Rheology Light Containing Bentonite NPs	Kjeldal, Vigleik Nicolai	Geir Hareland, geir.hareland@okstate.edu 405-744-9113	2020	Task 3/Cement Rheology Testing	gulf-cement-project.oucreate.com/Task 3/Cement Rheology Testing/Rheology Light Containing Bentonite NPs.xlsx	Cement Rheology Testing	TBD
Engineering	Tabular/Spreadsheet	Fluid Loss Testing	Fluid Loss Light Containing Bentonite NPs	Kjeldal, Vigleik Nicolai	Geir Hareland, geir.hareland@okstate.edu 405-744-9113	2020	Task 3/Cement Fluid Loss Testing	gulf-cement-project.oucreate.com/Task 3/Cement Fluid Loss Testing/Fluid Loss Light Containing Bentonite NPs.xlsx	Fluid Loss Testing	TBD
Engineering	Tabular/Spreadsheet	Fluid Loss Testing	Fluid Loss Light Containing Ground Cement A	Kjeldal, Vigleik Nicolai	Geir Hareland, geir.hareland@okstate.edu 405-744-9113	2020	Task 3/Cement Fluid Loss Testing	gulf-cement-project.oucreate.com/Task 3/Cement Fluid Loss Testing/Fluid Loss Light Containing Ground Cement A.xlsx	Fluid Loss Testing	TBD
Engineering	Tabular/Spreadsheet	Fluid Loss Testing	Fluid Loss Light Containing Ground Cement H	Kjeldal, Vigleik Nicolai	Geir Hareland, geir.hareland@okstate.edu 405-744-9113	2020	Task 3/Cement Fluid Loss Testing	gulf-cement-project.oucreate.com/Task 3/Cement Fluid Loss Testing/Fluid Loss Heavy Containing Ground Cement H.xlsx	Fluid Loss Testing	TBD
Engineering	Tabular/Spreadsheet	Tensile Bond Strength	Tensile Bond Strength Light Containing Bentonite NPs	Kjeldal, Vigleik Nicolai	Geir Hareland, geir.hareland@okstate.edu 405-744-9113	2020	Task 5/Tesnile Bond Testing	gulf-cement-project.oucreate.com/Task 5/Tesnile Bond Testing/Tensile Bond Strength Light Containing Bentonite NPs.xlsx	Tensile Bond Testing	TBD
Engineering	Tabular/Spreadsheet	Tensile Bond Strength	Tensile Bond Strength Light Containing Ground A	Kjeldal, Vigleik Nicolai	Geir Hareland, geir.hareland@okstate.edu 405-744-9113	2020	Task 5/Tesnile Bond Testing	gulf-cement-project.oucreate.com/Task 5/Tesnile Bond Testing/Tensile Bond Strength Light Containing Ground A.xlsx	Tensile Bond Testing	TBD
Engineering	Tabular/Spreadsheet	Tensile Bond Strength	Tensile Bond Strength Heavy Containing Ground H	Kjeldal, Vigleik Nicolai	Geir Hareland, geir.hareland@okstate.edu 405-744-9113	2020	Task 5/Tesnile Bond Testing	gulf-cement-project.oucreate.com/Task 5/Tesnile Bond Testing/Tensile Bond Strength Heavy Containing Ground H.xlsx	Tensile Bond Testing	TBD
Engineering	Tabular/Spreadsheet	Shear Bond Strength	Shear Bond Light Containing Bentonite NPs	Kjeldal, Vigleik Nicolai	Geir Hareland, geir.hareland@okstate.edu 405-744-9113	2020	Task 6/Shear Bond Testing	gulf-cement-project.oucreate.com/Task 6/Shear Bond Testing/Shear Bond Light Containing Bentonite NPs.xlsx	Tensile Bond Testing	TBD
Engineering	Tabular/Spreadsheet	Shear Bond Strength	Shear Bond Light Containing Ground Cement A	Kjeldal, Vigleik Nicolai	Geir Hareland, geir.hareland@okstate.edu 405-744-9113	2020	Task 6/Shear Bond Testing	gulf-cement-project.oucreate.com/Task 6/Shear Bond Testing/Shear Bond Light Containing Ground Cement A.xlsx	Tensile Bond Testing	TBD
Engineering	Tabular/Spreadsheet	Shear Bond Strength	Shear Bond Heavy Containing Ground Cement H	Kjeldal, Vigleik Nicolai	Geir Hareland, geir.hareland@okstate.edu 405-744-9113	2020	Task 6/Shear Bond Testing	gulf-cement-project.oucreate.com/Task 6/Shear Bond Testing/Shear Bond Heavy Containing Ground Cement H.xlsx	Tensile Bond Testing	TBD
Engineering	Tabular/Spreadsheet	30 Day UCS	30 Day UCS Ground Cement A	Kjeldal, Vigleik Nicolai	Geir Hareland, geir.hareland@okstate.edu 405-744-9113	2020	Task 6/UCS Testing	gulf-cement-project.oucreate.com/Task 6/UCS Testing/30 Days UCS Light Containing Ground Cement A.xlsx	UCS Testing/ UCS Results	TBD
Engineering	Tabular/Spreadsheet	30 Day UCS	30 Day UCS Ground Cement H	Kjeldal, Vigleik Nicolai	Geir Hareland, geir.hareland@okstate.edu 405-744-9113	2020	Task 6/UCS Testing	gulf-cement-project.oucreate.com/Task 6/UCS Testing/30 Days UCS Heavy Containing Ground Cement H.xlsx	UCS Testing/ UCS Results	TBD

Information Products Report

InfoProductType	DigitalResourceType	Title	FileName	Creators	PublicationYear	Publisher	RepositoryName	DOIorPersistentURL	DatasetReference
Models and Simulations	Text	Model Input "Life of Well"	PR1-FEA_Model_Input(Fig4)	Jarrett Wise	2018	Geir Hareland, geir.hareland@okstate.edu 405-744-9116	Task1/FEA_vs_Analytical	TBD	TBD
Models and Simulations	Text	Model Output "Life of Well"	PR1-FEA_model_Output(Fig4)	Jarrett Wise	2018	Geir Hareland, geir.hareland@okstate.edu 405-744-9116	Task1/FEA_vs_Analytical	TBD	TBD